Laboratory Experiments of Wave Attenuation by Mud

by

Nourah Mohammed Almashan

A dissertation submitted to The Johns Hopkins University in conformity with the requirements for the degree of Doctor of Philosophy.

Baltimore, Maryland

September, 2014

Abstract

Muddy deposits make up a large region of the world's coastal lands such as the Gulf of Mexico, the Louisiana coastline, and the Persian Gulf. These regions serve as valuable resources for the world's population for commerce, leisure activities, and sustainability. Human activities depend on the comprehensive understanding of the natural occurrences that take place in these coastal zones. The interaction between waves and the muddy sea bottom has profound effects on these human activities because the damping of waves in these regions creates turbidity, which can disrupt the natural habitat for marine and coastal life.

The purpose of this study is to better understand the mechanisms of water wave damping over mud as a function of water depth, wave height and period. In a series of laboratory experiments, the damping rate was determined for different wave parameters in intermediate and shallow water for a kaolinite mud bed. The results show that the damping rate is highly dependent on the rate of work performed by the waves on the bottom.

Damping in deep water was also observed in laboratory experiments. Water waves

ABSTRACT

propagating over a mud bottom in deep water are not affected by the bottom. However, two superimposed short waves can create a wave group that generates an associated long bound wave that will extend the wave pressure to the bottom and dissipate energy. In a series of laboratory experiments of various wave group parameters, the damping rate was measured with a variety of methods.

A theory for the nonlinear interaction of two short waves propagating with arbitrary angles in deep water was developed extending the work of Longuet-Higgins (1950). The theoretical expression of the water surface elevation of waves, the bottom pressure, the velocities were developed. A further series of laboratory experiments on mud behavior showed the damping rate of waves to be a function of the wave characteristics and the amplitude of the bottom response.

These findings will improve the theoretical understanding of wave damping mechanisms in shallow, intermediate and deep water. This in turn should enable authorities and planners to shape more effective long-term environmental policies for coastal regions to protect both land and marine life.

Primary Reader: Professor Robert Dalrymple

Secondary Readers: Professor Cila Herman and Professor Tak Igusa

Acknowledgments

I would like to express my continual gratitude to Professor Robert Dalrymple, my advisor in the Civil Engineering Department at Johns Hopkins University, for his constant support, advice and enthusiasm in helping me advance to this stage. He has guided me during my years at Hopkins, making it possible to succeed with my graduate studies.

I would also like to thank Kuwait University for funding my work and financially enabling me to achieve my goals in order to return and contribute to developing the critical infrastructure of my country. I hope to make positive change for the country and inspire the new generations. I am honored to represent Kuwait in my field of study and am grateful for the knowledge and experiences that the University has afforded me.

I would also like to thank all the Professors in the Civil Engineering Department at Johns Hopkins University: Professor Lian Shen, for all of his help and advice; Professor Takeru Igusa, for his help with statistics; Professor Benjamin Schafer, who serves as the chair of the Civil Engineering Department; and Professor Narutoshi

Nakata who, as a Structural Engineering professor, helped me advance in the Civil Engineering department.

To Lisa Wetzelberger, Vess Vessileva- Clarke, LaTanya Waith and Deborah Lantry, the administrative staff of the Civil Engineering Department, thank you for your kindness, help and patience. To Nickolay Logvinovsky, the Senior Instrument Designer at the Civil Engineering Department, thank you for preparing my experiments and fixing the machines when I needed to get things done. I am extremely grateful.

Also a very special thanks to the Mechanical Engineering department for providing me with classes related to my research and advancing my knowledge in the field. I would like to sincerely thank all of the professors in Mechanical Engineering particularly Professor Rajat Mittal who introduced me to the subject of Fluid Mechanics, which is the basis of my research. I would also like to acknowledge Professor Charles Meneveau for offering his wisdom and understanding of Fluid Mechanics. Thank you to Professor Cila Herman, a professor in mechanical engineering, who helped me to better understand renewable energy. I could not have done this without all of you.

Thanks to Professor Markus Hilpert, a professor in the Geography and Environmental Studies Department at Johns Hopkins University. With his help, I was able to solve all of my research-related mathematical equations, which at times seemed intimidating.

I would like to acknowledge my Coastal Engineering group in Steiff Building for sharing their knowledge. First I would like to thank Dr. Eric Maxeiner who intro-

duced me to the lab, and who I assisted on the monochromatic wave experimental tests in chapter three. Also I am very thankful for my friend Younes Nouri who was like a brother who helped me continue my research especially in wave group I really appreciate all his supports, I would like also to thank all the girls Varjola Nelko, Rozita Farahani and Khatoon Melic, it been a great experience and time working with them.

I would like to sincerely thank my friends from the University: Guoto Yi, Shengbai Xie, Hamid Reza Khakbour, Xin Guo, Yi Lui, Xi Zhao, Vahid Meimand, Brian Lindberg and Kara Peterman. We have spent the past four years working hard, sharing our thoughts, and encouraging one another. Thank you for sharing your knowledge and experiences with me.

Eternal thanks to my friends in Baltimore, Awdah Althunayyan, Fatima Kathem, Layla Alrasheed, Shaikha Alduaij, Dalal Alsharhan, and Chelsea Markle who were all there for me in times of need and for being my family while studying and working in the United States.

Finally, I would like to thank my mother, father, my loving husband Abdulaziz Alahmad, my sisters Nouf and Shaikha, and my brother Khaled for their endless patience, love, support and encouragement. Also, thanks to my lovely children, Ahmad and Reema, for their sacrifices in having their mother away while working. Their visits and love kept me energetic, optimistic and enthusiastic during my studies. Finally, my eternal gratititude goes to everyone who has contributed, in some way, to

my project, my studies, and my stability over these few years. You all have been the key to my success.

Dedication

It has been an invaluable and memorable experience pursuing my PhD in Civil Engineering. I have worked tirelessly in academic pursuits and towards my countrys scientific advancement in the study of critical environmental phenomena. While it has not been an easy or quick period in my life, I would like to dedicate my work and this thesis to my family, who have blessed me with their patience and support against all else. My mother and father have supported me through this experience by allowing me to focus on my studies in the United States, far from my home Kuwait, while they cared for my children. They continually encouraged me to pursue my work despite setbacks, despite struggles. For this I am ever grateful. Finally, I would also like to dedicate this thesis to my husband Abdulaziz Alahmad who supported me in pursuing my studies for the past four years. Even though I have had to travel and work away from my family for most of this time, he has been a rock of support. I love him for his dedication and inspiration.

Contents

List of Tables

List of Figures

Chapter 1

Introduction to wave dissipation by mud

1.1 Motivation

Water waves greatly affect the stability and consistency of the seabeds over which they pass. There are numerous ramification of the relationship between water and mud or sediment, such as modifying wave characteristics, erosion and liquefaction of the seabeds, the change in near-bed turbulence, sediment transport, and much more. Coastal engineers, oceanographers, scientists and commercial entities all have interest in the interaction between water and a muddy bottom layer because it is a critical environment that plays a part in commercial, political/military, and environmental interests. It is crucial that we understand that the interaction of water waves and

muddy seabeds affects wave energy and motion, thus contributing to a change in the sea environment. Large portions of the worlds coastal areas, such as the Gulf of Mexico, Atlantic coastlines of South America, and the Persian Gulf, have muddy seabeds. These areas are essential areas of the world that are highly trafficked and populated and, as such, it is necessary to understand every aspect about coastlines such as water energy and force, wave directional flow, and seabed composition for stability of offshore structures. This study hopes to contribute to research on the interaction between water waves and muddy bottoms and offer new insight to better understand the relationship and potential effects.

1.2 Objectives

As part of the Department of Defense's Multi-disciplinary University Research Initiative (MURI) on the mechanisms of fluid-mud interactions under waves, this research project contributes to the overall goal of understanding the various mechanisms that contribute to wave dissipation. In this study, we will focus on the effects of wave parameters on damping.

The first objective here is to study the water wave mechanisms that cause wave energy dissipation when passing over a muddy bottom in intermediate and shallow water depths. A series of experimental tests were conducted to examine the water and mud interaction within a wave tank with a focus on the change in wave height. This

study will examine the effects of additional wave parameters, such as wave period and water depth, and mud consolidation on the damping value as well.

The second objective of this study is to examine wave damping in deep water. An individual wave train propagating in deep water does not interact with the bottom, therefore any damping of waves in deep water is caused by other mechanisms such as sidewall friction or damping by a contaminated surface. Experiments using monochromatic waves were conducted to determine this damping. Two short waves were created in deep water with slightly different frequencies, which then form a wave group with associated long-bound wave. We examine the nonlinear effects of the sum and difference bound waves and the possibility of their interaction with the bottom. In particular, we will demonstrate that the length of the long bound wave can be long enough such that the bound long wave is in intermediate or shallow water, therefore feels the bottom. The following chapters provide context for reaching these primary objectives and offer research to corroborate our findings.

Chapter Two offers a summary of laboratory, theoretical, and field experiments as well as the theoretical models that have been used to study the various aspects of water waves and seabeds. These studies provided the basic framework for our research and allowed this project to expand on previous work regarding new parameters such as deep-water depth.

Chapter Three presents our laboratory experiments examining monochromatic wave attenuation by a muddy bottom layer and the relationship between the atten-

uation of water waves and different wave parameters including water depth, wave period, mud history, and wave amplitude. The relationship between wave height and attenuation is the particular focus of this research. The experiments were carried out in intermediate and shallow water. The findings of the laboratory results are compared with theoretical models.

Chapter Four presents a new study looking at wave damping in deep water. We demonstrate that wave damping in deep water can occur, though not in the same manner as shallow water waves. We found that two short waves, which individually do not interact with the bottom seabed, create a wave group with associated bound long waves that have sufficient length to feel the bottom, therefore causing wave damping. This mechanism is studied by conducting a series of experiments looking at the different wave parameters.

Chapter Five examines existing analytical theories about the superimposition of two short waves in deep water. The water surface elevation and pressure at the bottom layer were predicted in previous studies; however we expanded on this theory to test the short waves coming together with differing angles of incidence to offer a more realistic study of what occurs in nature.

Overall, the following research offers a comprehensive look at the subjects of water wave and mud interaction and presents new insight to deep-water wave damping. The goals of this research are to look at and present findings on the effects of wave height on attenuation in shallow to intermediate-depth water and to also examine the

mechanisms of deep-water damping as an understudied phenomenon. In doing so, we have found agreement with our findings and have also explored additional parameters during the process that have inspired future study and research on the subjects.

Chapter 2

Literature Review

2.1 Introduction

The interaction of water waves and sediment is critical for numerous aspects of marine activity. Many field campaigns on muddy coastal shelfs have been carried out in highly trafficked and vital parts of the globe, such as the Gulf of Mexico, the Gulf of Aden, the Mississippi River, off the coasts of Kuwait, India, and north-western South America to name a few (Mathew *et al.*, 1995; Robillard, 2009; Vinzon *et al.*, 2009), showing significant wave damping over the mud, that is, waves decaying in a distance of several wavelength.

The interaction of water waves with the muddy shorelines is the concern of many industries that require intimate understanding of ocean geography for their commercial interests. The shipping and trade industries rely on stable, long-lasting ports and

harbors and have concerns with seabed response to storms and shifts in water wave movement. Big industries such as those involved with offshore oil and natural gas drilling need to know the rheological composition of the seabed where they set up equipment and rigs for operations.

They invest billions of dollars into construction efforts but if the seabed is unstable or too porous and is transported by waves, a billion dollar structure could collapse from the base. Furthermore, the cities and communities that are located on or near muddy coastlines, like those of Kuwait and India, have concerns about how the ocean water can erode away the shoreline. Despite being a somewhat slow process, erosion on such a large scale completely undermines the marine habitat, causing marine animals and vegetation to die off, affecting the sustenance and income for local communities. Also, tourist destinations that depend on beautiful beaches and coastal sanctuaries need the necessary information to understand the potential outcomes of the changes in water movement, sediment transport, and storm stress on the seabed.

Research concerning the interaction of ocean water waves with muddy bottoms (Gade, 1958; Dalrymple and Liu, 1978; MacPherson, 1980; Nagai *et al.*, 1984; Traykovski *et al.*, 2000; Sheremet and Stone, 2003; Hsu *et al.*, 2013), provides a good framework for understanding the varying mechanisms involved in water-mud interaction and identifying the parameters for research. These studies address many types of wave interactions (i.e. direct wave interactions, indirect wave interactions, resonant wave-wave interactions, shear instability and turbulent mudflow interactions, and

large-scale broadband mechanisms) that are crucial elements in understanding wave attenuation; however there is much more to understand about wave attenuation.

Initiated by the Office of Naval Research within the U.S. Department of Defense in February 2006, this study contributes to the Multidisciplinary University Research Initiative: Mechanisms of Fluid-Mud Interactions Under Waves (MURI) project, a multi-national research program. The MURI project's goal was to research and study water waves propagating over muddy bottoms and how energy is lost in this process. Researchers at Johns Hopkins University, Massachusetts Institute of Technology, Woods Hole Oceanographic Institution, Boston College and Louisiana State University have collectively studied portions of the greater project to combine efforts for better understanding this phenomenon. Johns Hopkins, in particular, played a role in the laboratory program by performing a series of tests within wave tanks. Through this series of laboratory experiments, more information about the effect of wave parameters and mud behavior on the damping rate of waves and will help to understand the most effective and prominent damping mechanisms.

Previous studies typically focus on shallow water wave damping as it pertains to the coastlines and harbors where much commercial and public interest lies. These are the central areas of waterway traffic and tourism. Mud properties are very influential and there is a need for further study beyond what has already been done (Krone, 1963; Yamamoto and Schuckman, 1984; Barnes *et al.*, 1989; Shibayama *et al.*, 1990; Shibayama and An, 1993). These phenomena will be further examined in the following

chapters.

2.2 Wave Attenuation

Water waves, when interacting with a muddy bottom lose energy. This energy dissipation is known as wave attenuation. Attenuation occurs due to mud viscosity, bottom boundary layer thickness, sediment suspension, degree of bed porosity among other factors (Gade, 1958; Dalrymple and Liu, 1978; Sheremet and Stone, 2003; Foda, 1989; Allison *et al.*, 2000; Yamamoto *et al.*, 1983).

Foda (1989), extended the Benjamin and Feir (1967) sideband instability which created by surface wave propagating but over mud bottom. They observed that the energy transfer from the surface wave to the sideband which will interact with bottom and will dissipate high energy.

There has been significant study regarding the different causes and outcomes of wave attenuation, though most studies focus on the damping of water waves in shallow to intermediate depth water. The importance of wave damping is significant, as the following review will point out, because the change in wave energy can severely alter the bottom seabed properties. While there are many studies that address this topic, below is a robust sampling of relevant studies and research that gave this particular study the necessary background on which to base further research. Field tests, laboratory experiments and theoretical models provide a framework for understanding

relevant research on wave attenuation.

2.2.1 Field Experiments

Field tests allow scientists and researchers to examine water-mud interaction in a natural setting that includes the variability of natural conditions. There are various regions around the world of particular interest to scientists because of their seabed composition and unique locations for examining water-mud interaction and wave attenuation. The Mississippi River delta region, Florida coast, Brazil, Surinam, South Korea, and India are a few of the areas studied for wave attenuation. Each has a unique water source (be it an ocean, river, or lake) with distinct weather patterns and climate that have an affect on wave interaction.

Looking at features offshore of the Mississippi River delta and Louisiana inner shelf, Tubman and Suhayda (1976) take their study to the field in the river delta, measuring wave attenuation rates in shallow water. Their experiment showed that wave attenuation is highly dependent on the bottom layer bed properties. A muddy bottom is more significantly affective on damping than a porous sandy bottom. By using instruments deployed at two locations in the Mississippi river delta, in deep and relatively shallow water, Tubman and Suhayda focused on long wave propagation. They found that wave propagation in cohesive sediment environments differs significantly from well-sorted environments. Particularly after Hurricane Camille in 1969, some differences in the bottom properties and their traits were apparent when

two deep-sea oil platforms, designed to withstand wave overloads of up to 20–25 m in height, were completely toppled due to soil shear strength failures or mud fluidization.

Also Wells and Coleman (1981) conducted field experiments off the coast the Caribbean. They found that the attenuation of surface waves occurs when the surface layer of the seabed is composed of mud. Two years later Wells (1983) traveled to South Korea to examine wave attenuation when the surface layer of the seabed is mainly composed of mud. These studies all found agreement that the surface layer of the seabed causes maximum damping when it is muddy.

Moreover, examining attenuation around coastlines in the United States, but this time a lakeside shore, Jain (2007) performed field tests at Newnans Lake in northern Florida. Newnans Lake served as a natural example of a shallow body of water with a soft mud bottom.

Sheremet *et al.* (2011) expands yet on Tubman and Suhayda (1976) work and uses field observations of wave and sediment processes from two locations on the Atchafalaya inner shelf of the Mississippi River. Sheremet *et al.* (2011) reveal that wave dissipation is extremely high in shallow, muddy environments. Interestingly, this study found that the maximum dissipation rate occurs post-storm, when a fluid mud layers are present, which is inconsistent with findings of Faas (1995), which also studied the wave attenuation under storm conditions. The difference in the natural environment possibly contributes to the variation of effects on wave damping. Other studies observed damping in Louisiana but for short waves in deep water during

storms and this part will be explained in details in the next chapters (Allison *et al.*, 2000; Sheremet and Stone, 2003; Elgar and Raubenheimer, 2008).

The coast of Brazil has many mudy shorelines snd offshore deposits. Holland *et al.* (2009) describes a multi-national field experiment performed offshore of Cassino beach in southern Brazil. This experiment investigated the formation of offshore mud deposits and studied wave attenuation over the muddy deposits, and evaluated the performance of models for wave transformation. Despite some complications during the experiment period, the results of this field study are being used to improve the understanding of shoaling wave dynamics and sediment transport in the coastal zones. Also contributing to understanding the coastal habitat and water interaction, Vinzon *et al.* (2009) studied mud deposit formation, in particular. In field experiments, the attenuation of surface waves was observed when the surface layer of the seabed is mainly composed of mud, much like the findings of an earlier study, Wells and Coleman (1981).

Looking more at the results of wave attenuation when natural conditions are inconsistent, such as the formation of mud banks or when there is a storm that mixes up the bottom layer, Mathew *et al.* (1995) studied the dynamics of mud banks off the southwest coast of India. They found that the pre-mud bank wave intensity directly affect dimensions of the mud banks. The wave measurements indicated that wave energy, as a result, is almost completely dissipated before it reaches the coast when passing over the mud bank. These studies identified the important of wave

parameters and sediment transport as critical components of wave attenuation in a natural setting without controlled parameters.

2.2.2 Laboratory Experiments

There are many laboratory experiments that observe damping and the physical processes and modeling of wave-mud interactions. Laboratory experiments are used to test new hypothesis and verify or refute field and/or modeling tests while allowing researchers to tailor the test parameters to account for different outcomes. Gade (1957) was the first person that studied the wave attenuation over a soft bottom. He did experimental tests where the upper layer is Kerosene and the lower layer is water- suger solution to measure the energy dissipation. He found that the maximum attenuation of a wave occurs when the mud layer thickness is 1.2 times that of the bottom layer thickness.

Hoping to fill in some of the gaps that field studies have left, Yamamoto *et al.* (1986) measured wavelength and damping of water waves passing over a clay bed. The study found that wave dispersion is related to the mud motion and that mass transport in a clay bed is proportional to the wave energy dissipation in that bed (Vinzon and Mehta, 1998).

De Wit (1995) studied wave action in a wave-current flume and an oscillating-water tunnel with artificial sediments and a marine mud mixture, creating a two-layer model. This study showed that fluid mud was made when wave height exceeded

a threshold value, creating a shear stress on the bed and fluidizing the mud. The wave motion created a movement of the mud layer, affecting its density and directly affecting wave attenuation.

Hu and Wai (2001) looked at the wave energy dissipation and the movement of the mud layer. They found that the wave-damping coefficient is a function of the mud density and the wave height. Their study draws on the previous work on sediment transport through erosion of the mud bed and transport in the mud layer (Maa and Mehta, 1987; Mehta, 1991; Shibayama *et al.*, 1989). The importance of looking at mud transport as it effects wave attenuation is critical because, in natural environments, transport is inevitable. Transport occurs under a variety of conditions, as the field study portion demonstrates. Unfortunately we didn't test the effect of sediments transport on damping in our laboratory tests but it is important to mention the important parameters that effect the damping. Taking a new approach on wave propagation, Shen *et al.* (2003) divided the incident and reflected waves propagating over a muddy bottom and looked at the dissipation ratios of both. This was the first study to isolate incident and reflected waves as such and independently test their dissipation rates.

Another factor to test is the influence of wave period in wave damping. de Boer *et al.* (2009) identifies the dispersion equation for deep to shallow water and a thin mud layer, testing the theory of Kranenburg (2008) through flume experiments. They based their study on the dispersion equation based of a two-layer model (De Wit, 1995;

Kranenburg, 2008). The experiment found that wave damping changed for the three different wave periods that were tested, linking wave period to the intensity of the damping.

More recent experiments on wave attenuation have begun to address additional parameters such as different bed composition, which cause damping in natural settings. Koftis *et al.* (2013) carry out experimental studies in a wave flume, looking at the effects of the Posidonia Oceanica meadows on damping and velocity of irregular waves. Results show good agreement for theoretical studies that have also assumed that energy loss of a wave passing over vegetation is a result of drag forces (Tang *et al.*, 2013). There are studies that address other bed makeups which affect wave attenuation, though they are not the focus of this particular study but are worth mentioning (Augustin *et al.*, 2012; Ma *et al.*, 2013; Ogus *et al.*, 2013).

The use of experimental studies is critical to offer careful, calculated research that can affirm, refute, or question research performed in field and theoretical experiments. The following is a sampling of experimental research including comparisons and contrasts of their findings would explain the value of their work to the field. The following identifies key studies looking at wave height versus attenuation, wave period versus attenuation, mud density versus attenuation, water depth thickness, mud thickness, attenuation in the sidewall, and attenuation versus shear strength of the bottom layer.

2.2.2.1 Laboratory Results for Wave Height Effects

Yamamoto and Schuckman (1984) expand on Yamamoto (1983) and conducted wave tank experiments to observe wave interactions with clay beds, testing the bed composition, wave height, and period on energy dissipation. They observed that the attenuation increases as the wave height increases. Soltanpour *et al.* (2010) also found that same results. This result makes sense because as the wave gets bigger the pressure at the bottom with increase and the damping will increase.

On the contrary, Nagai *et al.* (1984) used bentonite clay beds to tests the attenuation coefficient. They found that attenuation decreases with wave height increases. The same result was found by Sakakiyama and Bijker (1989), who studied mass transport of sediment theoretically and experimentally. They explain this result by the nonlinearity of shear stress of mud layer when wave propagate over it.

Finding two different results for wave height and attenuation, Zhang and Zhao (1999) related wave damping to the mud density. With hard mud (higher density) they found that attenuation decreases as the wave height increases, meaning the higher the wave, the greater the energy dissipation (Nagai *et al.*, 1984; Sakakiyama and Bijker, 1989). With soft mud (low density) they found that attenuation increases as wave height increases (Yamamoto and Schuckman, 1984; Soltanpour *et al.*, 2010).

To reach these conclusions, they looked at the effect of wave parameters such as wave frequency and height and how they affect the attenuation coefficient. They found that mud density is an important factor that effects the wave attenuation and

that maximum attenuation occurs at critical density 1341 kg/m^3. The interesting part of these experiments is that they conclude that the wave height increase and decrease with wave attenuation and it largely depends on mud density. They also numerically developed a multi layer hydrodynamic model to predict the wave attenuation and mass transport velocity for regular and irregular waves.

2.2.2.2 Laboratory Results for Wave Period Effect

Studies by Tsuruya and Nakano (1987), Sakakiyama and Bijker (1989), Zhang and Zhao (1999), have found that wave attenuation increases with wave period until it reaches a maximum; then it decreases. Tsuruya and Nakano (1987) found that the peak occured at a wave period is around 0.8 s at water depth= 20 cm and mud depth= 19 cm. Their results were compared with Dalrymple and Liu (1978) viscous fluid theory and found to be in agreement when the water depth was 20 cm and slightly different when the water depth was 30 cm.

As previously discussed, Sakakiyama and Bijker (1989), Zhang and Zhao (1999) also addressed this phenomenon and found that the maximum damping occurs at critical period of 1 s and they compare their results with Dalrymple and Liu (1978) and showed a good agreement. Most recently, Hsu *et al.* (2013) while finding agreement with the results of Tsuruya and Nakano (1987), Sakakiyama and Bijker (1989), Zhang and Zhao (1999), they also observed that in some cases, where the mud density is particularly low, the wave attenuation might increase again. They performed

laboratory experiments and numerical modeling of wave attenuation, finding that the wave-averaged bottom stress is correlated with the damping rate in intermediate waves.

2.2.2.3 Laboratory Results for Mud Density Effect

In addressing the relationship between mud density and wave attenuation, for which there are numerous studies, Nagai *et al.* (1984), Sakakiyama and Bijker (1989) found that attenuation increases with lower density mud and decreases with higher density mud. Sakakiyama and Bijker (1989) found that at low frequency the attenuation coefficient is high for soft mud layer when the density is 1300 kg/m^3 and the attenuation coefficient is low for mud layer when the density is 1370 kg/m^3. Studies finding similar results include Zhang and Zhao (1999), Hu and Wai (2001), Hsu *et al.* (2013), who also observed that the wave attenuation is directly related to mud density. There needs to be further study to identify critical factors and potential outcomes of mud density changes and attenuation of water waves because many studies address this point yet there are still inconsistencies in the research.

2.2.2.4 Laboratory Results for Rheological Properties Effect

A basic understanding of rheological properties of mud is fundamental to many of the studies mentioned above. While most studies briefly discuss how rheology plays a role in other wave-mud interaction phenomena, it is critical to establish a basis

of literature and research projects that have advanced the study of mud properties. A pivotal analytic study on rheological properties offered by Barnes *et al.* (1989), provides a basic background and theoretical discussion about rheology as a scientific discipline.

Rheology, as invented by Professor Bingham of Lafayette College, studies the deformation and flow of matter. This book also introduces the reader to viscoelasticity as a medium between a viscous fluid and a purely elastic response, which is a liquid whose behavior has somewhat of a memory characteristic. Additional studies such as Maa and Mehta (1988, 1990), Mehta (1991), Shibayama and An (1993), Jiang and Watanabe (1995), also provide further insight.

2.2.2.5 Laboratory Results for Side Wall Effect

A relatively neglected factor in wave attenuation is the role of the sidewall during wave experiments. Tsuruya and Nakano (1987) found the wave amplitude is at a maximum in the center of the tank and a minimum at the walls.

In conclusion, the use of laboratory experiments allows researchers to test the various parameters of attenuation and interchange different wave characteristics and bottom layer features to see a variety of outcomes. This allows for comparison of experimental findings with those in the field or with theoretical models, which also study wave attenuation but within the framework of other theorist's findings.

2.2.3 Theoretical Models

A variety of theoretical models of wave damping have been developed to by differ in their treatment of the rheology of the mud. Modeling details are discussed in further detail in the following sections. The models differ in their treatment of the rheology of the mud. In this section, the models (viscous, visco-elastic, poro-elastic, elastic, visco-plastic, visco-elastic-plastic) will be presented along with relevant research and examples to demonstrate their successful application.

2.2.3.1 Elastic Model

A useful theoretical tool is the elastic model. This model assumes the rheological properties of mud is an elastic solid. Mallard and Dalrymple (1977) offer an analytic solution for water waves propagating over a deformable, elastic bottom. The water is assumed to be constant depth so that the shear stress of the soil can be obtained. Expanding on this, Dawson (1978) uses numerical modeling, looking at the response of soil beneath water as studied by Mallard and Dalrymple (1977). In the elastic model, no damping is occurs.

2.2.3.2 Viscous Model

The viscous mud model is very widely used in the field of wave attenuation and is often used for comparisons with field experiments because of its simplicity. Its use of the two-layer fluid system provides a simplified way for researchers to hone in on

certain test parameters.

Gade (1958) is the most well-known and cited study on the effects of a non-rigid, impermeable bottom on surface waves in shallow water. He used a two-layer model with a rigid bottom and treated the water as an inviscid fluid and the mud as a highly viscous fluid. He developed linear solutions for wave attenuation. He concluded that maximum wave attenuation occurs when the fluid mud layer thickness is 1.2 times the water layer thickness. Taking Gade (1958) as a basis for their study, Dalrymple and Liu (1978) extended his work by developing a model that characterized the bottom mud as a viscous fluid but they also included the viscosity in the upper layer to find a solution for the two layer problems for both shallow and deep water conditions. They also developed a boundary layer model and the solutions to calculate the wave attenuation. They found that the maximum damping occurs when the mud layer is equal to the boundary layer thickness in the mud. They compared their results with Gade (1957, 1958) experiments and found good agreement.

Many viscous experimental and theoretical models have been developed since their work such as Jiang and Zhao (1989), Jiang *et al.* (1990), Ng (2000), which are often used in comparing the experimental results. Jiang and Zhao (1989) took a new approach and examined solitary wave motion over a soft fluid mud. Using laboratory experiments of mud from the New Port, Tianjin, the theoretical calculations showed agreement with experimental data. It was found that the waves attenuated much faster than the rate determined by Keulegan (1958) over a rigid smooth bed. Also,

the higher the density of the fluid-mud means greater viscosity and the greater the viscosity, the greater the energy dissipation of the wave will be. Taking these same features of the model, Jiang *et al.* (1990) expand Jiang and Zhao (1989) model and look at cnoidal water waves passing over fluid-mud and the energy dissipation by adopting a two layer viscous fluid model with boundary layers at the water-mud interface and at the rigid bottom. It was found that exceptionally high rates of attenuation can occur such that waves are almost completely damped in several wavelengths. This has been observed both in field investigation and in laboratory experiments. For nonlinear, shallow waves, this study finds analytical solutions for the velocity in the boundary layers and for the attenuation of the wave heights over a distance.

In addition, Ng (2000) developed new solutions for wave attenuation while examining the mud transportation caused by wave motions. He studied water waves propagating on the waters surface overlying a thin layer of a laminar viscous mud. The mud was assumed to be Newtonian and homogeneous. This study used the important limiting case when the mud depth is comparable to its Stokes boundary layer thickness. This case was important because the damping rate of waves was found to reach its peak when the mud layer is only 30 - 50% thicker than the boundary layer, as found by Dalrymple and Liu (1978). Ng wanted to look at the mud layer as it mimics most marine environments; where the mud layer is typically much thinner than the overlying water layer, as also found by Mei and Liu (1987). Analytical solutions were sought for the fluid velocity fields, interfacial wave characteristics, and wave-damping

rate. Ng's study also looked at the effects of the mud layer thickness, density, and viscosity ratios on these factors. He found that denser mud is more uneffected under the wave activity, which decreases wave attenuation for smaller waves. The mass-transport velocity of the mud increases with the mud layer thickness, but decreases with the density contrast. These analytical results expand our understanding of the interaction between surface waves and a muddy bottom.

The viscous model has been used in many research areas. Looking at nonlinear surface waves, Kaihatu *et al.* (2007) look at fluid-mud layer on nearshore nonlinear wave-wave interactions using a series of laboratory experiments with a nonlinear wave model. They also adjusted for bottom layer dissipation, which allows for calculating the wave-damping rate. Numerical tests showed that damping of high frequency waves occurs. Their study found good comparison with De Wit (1995) in regards to wave height.

Winterwerp *et al.* (2007) further expanded on Gade (1958) and the two-layer model to predict wave height and attenuation in the Guyana coastal system. Input to the wave damping module considered the extension, thickness, density and viscosity of the fluid mud layer. Their findings were validated by attenuation studies also carried out in a laboratory wave flume and find good agreement. The model predicted significant wave attenuation and the computed changes in wave energy agreed numerically with measurements taken place in Surinam, whereas the decrease in significant wave height agrees with historic observations along the Guyana coast.

The viscous model is rather easy to assume because it involves the least complex rheology and water parameters for performing experimental and modeling studies (Kranenburg, 2008; Kranenburg *et al.*, 2011).

2.2.3.3 Viscous-Elastic Model

The viscous fluid mud model does not address the complexities that mud and sediment have in a natural state. Most researchers assume or predict mud rheology, but this can leave room for error when looking at the mechanisms of wave damping. Within visco-elastic modeling, the muddy bottom layer over which water waves pass is assumed to be a semi-elastic material.

Hsiao and Shemdin (1979) review previous studies like Rosenthal (1978), Yamamoto *et al.* (1978) and look at wave dispersion and dissipation by the interaction of muddy bottoms and water waves. MacPherson (1980) developed a model that looked at the wave attenuation assuming an inviscid fluid (water) propagating over an incompressible visco-elastic muddy bottom. This model accounted for a variety of depths of either the upper or lower layer. MacPherson used the Voigt model to study the mud rheology and to solve the dispersion relationship and wave attenuation. He concluded that the viscosity and elasticity values of mud are extremely important and are related to the attenuation coefficient. Hsiao and Shemdin (1979) assumed the same as MacPherson (1980) but found that the dynamic boundary conditions along the interface between the water and the mud are different.

Maa and Mehta (1990) further expand upon the work of Dalrymple and Liu (1978) by using a multilayer Maxwell visco-elastic model to examine coastal mud responses to waves. The mud bed is layered with a viscoelastic material with constant density, viscosity, and elasticity for simulating energy dissipation. Wave attenuation is found to depend on the degree of bed consolidation and the type of sediment. This model helps to study the shear stress of the bed required for re-suspension rate calculations. There are many other researchers that have also used the Maxwell visoelastic model such as Maa (1986), Rodriguez (2009), Rodriguez and Mehta (2000).

Using a Voigt model like that used by MacPherson (1980), Zhou and Wang (1992) looked at wave attenuation in a two layer fluid system looking at wave decay for different water depths. The results are compared numerically and found to be in good agreement. Piedra-Cueva (1993) also expanded on MacPherson (1980) except he did not consider water as an inviscid fluid. Instead, his study considers the visco-elastic bottom under small amplitude waves showing that the attenuation coefficient is related to the resonance affect. The visco-elastic model is widely used to study these effects of sediment transport and fluidization, which certainly affects wave attenuation as these studies have shown.

The viscoelastic model has been used in many laboratory experiments to investigate the effect of various parameters on damping rate. Lian *et al.* (1999) were interested in mud transport and particularly how it influences the shoaling of waterways. Using a nonlinear viscoelastic model, the mud velocity is found and compared

to flume experimental results to find good agreement (Shibayama *et al.*, 1989). They considered irregular waves and wave-current conditions that had previously not been the focus of experimental study. Zhang and Ng (2006b) also looked at the interaction between surface waves and a viscoelastic muddy bottom, assuming that the mud layer is comparable in thickness with the wave boundary layer and is much smaller than the wavelength. A Stokes boundary layer model determined the mud motions under these waves and the rheological properties of the mud were further studied.

In addition, Zhao *et al.* (2006) expand on the work of the multilayer modeling and initially used numerical modeling to study the interactions between waves, current, mud and turbulence. The equations of mud transport are then found through using a visco-elastic model to study the properties of mud. These results are found to be in good agreement with the experimental results. Their study found new evidence that the rate of wave attenuation increases in the opposing currents and decreases in the following currents. Also, the opposing currents have more significant effects on the rate of wave height attenuation than the following currents and the effect of a current on wave attenuation on a muddy bottom is larger than on a rigid bottom. Finally, the mud transport rate was found to increase in the following currents but decreased in the opposing currents and the rate of wave height attenuation on the mud bottom is greater than on a rigid one.

Moreover, Liu and Chan (2007) looked at the effects of a thin visco-elastic layer on wave propagation to find the damping rate, dispersion relationship with wave

frequency and number as well as the velocity of the water column and mud layer. It was found that attenuation hits a maximum value when the mud layer thickness is about the same as that of the boundary layer, the same as Dalrymple and Liu (1978). Muddy bottom layers are found to be more influential on wave damping and fluidization and creation of the boundary layer. Most studies have assumed or predicted the mud rheology for the purpose of study but these assumed parameters are not necessarily reflective of what occurs naturally. Therefore, there needs to be additional study on the subject, as will be discussed in further detail in following sections.

2.2.3.4 Visco-Plastic Model

Visco-plastic model or Bingham fluid model uses a two-layer model but assumes the fluid bottom layer is a visco-plastic material. For a Bingham-plastic muddy seafloor, the mud moves either like a solid or like a viscous fluid (shear flow) depending on the magnitude of shear stress. Velocities inside these two different flow regimes and the locations of the yield surfaces vary as functions of water-mud interfacial pressure and the properties of the Bingham-plastic mud.

The visco-plastic model, as used by Krone (1963), Tsuruya *et al.* (1986), Otsubo and Muraoka (1988), is employed to study the rheological property measurement to help understand the dynamics of muddy beds. Krone sought to find the stability of sediments during transport to help in understanding shoaling processes. Mei and Liu

(1987) expand on Krone (1963) by studying the Bingham plastic behavior of river mud with a high concentration of sediment. The study looks at wave damping of a solitary wave across a thin layer on both horizontal and sloping mud beds Tsuruya *et al.* (1986).

Later study by Zhang *et al.* (2003) used this two-layer model with a visco-plastic fluid bottom to solve boundary value problems. Results show that the complex non-linear properties of wave attenuation over a muddy bed, such as the wave dissipation rate according to wave height, can be explained within this model.

2.2.3.5 Poro-Elastic Model

The poro-elastic model assumes a certain permeability of the bed, thus affecting energy dissipation of water waves. The attenuation of waves propagating over poro-elastic beds with non-linear Coulomb internal damping is studied in laboratory experiments in Yamamoto (1982b).

Looking at the Mach number, the ratio of the propagation velocity of the water wave to the shear wave velocity, wave damping is found to be small when the Mach number is small and vice versa. Large waves damp out more quickly and small waves damp slower. The shear Mach number is found to be larger in a very soft fluid-like mud. In a later study with Yamamoto and Takahashi (1985) they used a poro-elastic model to look at wave damping by wave-soil interactions quantitatively. They found that the Coulomb friction between soil grains is by far the most important wave

damping mechanism in soft soil beds, for example with clays and silts, finding that large waves damp much quicker than small waves Yamamoto *et al.* (1983). Yamamoto *et al.* (1978) also include the porosity in the bottom layer of there model.

2.2.3.6 Visco-Elastic-Plastic Model

The visco-elastic-plastic modeling is developed basing the fluid mud layer as a viscoelastic fluid and with shear stress in the mud layer exceeding the yield stress Shibayama *et al.* (1990). This study looks at two forms of transport: mud mass transport in the mud layer and suspended mud transport in the water layer. Results of the new numerical model are compared with laboratory results.

Shibayama and An (1993) later used this modeling to help predict the behavior of wave-mud interaction. This rheological model can be considered as a visco-plastic model where the elastic part has been replaced by a viscoelastic state. Considering that the elastic part of the Bingham model, in the upper part of mobile mud, is usually neglected in wave-mud interaction studies, the visco-elastic-plastic model seems to be a better choice that takes into account the behavior of mobile mud at both low and high shear stresses. The shear modulus and viscosity of this study are later calculated for that of Oveisy (2009). The results of the laboratory experiments are in agreement.

2.2.3.7 Additional Models

There are several additional models that have been used to study water-mud interaction such as the electro-viscous model which used by Aijaz and Jenkins (1994) and pseudo-plastic model used by Zhang *et al.* (2003). The theoretical models discussed in the previous sections are critical components to validating field and experimental studies and also for highlighting the array of research devoted to understanding wave-mud interaction with the phenomena of attenuation and the changing in wave characteristics due to propagation over a seabed.

The models discussed for the purpose of this research (elastic, viscous, visco-elastic, poro-elastic, visco-plastic, visco-elastic-plastic) offer unique findings that show variations in damping effects and also emphasize the need for further research regarding subjects such as rheology and sediment transport.

2.3 Additional parameters for study

Additional parameters for understanding the process and contributors to wave damping will be mentioned but not reviewed in depth. Sediment transport, fluidization of mud, shear stress, and bed environment all have a role in attenuation.

2.3.1 Mud mass transport

Mud mass transport under the influences of waves, gravity and suspended sediment in the water layer are the main mechanisms of mud transport in estuaries and coastal regions. Understanding how and why sediment shifts and moves and what can occur during and after this shift is a key component of understanding effects of erosion, bottom layer softening, and liquidation of mud to create a fluid boundary layer (Yamamoto, 1982a; Shibayama *et al.*, 1986; Nagai *et al.*, 1984; Mei and Liu, 1987; Ross and Mehta, 1990; Ng, 2000; Soltanpour *et al.*, 2003; Geyer *et al.*, 2004; Traykovski *et al.*, 2000).

There is a good amount of research on sediment transport. Much of this complements studies on wave attenuation and boundary layer fluidization; however it is important to reiterate relevant research on the subject to give a framework for this projects parameters. The following studies highlights some of the most recent studies on mud mass transport: Oveisy *et al.* (2009), Shibayama *et al.* (1990), Kessel and Kranenburg (1996), Jaramillo *et al.* (2009), Torres-Freyermuth and Hsu (2010), Sheremet *et al.* (2011), Winterwerp *et al.* (2012).

2.3.2 Fluidization of mud

The fluidization of mud is another factor to consider. The fluidization or liquefaction of bottom layer mud is the main proponent in erosion and break down of

coastline. It also contributes to sediment transport and the damping and breaking of water waves passing over top. Two strong studies focusing on the effects of storm interaction with coastal land are Sheremet and Stone (2003) and Traykovski *et al.* (2000) studies. These are primarily river continental shelf projects that study how storms challenged can strongly interact with the bottom and cause a high damping. Sheremet and Stone (2003) found that there is a significant damping of high frequency, short waves. They looked at wave propagation on the Louisiana inner shelf using simultaneous measurements at two shallow water ocean observatory sites. One site was mostly a muddy bottom and the other was mostly sandy bottom. Contrary to the expectation that wave dissipation via mud is only important for long waves that directly interact with the bottom, their study showed significant damping of high frequency short waves. Their numerical simulations showed that other factors such as refraction or depth did not account for the scale of the observed effects. Sediment re-working during storms suggests that these effects are related to sediment re-suspension processes.

Traykovski *et al.* (2000) found that during periods of low-concentration suspended sediment transport, when there is no fluid mud layer present, there was either erosion or no change in bottom elevation. What both studies found was that the sediment particles of the muddy bottoms began to separate under intense pressure from the storms, thus creating a liquid mud bottom layer that interacted with the overlying fluid layer and creating the greatest damping values. Also, more useful studies have

looked at the mechanism of erosion and the creation of fluid mud: Maa and Mehta (1987), Mallik *et al.* (1988), Ross and Mehta (1990), Liu and Mei (1990), Feng *et al.* (1992), De Wit (1995), Kineke *et al.* (1996), Bai *et al.* (2002), Kranenburg (2008), Soltanpour and Haghshenas (2009), Chan and Liu (2009).

2.3.3 Shear stress

Shear stress is another factor that affects wave attenuation, the rate of erosion and mud liquefaction, as well as the overall movement of water waves. As with sediment transport, stress is often a complimentary finding to wave attenuation (since the two are related) as well as with rheological properties, water movement and other characteristics of interest for marine studies. The following is a collective of the relevant studies that highlight shear stress: Mallard and Dalrymple (1977), Dawson (1978), Thimakorn (1980), Maa and Mehta (1987), Maa and Mehta (1990), Mimura (1993), Liu and Mei (1993b), Liu and Mei (1993a), Chou *et al.* (1993), Jiang and Watanabe (1995), Jiang and Watanabe (1997), Safak *et al.* (2010), Mei *et al.* (2010).

2.3.4 Bed environments

The understanding of bottom layer, bed environments, mainly the underwater vegetation, is another aspect of wave-bottom layer interaction that plays a role in aforementioned affects such as wave attenuation, sediment transport, and wave mo-

tion. The presence of vegetation, despite the density and porosity of the bed, must be understood as another parameter though less focus has been given to such research. Some studies in the past decade have given attention to wave damping as waves propagate over various vegetation and have found that vegetation generates unique pressured currents (Augustin *et al.*, 2012; Ma *et al.*, 2012).

Other studies have found that wave attenuation decreases when passing over vegetation, but there is still a lack of understanding of vegetation-flow interaction and sedimentation transportation (Ogus *et al.*, 2013; Kim and Lee, 2013). Some studies have found that at the edges of the vegetation beds, energy transfer in spectral wave velocities goes from long to short wave periods and that the vegetation actually attenuates longer waves (Koftis *et al.*, 2013; Tang *et al.*, 2013).

Looking at the previous literature and research projects conducted regarding the interaction between water waves and mud and the many physical characteristics that are attributed to and a result of their interaction, this study will build off of this theoretical and experimental framework to address the issues that will be raised in the following sections. It is evident that there is significant study on wave and mud properties, the interaction between water and mud, and the primary causes of attenuation; however there is a need for further study on several of the aforementioned aspects.

2.4 Discussion

Studies prove that waves propagating over a muddy bottom layer will dissipate energy and will cause the wave to attenuate. While some factors such as bed viscousity and water depth are more crucial to attenuation, other factors play a small role. What can be determined from this extensive review of relevant studies and literature is that knowledge of mud properties is the most significant constraint to this research. Inconsistencies in findings and assumptions of characteristics and parameters for study have left gaps. While findings have made great successes in the field of wave attenuation study, there are still many challenges to overcome. By looking at this relationship between fluids and dense viscous deposits underneath, it is observed that there are extreme inconsistencies with wave attenuation coefficients and wave damping trends.

The major general findings when reviewing the research presented are that the damping depends on wave amplitude and wave period also plays a role, as does the consistency of the bottom layer. Studies found that attenuation increases as wave height increases (Yamamoto and Schuckman, 1984; Soltanpour *et al.*, 2010) while others have found that attenuation decreases with wave height increases (Nagai *et al.*, 1984; Sakakiyama and Bijker, 1989). Zhang and Zhao (1999) found both results in their study on wave height and attenuation related to the mud density. While (Tsuruya and Nakano, 1987; Sakakiyama and Bijker, 1989; Zhang and Zhao, 1999) found that wave attenuation increases with wave period until it reaches a critical

peak; then it decreases. They also observed that in some cases, when mud density is low, the wave period could increase ((Jaramillo *et al.*, 2009; Sheremet *et al.*, 2011; Winterwerp *et al.*, 2012). The varying values of the attenuation coefficient are due to the wave interactions with the different levels of mud layer consolidation underneath Nagai *et al.* (1984), Yamamoto and Schuckman (1984).

In addressing the relationship between mud density and wave attenuation, it is also found that attenuation increases with low-density mud and decreases with hard density mud Nagai *et al.* (1984), Sakakiyama and Bijker (1989). What is clear is that there needs to be further study to identify critical factors and potential outcomes of mud density changes and attenuation of water waves. Many studies find inconsistencies in their research, which is a point that this work attempts to clarify. Basic understanding of rheological properties of mud is fundamental because rheology plays a role in other wave-mud interaction phenomena (Gade, 1958; Soltanpour and Samsami, 2011). Understanding the characteristics of rheological properties is critical because they can completely change how water reacts. Mud properties are very influential and there is a need for further study beyond what has already been done (Krone, 1963; Yamamoto and Schuckman, 1984; Barnes *et al.*, 1989; Shibayama *et al.*, 1990; Shibayama and An, 1993). Further research might look at various aspects uncovered during this study, though moderately explored, such as deep-water damping.

Deep-water wave damping, despite its importance, is rarely studied as a majority

of the previously discussed studies use shallow water and coastal waters for their research. However the importance of understanding the mechanisms of deep-water wave damping are of interest for offshore commercial interests. What is known is that the level of damping depends on the depth of the water; high damping is a result of a lower water depth and lower damping is the result of a higher depth of water. We know that an individual wave train does not feel the bottom but Sheremet and Stone (2003) observed that short waves were damped in deep water. This issue will be further explored in the following chapters to add clarity to the research and present new findings that inspire further research on the subject.

Chapter 3

The Laboratory Experiments of Monochromatic Wave Attenuation by Muddy Bottom

3.1 Introduction

The attenuation of waves propagating over a kaolinite mud has been examined by conducting a series of monochromatic wave tank experiments in intermediate water depth. Various test conditions included different wave periods, incident wave heights, water depth, and mud history. Results show a variety of attenuation coefficient values.

Observations shows that wave damping can both increase and decrease with wave height depending on wave period. Additional tests have been performed in shallow

water conditions, yielding high attenuation coefficients. Results shows mud rheology is a significant variable that contributes in understanding the wave attenuation value. With a better understanding of the behavior of mud properties and mud transport, there will be a clearer vision about the attenuation value.

3.1.1 Schematic description

Consider a two layer fluid system with an upper layer of water with a density, viscosity and thickness of (ρ_1, ν_1 and d_1), respectively, and a lower layer of mud (ρ_2, ν_2 and d_2). The total depth of the system is $h = d_1 + d_2$. Figure 3.1 is a definition sketch for the two-layer water-mud system.

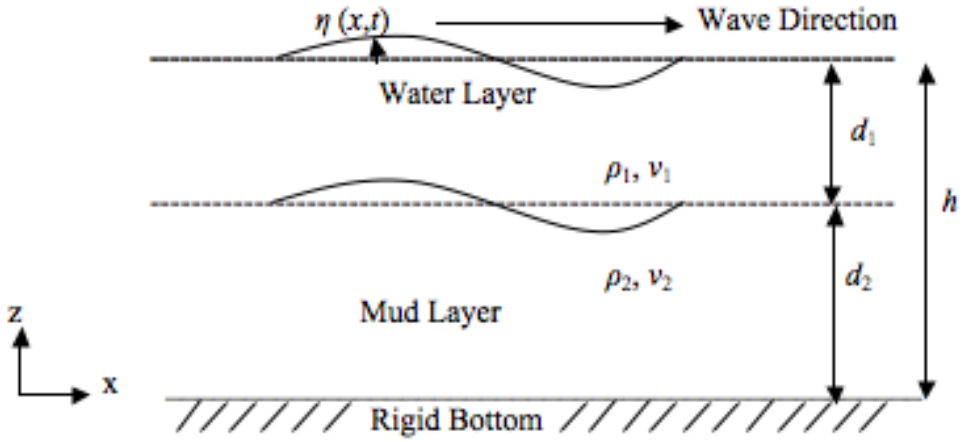

Figure 3.1: Schematic description of water-mud system.

CHAPTER 3. THE LABORATORY EXPERIMENTS OF MONOCHROMATIC WAVE ATTENUATION BY MUDDY BOTTOM

The water surface displacement is described by:

$$\eta = a\cos(kx - \sigma t) \tag{3.1}$$

where η is the surface elevation, a is the wave amplitude, k is the complex wave number, x is horizontal distance in the direction of wave propagation, σ is the wave angular frequency and t is time. Separating the two parts of the complex wave number, $(k = k_r + ik_i)$ the linear wave system expression becomes

$$\eta = ae^{-k_i x}\cos(k_r x - \sigma t) \tag{3.2}$$

The imaginary component of the wave number, k_i, describes exponential decay of the amplitude and defines the damping of the system. If we assume our schematic system consist of only water layer with solid bottom (no mud), the dispersion relationship can be obtained by the linear wave theory (Dean and Dalrymple, 1991) as

$$\sigma^2 = gk\tanh(kh) \tag{3.3}$$

where $\sigma = 2\pi/T$ and $k = 2\pi/L$. Equation (3.3) says that the L (wave length) or k (wave number) can be determined from T (wave period) and h (water depth). In two layer water mud system, the dispersion relationship is different than the one layer system due to the presence of the mud. Various theoretical models derived the dispersion relationship and they are vary depending on the behavior of bottom layer material: viscous (Gade, 1958; Dalrymple and Liu, 1978; Ng, 2000), visco-elastic (MacPherson, 1980; Rodriguez, 2009), poro-elastic (Yamamoto and Takahashi, 1985), elastic (Mallard and Dalrymple, 1977).

3.2 Experimental methods

In this study, a large wave flume was used to generate waves over a bottom layer of mud. The goal of this study is to look at the effect of the wave characteristics such as wave period, wave amplitude and history of the mud on the wave attenuation.

3.2.1 Test facilities

All experiments were performed at the Coastal Engineering Laboratory at Johns Hopkins University. The laboratory wave tank measures 18.3 m long by 2.5 m wide with walls measuring 1.8 m high (see Figure 3.2). About 6 m of each of the sidewalls is made of clear glass paneling to allow for clear viewing of the test area.

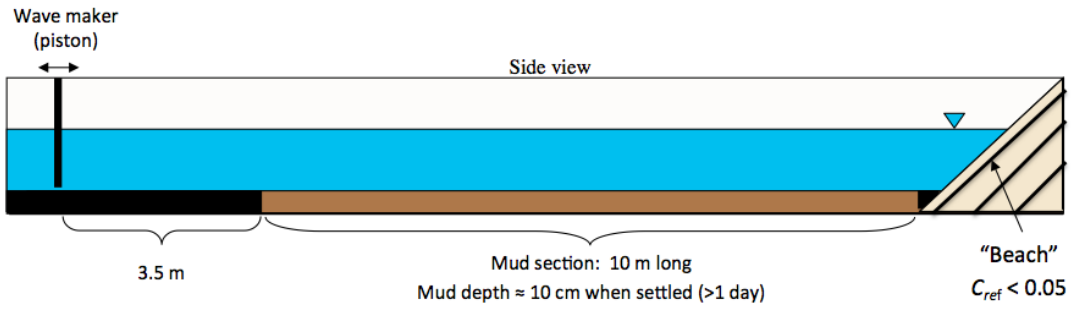

Figure 3.2: Side view of the Johns Hopkins University laboratory wave tank with length = 18.3 m, width = 2.5 m and depth = 1.8 m. Also shown is the false bottom and mud section that is 10 m long and about 12 cm of mud height.

The tank has a piston-style wavemaker with four individual flat paddles that moved in unison to generate waves. The pistons are driven by a hydraulic pump and their positions are measured by using four Linear Variable Differential Trans-

formers (LVDT) displacement sensors. The motion of the wavemaker is controlled by a computer program written by Varjola Nelko with National Instruments (NI) LabVIEW software package through a Proportional Integral Derivative (PID) feedback algorithm.

The program minimizes the difference between the desired paddle position and the measured (see Figure 3.3). Wave reflection from the "beach" with a slope 1:15 (opposite from the wavemaker) is about 5% comprised of several layers of Flex Matala filter material packed in four stainless steel cages to avoid reflection (see figure 3.4). A ramp is installed in the tank beginning from the wavemaker and extending to the mud section to hold the mud in place. There is a 10 m long test section, which is slightly recessed (12 cm) and holds a layer of mud (see figure 3.5). Wave measurements were performed using two sets of gages: eight acoustic gages (Senix TS-30S) and six capacitance gages (Akamina AWP). These gages were used to sample the surface elevation at 100 Hz (see figure 3.6). The sensors were aligned along the centerline of the tank over the test section (see Table 3.1).

Capacitance gages, although generally more accurate than acoustic gages, have additional difficulties in muddy water. Clay particles, which have polarity, tend be attracted to the electrical field that is created by the capacitance probe.

For monochromatic waves of constant amplitude this results in clay particles collecting on the surface of the probe around the peak height of the wave that causes a slight clipping of the signal (see Figure 3.7). Dr. Eric Maxeiner figure out a so-

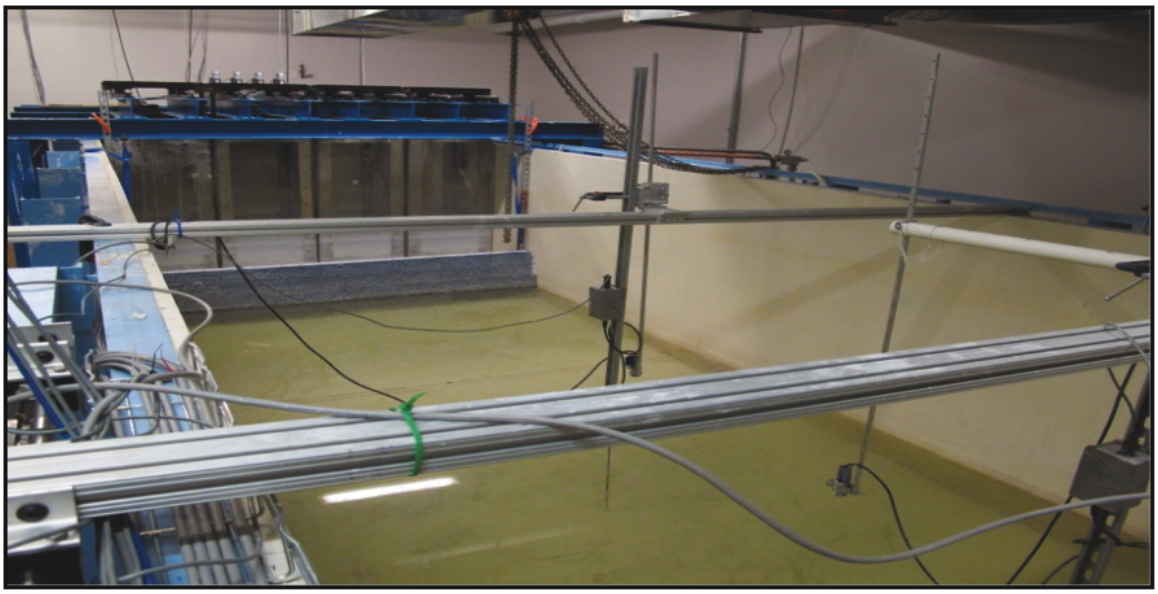

Figure 3.3: The wavemaker with four individual flat panels to create directional waves and the cross bars that hold the sensors.

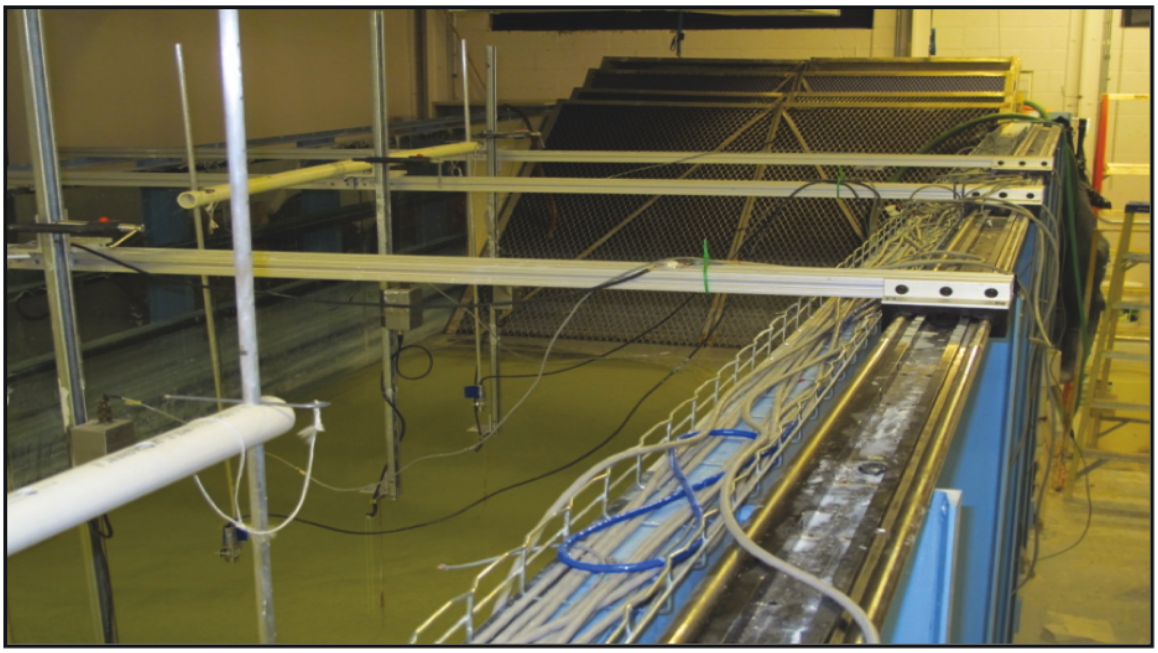

Figure 3.4: The wave tank, beach end with the cages layers with wave absorbing material.

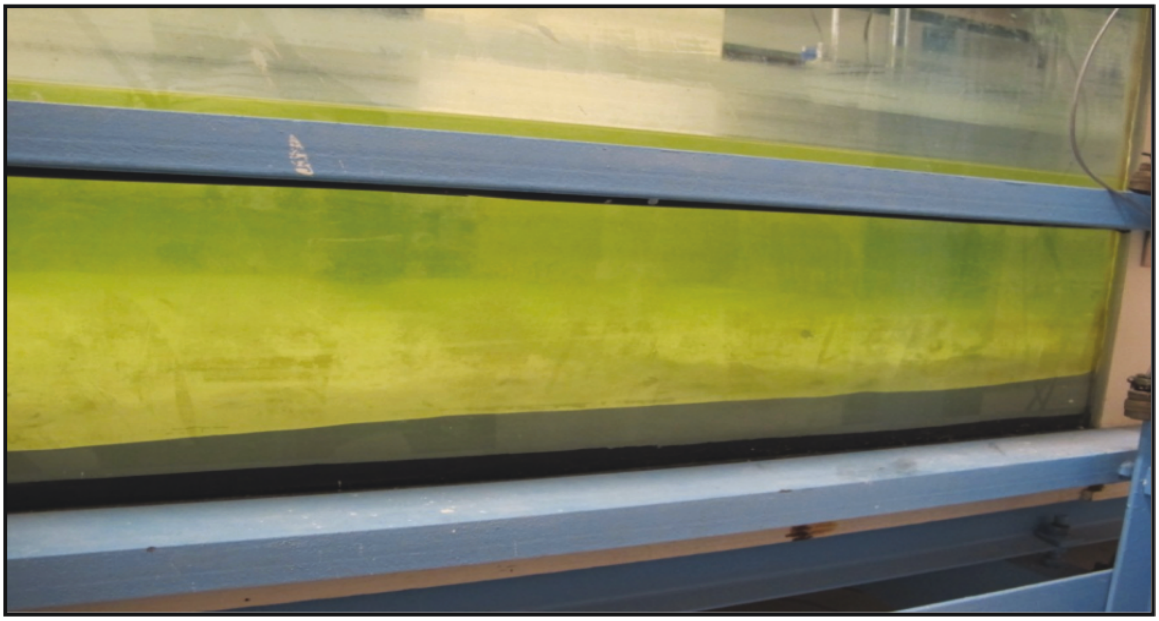

Figure 3.5: The tank bottom has a 10 m long test section filled with clay and the top layer is water.

lution to reduced the clipping of the signals to a reasonable amount by cleaning the probes off with fresh water (using a spray bottle) before each run. The amount of clipping appeared to be largely independent of wave height and was the same for all six capacitance probes.

3.2.2 Mud preparation

The mud for this study is a mixture of water and pulverized kaolinite clay that is produced by Edgar Minerals, INC. The mud thickness and density are variable depending on how consolidated the mud is and the amount of mud in the test area. Mud consolidates over time and, if allowed to settle for too long, becomes so consolidated that it acts as a solid boundary and does not interact significantly with the surface

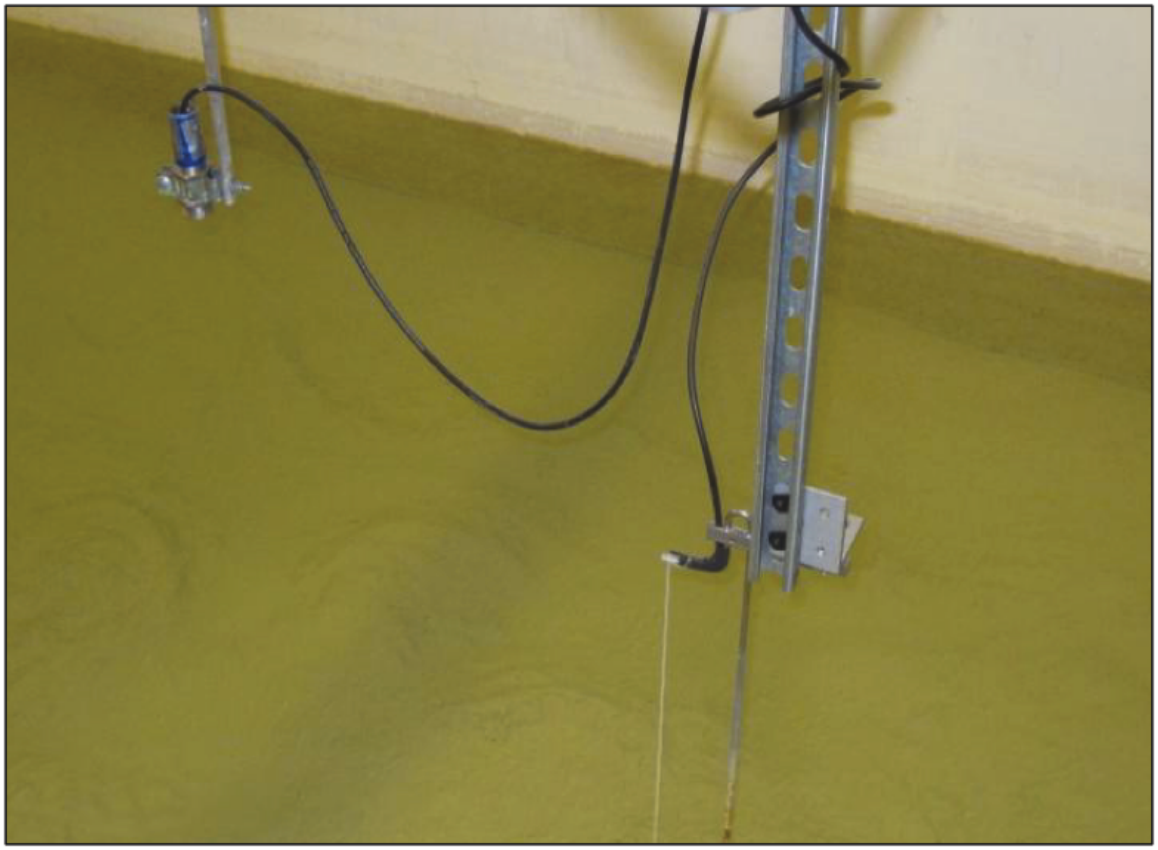

Figure 3.6: The Senix and the AWP sensors which are aligned along the centerline of the tank and used to sample water surface elevation at 100 Hz.

waves. If the mud layer is fully mixed into the water column and does not have a significantly different density than the overlying water, then it does not behave as a distinct layer and the wave attenuation is very small.

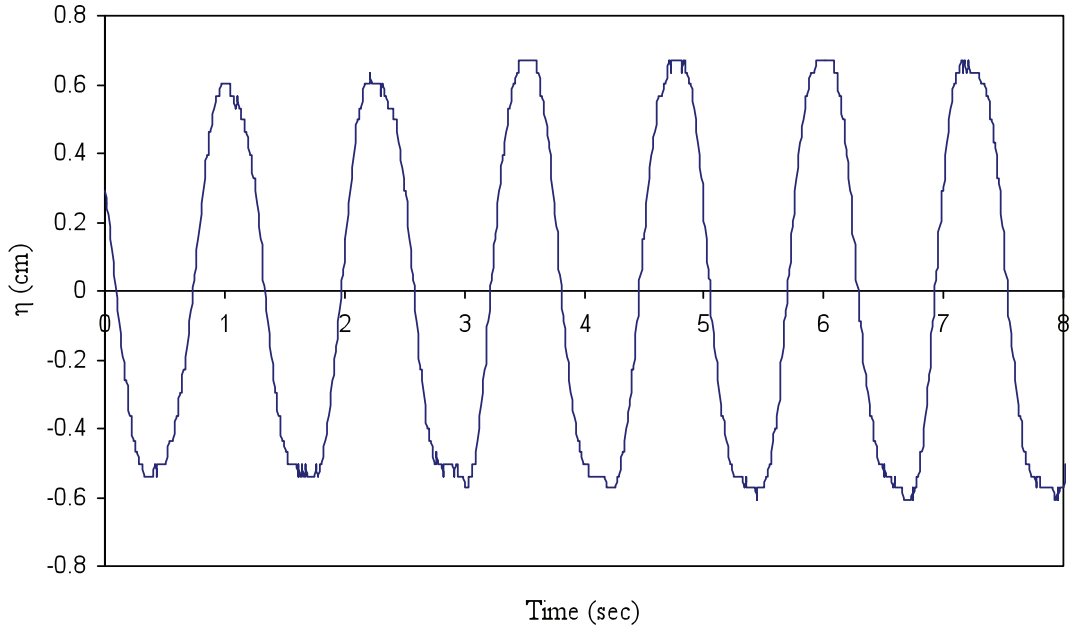

Figure 3.7: Observed clipping of the wave crests in the AWP sensor#4 for the test that taken in 07/18/2011 with wave period T= 1.24 s and water depth h= 0.44 m.

3.3 Calibration coefficient and sensor location

All data file are initially saved in LabVIEW Measurement (.lvm) format and then are converted to the text format (.txt). The format of the file name is presented as (YYMMDD_S#_T#_run#.txt). For instance, the file (110720_S1_T0p95_run1.txt) means that this test has been taken on July, 20th 2011 with a wavemaker stoke equal to one cm, the wave period is equal to 0.95 s and it was the first run for this test. The data file consists of several columns. The first column is the time in seconds for the test, the next columns are the reading for each sensor in volts and the frequency

(f) is equal to 100 Hz. For each run, there should be two data file for the Senix and AWP sensors. In order to calculate the water surface elevation (η) in centimeters, the reading in voltage (V) should be multiplied by a calibration coefficient.

3.3.1 Calibration coefficient

For each test, the sensors were calibrated outside the tank by using a traverse and water filled container. For seven different water levels, a reading in voltage (V) is measured. The calibration coefficient (cm/volt) will be the slope of the straight line of the graph of the voltage (V) and the water levels (see Figure 3.8). For example, the equation for the fitted line is 3.315x - 9.9681 and the regression coefficient R^2 = 0.9999, showing a linear relation between the voltage and water level. Table 3.1 shows the calibration coefficient for the different Senix and AWP gages. The sensors were calibrated before and during a test several times and the calibration coefficients did not show any significant changes.

3.3.2 Sensor location

The two types of sensors are located at fixed positions from the wavemaker. For each, sensor calibration coefficients were obtained (see Table 3.1).

Table 3.1: Sensor location and calibration coefficient for eight Senix gages and the six AWP gages.

Gage	Senix			AWP		
No. #	Distance from wavemaker (cm)	Calibration Coefficient (cm/volt)	Offset	Distance from wavemaker (cm)	Calibration Coefficient (cm/volt)	Offset
1	382	-2.5	9.949	373	3.407	9.979
2	500	-2.5	9.969	554	3.770	9.983
3	654	-2.5	9.985	707	3.402	9.987
4	805	-2.5	9.983	861	3.388	9.985
5	805	-2.5	9.996	1003	3.382	9.959
6	867	-2.5	9.977	1092	3.315	9.968
7	953	-2.5	9.989	—	—	
8	1097	-2.5	9.996	—	—	

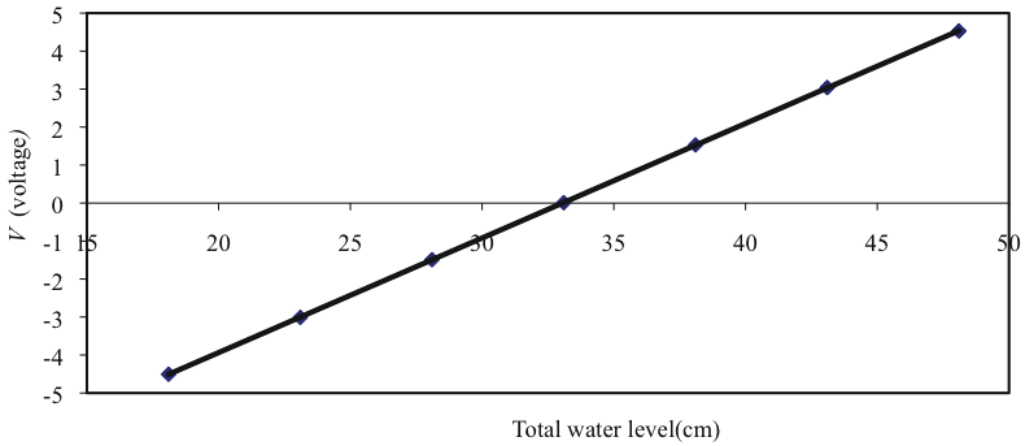

Figure 3.8: The calibration coefficient (cm/volt) for the AWP sensor#6 is the slope of the straight line depicting voltage versus total water level. Calibration coefficient is 3.315 cm/volt for this gage.

3.4 Water surface elevation

The water surface elevation (η) for each sensor was calculated by multiplying all the data that was measured from the sensors by the calibration coefficient that was calculated in section 3.3.2. Figures 3.9 and 3.10 show the results of the water surface elevation for all gages from experiment (110709_S2_T1p24_run1.txt). The eight Senix gages are designated with an S and the six AWP gages are designated with an A. For example, sensor number 2 for the Senix gages is designated with an S2 and sensor number 4 at location 861 cm from the wave paddle for the AWP gages is designated with an A4.

The measured water surface elevations (η) for all sensors are converted to the wave heights (H) for each individual waves by using the zero-upcrossing method that was described in Whitford *et al.* (2001). For each individual wave, the maximum wave

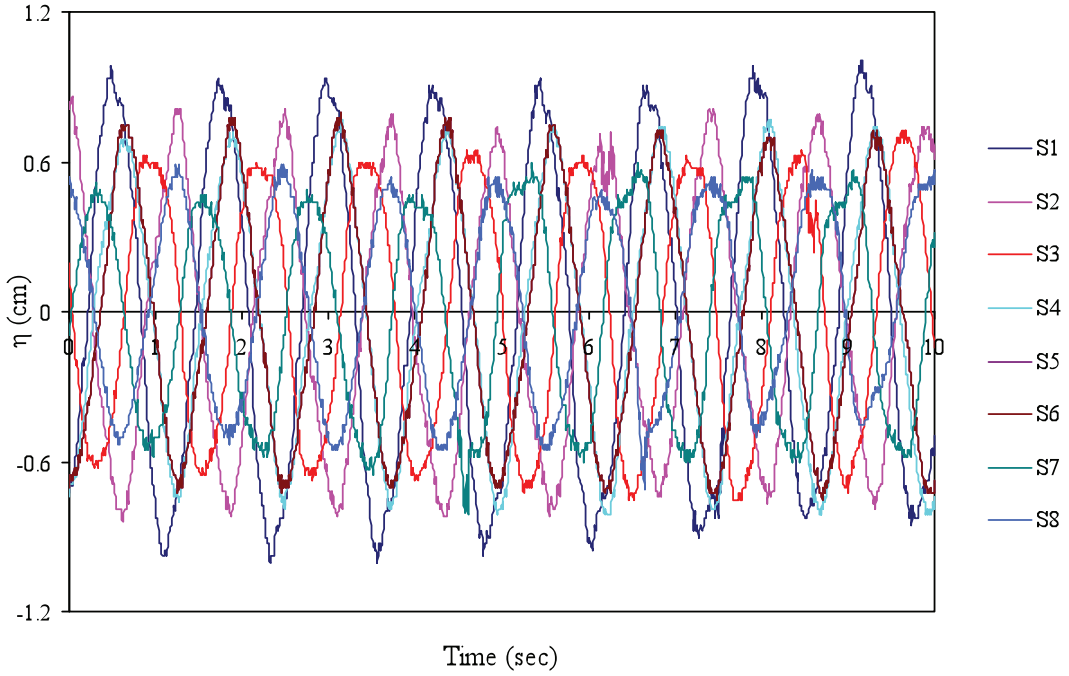

Figure 3.9: A sample of measured water surface elevation versus time for all Senix sensors in an experiment that has been taken in 07/19/2011 with wave period T= 1.24 s. The damping of the waves results in smaller heights.

crest minus the maximum wave trough will be defined as the wave height for a given wave period (T). The average of all wave heights of the total of the individual wave divided by two, which yields the wave amplitude (a) for each sensor.

3.5 Analysis

Tests were conducted for different wave frequencies, wave periods and wave heights. For each test condition, the wave attenuation coefficient was measured by using the least squares method. The wave attenuation coefficient was taken by fitting an expo-

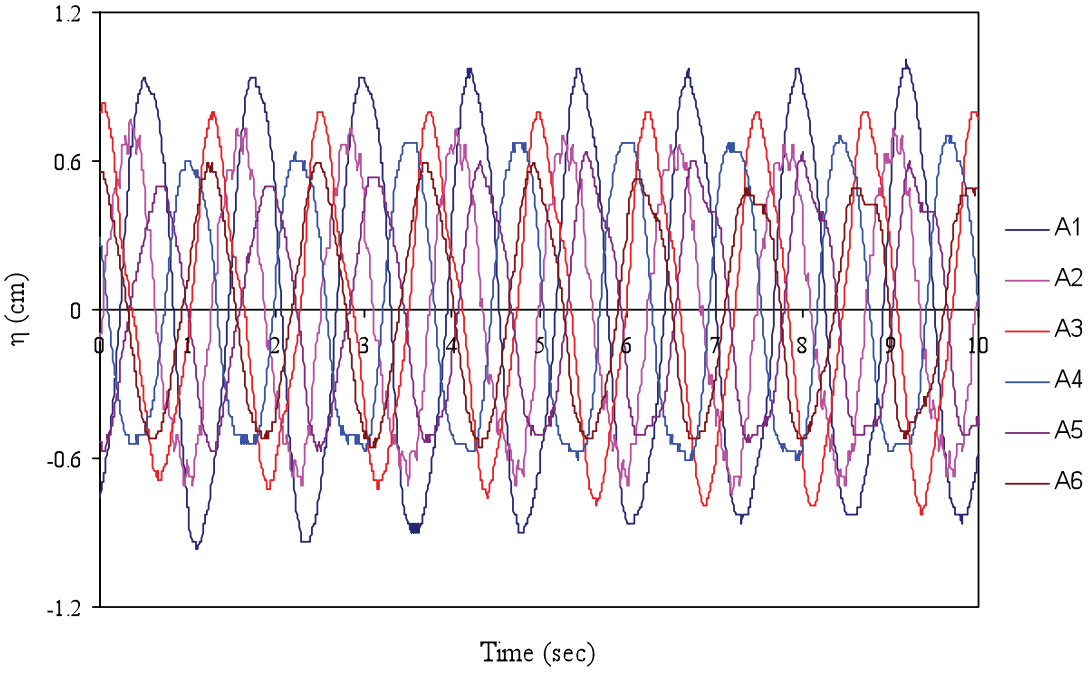

Figure 3.10: A sample of measured water surface elevation versus time for all AWP sensors in an experiment that has been taken in 07/19/2011 with wave period T= 1.24 s. The damping of the waves results in smaller heights.

nential curve to measure the average wave amplitude versus distance (x_i, i= 1,2,..,8) and calculating the exponential coefficient and the average of three repetitive tests. The distance (x) was the distance between the sensor locations and the wavemaker. The time duration for each test was two minutes for each test. The wave attenuation coefficient k_i (m^{-1}) is defined by the equation:

$$H(x) = H_0 e^{-k_i x} \tag{3.4}$$

where H_o is the wave height at x=0, and $H(x)$ is the wave height at any propagation distance x. Figure 3.11 (plotted logH vs x) represent attenuation coefficients calcu-

lated from an experiment that has been taken in 07/14/2011 with same wave period, water depth and varying the stroke.

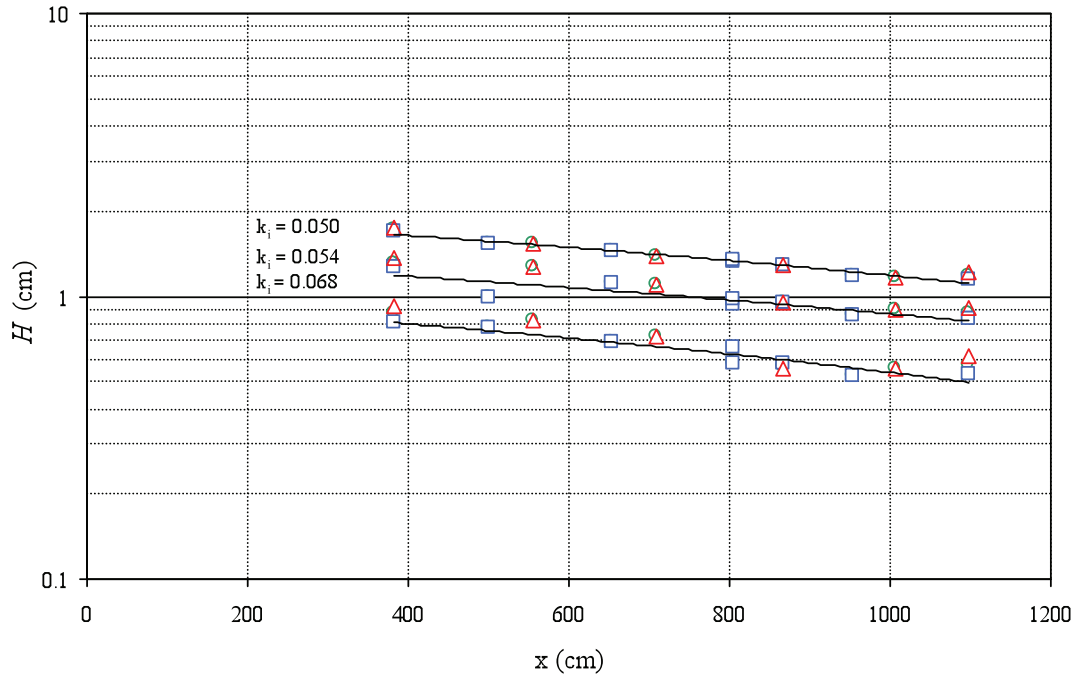

Figure 3.11: Attenuation coefficients as a function of wave amplitude for various tests that have been taken on 07/14/2011 for wave period T= 1 s and water depth h= 0.44 m. (H) for the AWP and Senix combined sensors (○); (H) for the Senix sensors (□); (H) for AWP sensors (△)). k_{i1} when stroke = 1.2, k_{i2} when stroke = 1.6 and k_{i3} when stroke = 0.8.

3.6 Experimental data

The first experiments in the study did not produce a damping value, which lead to questions about the nature of the damping. Yamamoto *et al.* (1986) first concluded that damping occurs at a greater rate in softer mud, which was followed by Sheremet

and Stones experiment on the interaction of water with a porous and weaker bottom layer that was the result of a shifting of the bottom layer sediment. After review of the Sheremet and Stone (2003) and Traykovski *et al.* (2000) research, it became apparent that, in the field after the mud was stirred by storms, damping was much more noticeable. Moreover, Dalrymple and Liu (1978) who studied the interaction of water and mud and developed the visous fluid model reported that the maximum attenuation coefficient would occur when the thickness of mud layer and the water layer are 50% .

This led our team to realize that we must physically stir the mud in order to reproduce this same type of storm effect. The wave attenuation coefficient was first identified in testing on February 2011. Before that, tests over consolidated sediments revealed relatively low attenuation coefficients. For each test condition such as the wave period, water depth, and wave amplitude, there are different attenuation coefficients. There are 256 experiments between 2/4/2011-08/04/2011 at the Johns Hopkins University Coastal Engineering Laboratory carried out by Dr. Eric Maxeiner and later by the current author. Appendix A presents the wave attenuation coefficient for all the experimental tests that were taken by Eric Maxeiner and Nourah Almashan. Most of the tests were in intermediate water and the results shows high wave attenuation coefficient (see Figure 3.12).

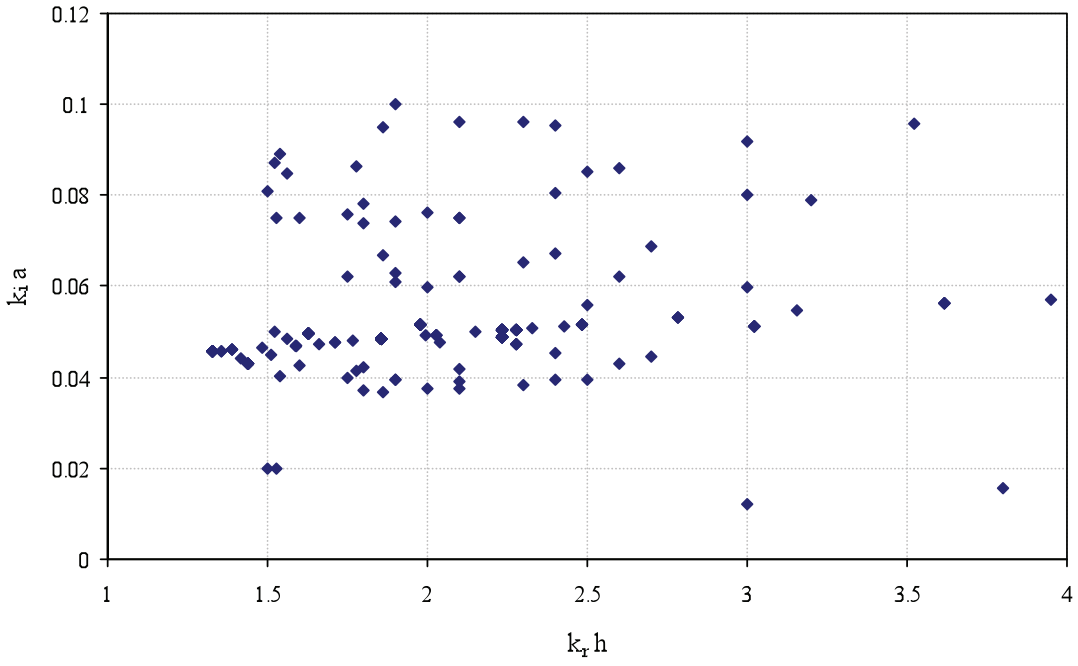

Figure 3.12: The normalized wave amplitude ka versus the normalized water depth $k_r h$ for some of the experiments that have been taken in Johns Hopkins Coastal Engineering Laboratory, showing the vary of parameters studied.

3.7 Results and discussion

Four parameters were used as independent variables: wave frequency, wave amplitude (initial/undamped), total water depth and mud layer thickness. Wave periods were generally between 0.7 and 2 seconds, which equates to sampling 60 to 170 waves. Significant wave attenuation was observed for a variety of test cases (see Figure 3.13). All wave attenuation coefficients were plotted for the 256 experiments. For most conditions, the damping coefficient was between 0.01 and 0.06 m^{-1}. The plots are grouped to see the effect of the wave attenuation coefficient on varying test conditions.

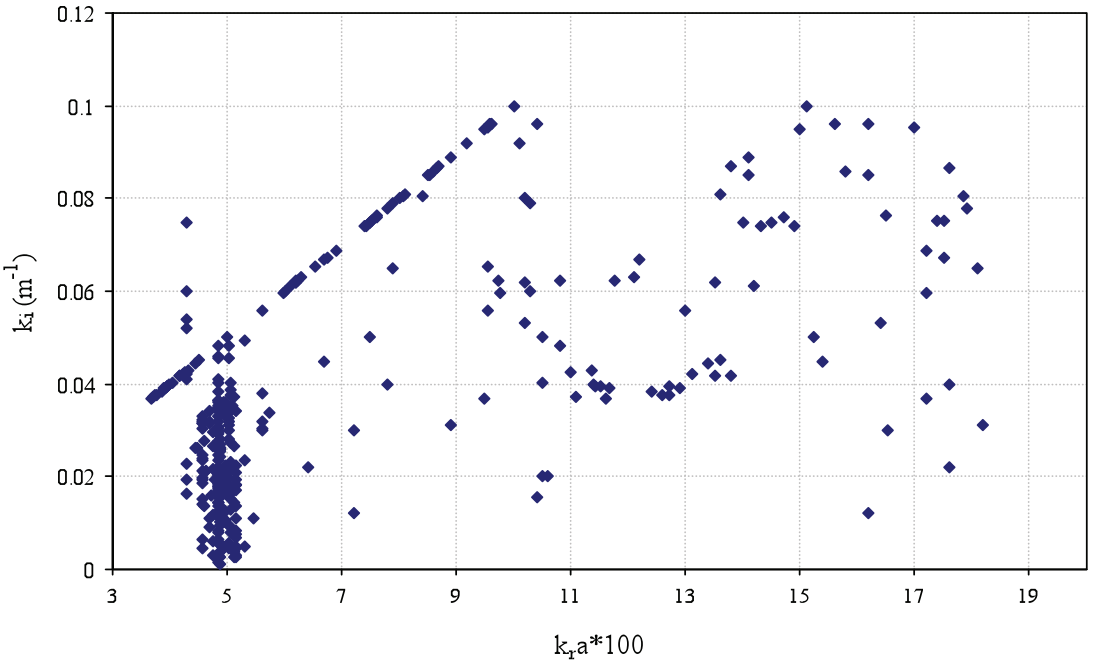

Figure 3.13: Wave attenuation coefficient versus $ka\times100$ for all experiments with water depth of 0.44 m and wave period (T= 0.7- 2.0 s).

3.7.1 Effect of wave amplitude on damping

One area of particular interest in this study is finding the effect of the initial amplitude on the wave attenuation coefficient. This was examined by generating monochromatic wave trains of different amplitude for a given wave period and water depth. 154 tests are plotted and were presented in Figure 3.14 and 3.15, as the measured attenuation coefficients versus initial wave amplitude. The figures show two different results for the wave attenuation. Both tests have the same input parameters (h= 44 cm, d_2= 12, ρ= 1307 kg/m^3) but the wave period (T) is different.

In Figure 3.14, Varying the wave amplitude of a wave period of 0.9 s showed that

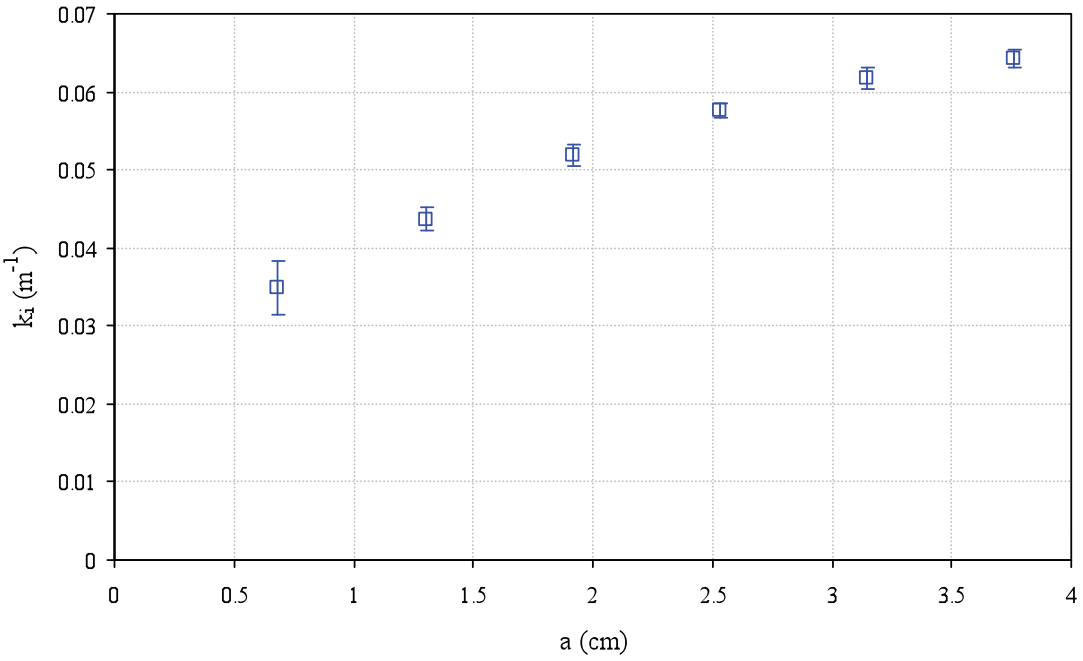

Figure 3.14: The attenuation coefficient versus the wave amplitude for 07/19/2011 tests (h = 0.44 cm, ρ= 1307 kg/m^3, d_2= 12 cm, T= 0.9 s).

wave damping increased with an increase in wave amplitude at water depth of 0.44 m as seen by Yamamoto and Schuckman (1984), and Soltanpour *et al.* (2010), yet with other tests damping decreased while wave amplitude increased (at water depth of 0.44 m and wave period T= 1 s) as seen by Nagai *et al.* (1984), and Sakakiyama and Bijker (1989), see Figure 3.15. Zhang and Zhao (1999) also observed the damping both increased or decreased with increase wave height. They related the relationship between the damping and wave height with mud density. They concluded that when the mud is soft the damping will decrease with increase the wave height and if the mud is dense the damping will increase with increase wave height.

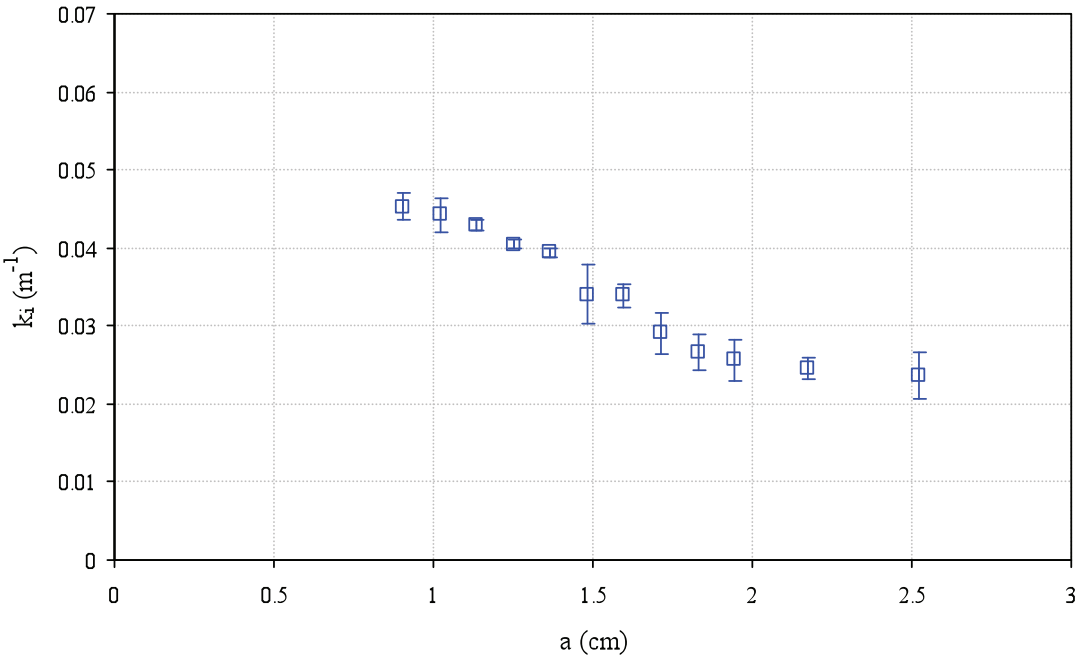

Figure 3.15: The attenuation coefficient versus the wave amplitude for 07/19/2011 tests (h= 0.44 cm, ρ= 1307 kg/m^3, d_2 =12 cm, T =1 s).

Interestingly, we observed in our experiments that the damping increased with either an increase or a decrease in wave height for nearly constant mud densities. We explain our results by looking at the rate of work done in the bottom. From the first law of thermodynamics, the change in internal energy of a system is equal to the heat added to the system minus the work done by the system. In our case there is no heat source add to system and the change of internal energy can be written:

$$\frac{dE}{dt} = -\dot{W} \tag{3.5}$$

where W is the rate of work done by the system. At the same time the change in

internal energy can be written as

$$\frac{dE}{dt} = C_g \frac{dE}{dx} \tag{3.6}$$

where C_g is the group velocity. We also know from linear wave theory that the total average energy per unit surface area is equal to

$$E = \frac{1}{8}\rho g H^2 \tag{3.7}$$

where H is the wave height and g is the acceleration due to gravity. By substituting equation (3.6) into (3.5), we find that the rate of work is proportional to the attenuation coefficient

$$\dot{W} = 2C_g E_i k_i \tag{3.8}$$

This means that, if the rate of work done by the waves is increased, the attenuation coefficient is increased and the opposite is true. So the rate of work is the key to have different results for the wave attenuation. The rate of work in the bottom due to wave pressure is related to the pressure at the bottom and the vertical velocity. The bottom pressure at the bottom and the vertical velocity can be written as:

$$P = |P| \cos(\sigma t + \theta_p) \tag{3.9}$$

$$V = |V| \cos(\sigma t + \theta_v) \tag{3.10}$$

Starting from rate of work equation, the average rate of work over a wave period is

$$\dot{W} = -\frac{1}{T}\int_0^T PV\, dt \tag{3.11}$$

Equation (3.10) can be written as

$$\dot{W} = -\frac{1}{T}\int_0^T |P||V|\cos(\sigma t + \theta_p)\cos(\sigma t + \theta_v)\,dt \tag{3.12}$$

From the equation (3.11), the rate of work depends on the pressure at the bottom (P), the vertical velocity at the bottom (V) and the phase shift between the pressure and vertical velocity. By integrating equation (3.11) and using the trigometric identities, the rate of work is

$$\dot{W} = \frac{|P||V|}{2}\cos(\theta_p - \theta_v) \tag{3.13}$$

which is strongly dependent on the phase difference between pressure and vertical velocity. Using MacPherson visco-elastic model (1980) and by using the viscosity and elasticity parameters of the mud from Nouri (2013), the rate of work and the phase shift difference of pressure and vertical velocity is calculated for two representative wave periods T= 0.9 s and T= 1 s. Figure 3.16 shows the phase shift for the pressure and vertical velocity and Figure 3.17 shows the rate of work for the case of wave period of 0.9 s.

In Figure 3.16, both the phase shift in pressure and vertical velocity are increasing with increasing the wave amplitude and the difference between them is constant. For equation 3.5, the rate of work is increasing with the wave amplitude, see Figure 3.17.

On the other hand, looking at the tests when the wave period (T= 1 s), the damping is decreasing when the wave amplitude is increasing. Figure 3.18 shows the phase shift for the pressure and vertical velocity for the case (T= 1 s).

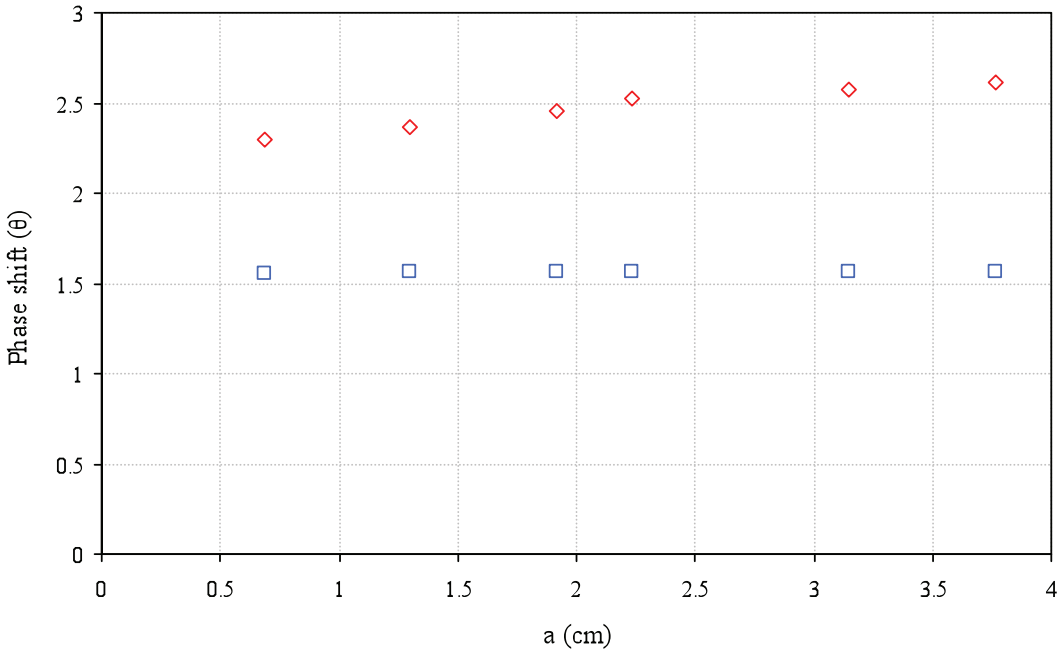

Figure 3.16: The phase shift of the pressure (□) and phase shift of the vertical velocity (◊) for tests (h= 0.44 cm, ρ= 1307 kg/m^3, d_2= 12 cm, T= 0.9 s).

The results shows that when the phase shift of the pressure is in phase with the phase shift of the vertical velocity, the rate of work will increase. Also when the phase shift of the pressure is out of phase with the phase shift of the vertical velocity, the rate of work will decrease and it vary depending on the difference between the phase shift for the pressure and vertical velocity. In the case were the amount of the phase shift of pressure and vertical velocity are equal, the rate of work will be maximum. Figure 3.19 shows the rate of work for T= 1 s.

Comparing the experimental results with MacPherson (1980) viscoelastic model using the viscous and elastic parameters from Nouri (2013) shows a good agreement.

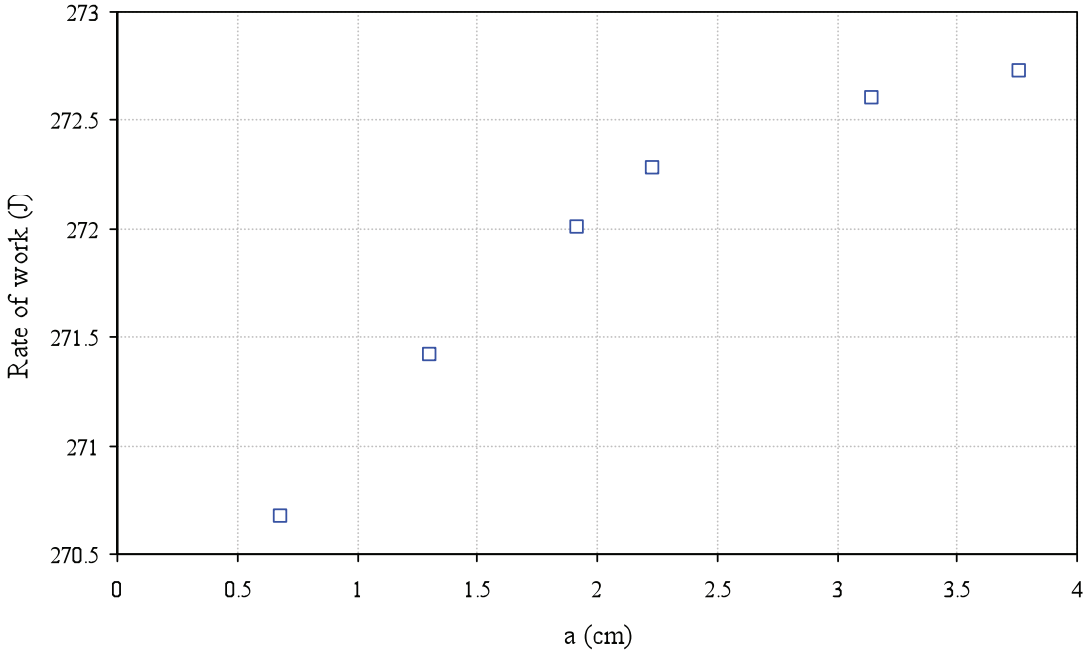

Figure 3.17: The rate of work versus the wave amplitude for tests (h= 0.44 cm, ρ= 1307 kg/m^3, d_2 =12 cm, T= 0.9 s).

We also used the attenuation coefficient experimental data and used the MacPherson (1980) viscoelastic model to predict the mud parameters to get the same attenuation coefficient as the experimental results and are presented as dash line in Figure 3.20–3.21. Figure 3.20 is the results for T=0.9 s and Figure 3.21 is the results for T=1 s .

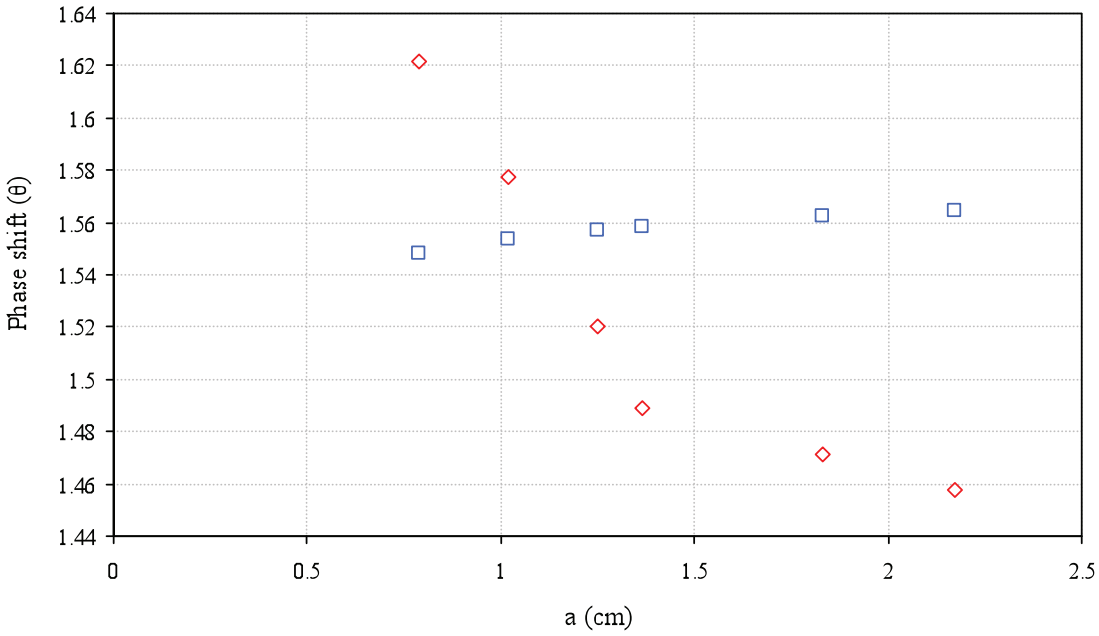

Figure 3.18: The phase shift of the pressure (□) and phase shift of the vertical velocity (◊) for tests (h= 0.44 cm, ρ= 1307 kg/m^3, d_2= 12 cm, T= 1 s).

3.7.2 Effect of wave period and water depth on damping

In this section we examined the effect of wave period on the damping. Previous studies (Tsuruya and Nakano, 1987; Sakakiyama and Bijker, 1989; Zhang and Zhao, 1999; Hsu *et al.*, 2013) among others, show that damping depends on wave period and they observed that the damping increases with increasing wave period until it reach a peak then decreases. To study this relationship, tests were carried out with a fixed water depth and varying wave periods. Tests were run for two minutes and then repeated three times and averaging the results. Testing has shown, for certain

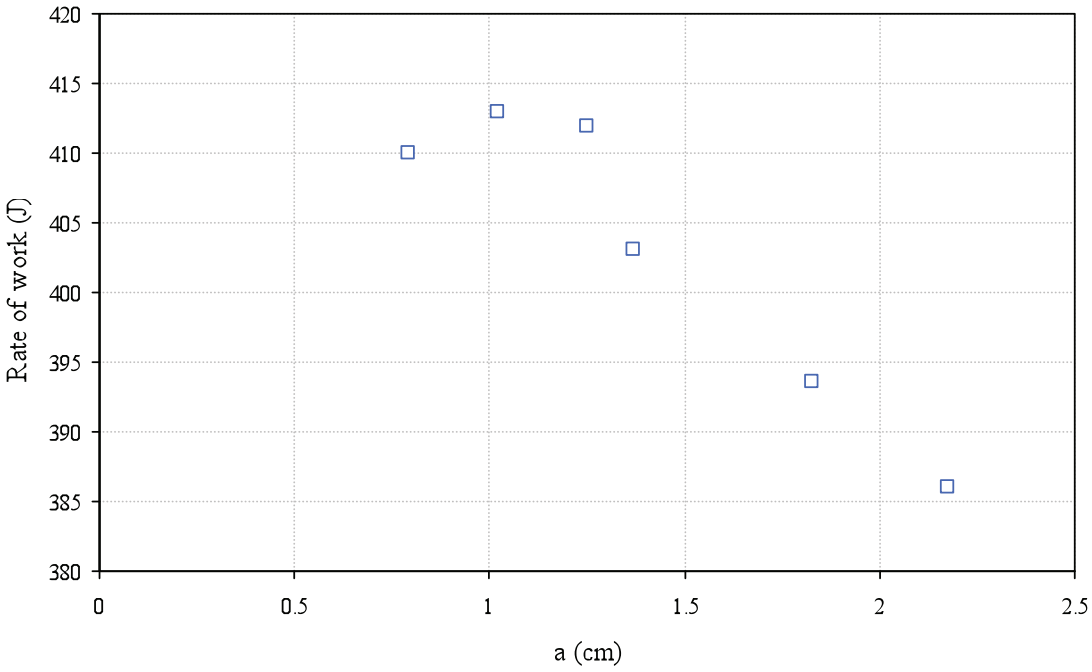

Figure 3.19: The rate of work versus the wave amplitude for tests (h= 0.44 cm, ρ= 1307 kg/m^3, d_2= 12 cm, T= 1 s).

cases, a wide variety of wave attenuation coefficient for a given test conditions. The damping can increase or decrease with wave period. The results of the attenuation coefficient are shown in Figures 3.22 for different wave periods.

Figure 3.22 shows all experiments that have been taken on 06/23/2012 with water depth 0.40 m and mud depth 0.12 m , 06/23/2012 with stroke 2 cm, water depth 0.44 m and mud depth 0.12 m. Wave periods were chosen (T= 0.7, 0.8, 0.9, 1, 1.2, 1.4, 1.6, 1.8, 2) s. Two different results were observed, the attenuation coefficient increases with increases the wave period for tests that have be taken on 06/23/2012 with water depth 0.40 m. On the other hand, the attenuation coefficient decreases with increases

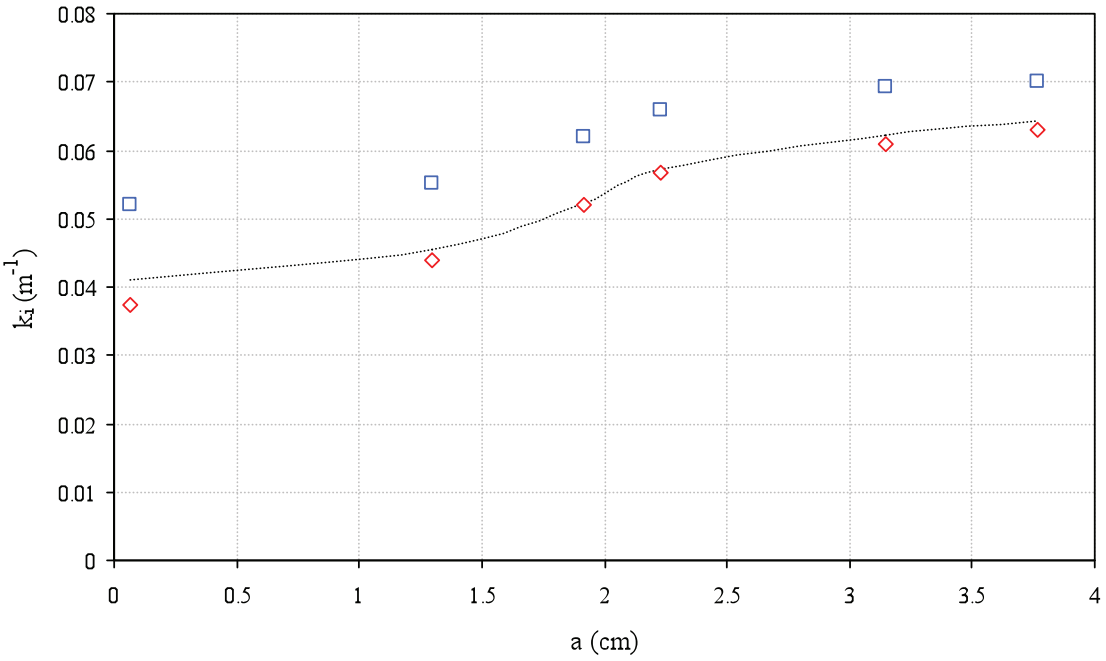

Figure 3.20: The results for tests (h= 0.44 cm, ρ= 1307 kg/m^3, d_2= 12 cm, T= 0.9 s).(□) experimental results.(◊) MacPherson results.(—) predicted mud properties by using (MacPherson, 1980).

the wave period for tests that have be taken on 06/23/2012 with water depth 0.44m. We should piont out the wave amplitude varies in each test and the results are different that what we observed in section 3.7.1. As a result we can conclude that the wave period effect on the wave damping.

These observations are interesting, for the same tests condition and with changing the water depth we found two different results. Again looking at the rate of the work done by the bottom, we use MacPherson's (1980) viscoelastic model and rheology data from Nouri (2013) to calculate the rate of work and the phase difference between the bottom pressure and vertical velocity. The rate of work increased with increase wave

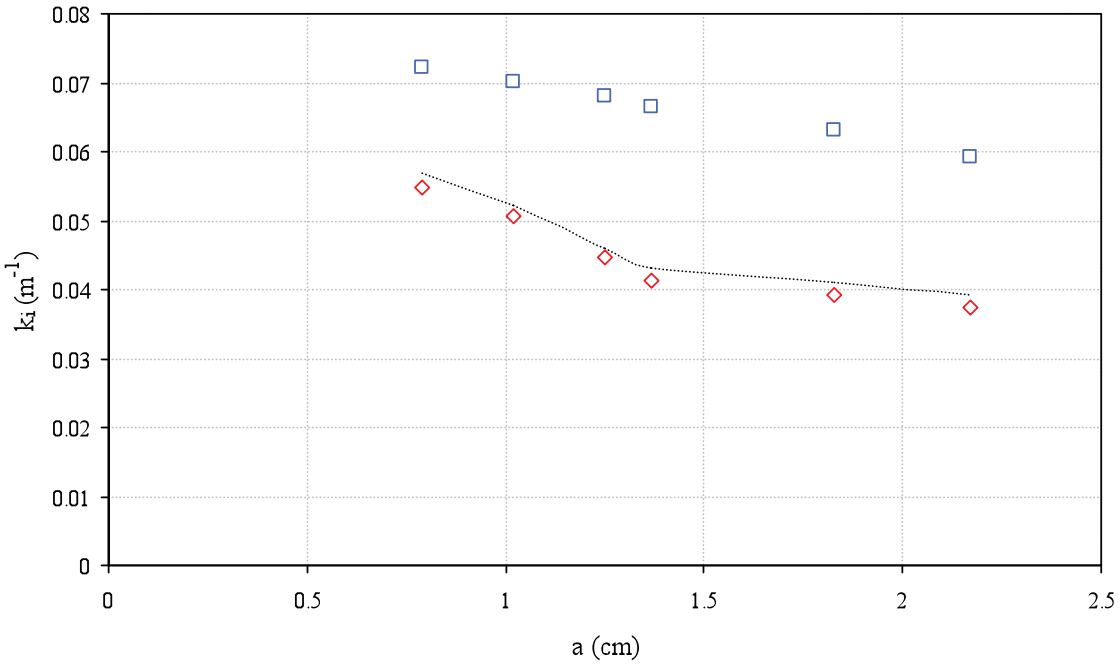

Figure 3.21: The results for tests (h= 0.44 cm, ρ= 1307 kg/m^3, d_2= 12 cm, T= 1 s).(□) experimental results.(◊) MacPherson results.(—) predicted mud properties by using (MacPherson, 1980).

period in the case where the water depth is 0.40 m and decreased with increase in wave period in the case of water depth 0.44 m (Figure 3.23). This was explained by measuring the difference in phase shift between the bottom pressure and the vertical velocity and we found that for the case of water depth 0.4 m the bottom pressure and vertical velocity was in phase which increases the rate of work. The opposite behavior for case where the water depth is 0.44 m, the bottom pressure and vertical velocity was out of phase which decreases the rate of work.

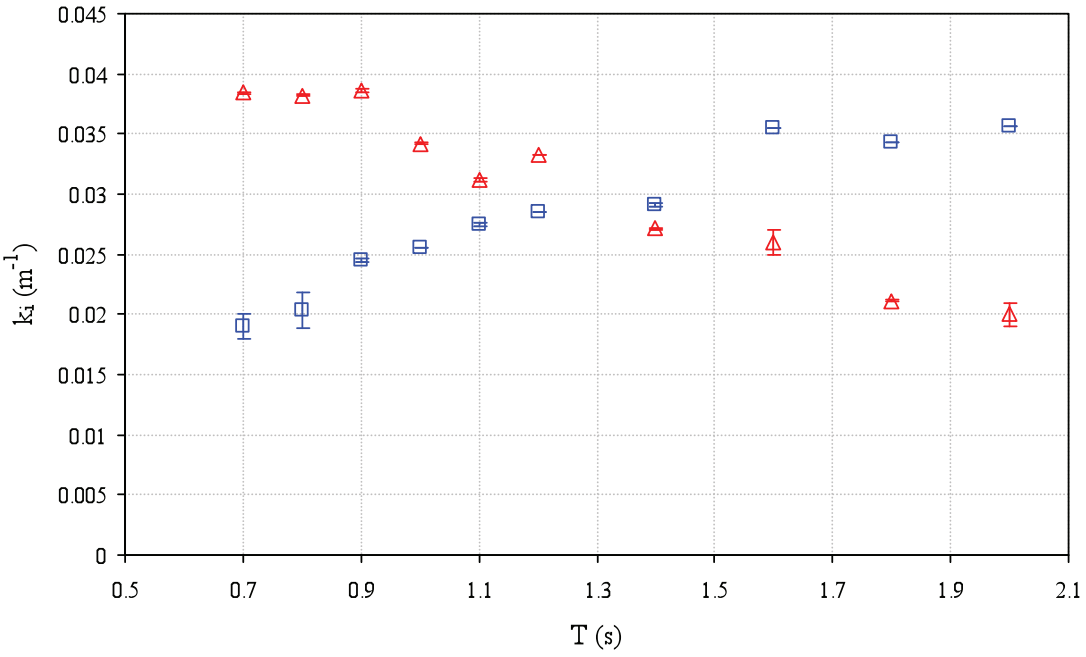

Figure 3.22: Attenuation coefficient versus wave period for all experiments performed on 06/23/2012 with water depth of 0.40 m and 06/23/2012 with a water depth of 0.44 m, mud depth of 0.12 m and varying wave periods (h= 0.40 m (□); h= 0.44 m (△)).

3.7.3 Effect of mud history

Looking at the relationship between damping and mud density, the attenuation coefficient was also tested for the varying mud densities. Sakakiyama and Bijker (1989) measured the attenuation coefficient for different mud densities and wave frequencies. They used water and kaolinite for their tests with fixed test parameters of mud depth at 0.09-0.095 m, fixed water depth at 30 cm, and a wave period from 0.6-2 s. Their conclusions showed that the most dense mud, which has a value of ρ= 1370 kg/m^3, has a smaller wave attenuation coefficient than the softer mud, which has a

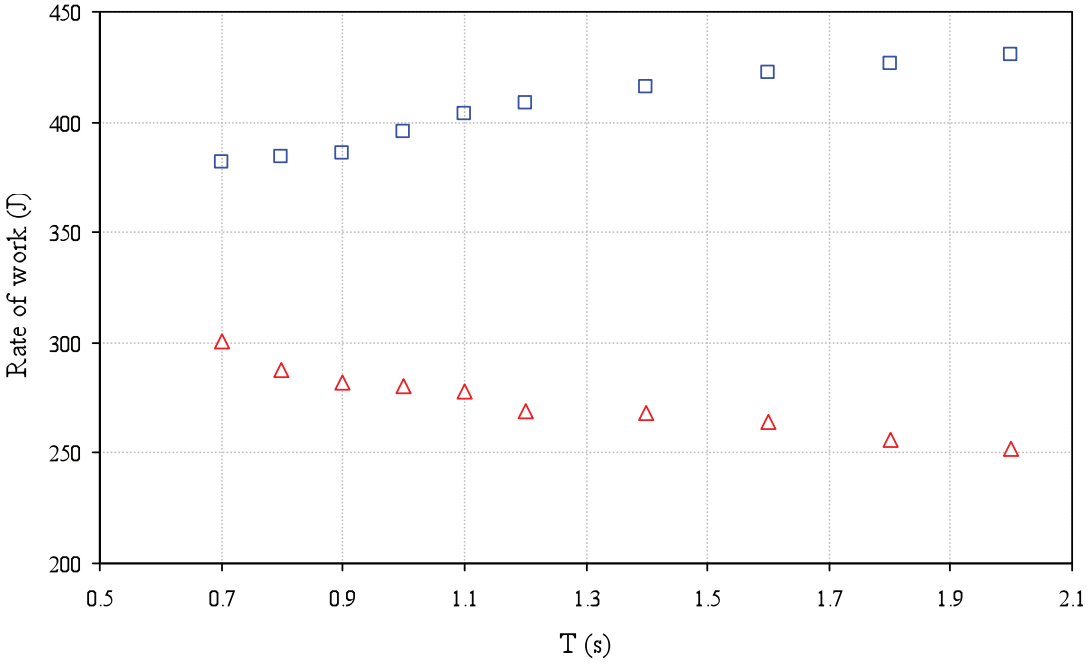

Figure 3.23: The rate of work versus the wave periods for tests taken on 06/23/2012 (ρ=1307 kg/m^3, d_2=12 cm, S=2 cm, h=0.40 m (□) and h=0.44 m (△)).

value of ρ= 1300 kg/m^3.

The objective of our experiments was to compare the damping value with the time since mixing the mud and to measure the damping the mud consolidated. Coussot and Piau (1994) observed that kaolinite-water mixture has time-dependent properties and the kaolinite changed its particle structure during the tests. Also Faas (1985), proved that the fluid mud has time and density dependency. (Maa and Mehta, 1987; Yamamoto and Schuckman, 1984) among others, conclude that the wave attenuation is depending on the mud properties.

To test that relationship we thoroughly mixed the mud for 20 minutes and allowed

the mud to settle for 1 hour. Then we ran the wavemaker with h= 44 cm, S= 2 cm, T= 1 s, for 2 minutes. Then we repeated the test twice more and averaged the resulting damping value for the three runs. Between each run we allowed the tank to settle for 5 minutes. Four hours after the initial mixing, we repeated the above procedure without remixing the mud at all. The results show that the damping value decreased by approximately 20% between the two sets of tests. Twenty-five hours after the initial mixing we repeated the test procedure again without doing any remixing of the mud. The results show the damping value decreased only slightly (10.5%). Finally, 29 hours after the initial mixing we repeated the procedure without remixing and found the damping value increased slightly (1.7%). This entire procedure of mixing and testing over a 29-hour period is repeated 3 times over a time period of 3 continuous weeks.

In all three weeks of testing we found the damping value decreases with time since mixing. While this trend was consistent over the three weeks of testing, the absolute damping values differed from week to week. This is unexpected as we attempted to use an identical procedure prior to testing for each week. It is still possible that human error or the behavior of mud caused the results to vary week to week. We believe that the slightly higher damping value at hour 29 is due to running the wave maker for multiple different tests between the hour 25 tests and the hour 29 tests. This makes sense as the mud is partially remixed by the waves. Figures 3.24 shows the results of the damping value with input data (h= 44 cm, S= 2 cm and T= 1 s)

versus the time of stirring.

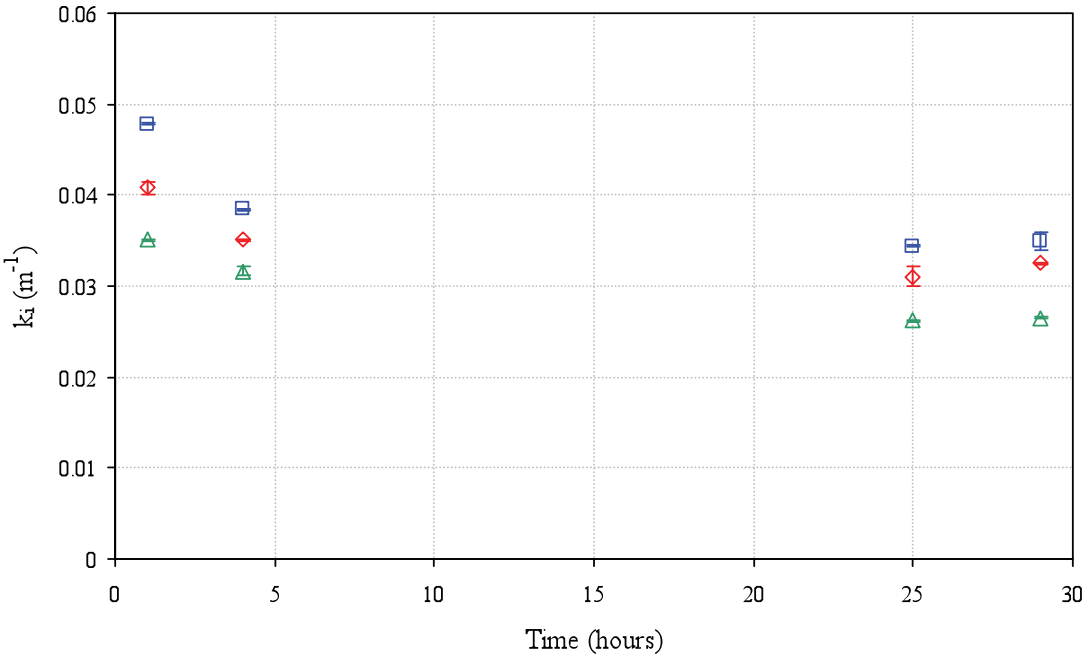

Figure 3.24: Damping value versus time of stir-up the mud with input data (h= 44 cm, S= 2 cm and T= 1 s) for three continuous weeks (08/28/12-08/29/12 ((□), 09/04/12-09/05/12 (◊) and 09/11/12-09/12/12 (△))

.

We also compare the damping value with different wave periods and look at the mud consolidation effects. To do so we fixed h= 44 cm, S= 2 cm, and varied the wave period T= 0.9, T= 1.0, and T= 1.24 s. To test that relationship we thoroughly mixed the mud for 20 minutes and allowed the mud to settle for 1 hour. We ran the wavemaker for 2 minutes with the first wave period (T= 0.9 s). Then we repeated the test twice more and averaged the resulting damping value for the three runs. Between each run we allowed the tank to settle for 5 minutes. Then we changed the

wave period to T= 1.0 s and repeated the procedure.

Finally we repeated the procedure again for T= 1.24 s. We let the mud to settle and then repeated the entire procedure (T= 0.9 s, T= 1.0 s, T= 1.24 s with S= 1 cm and h= 44 cm) at 4 hours, 25 hours, and 29 hours after the initial mixing. Our results displayed in figures 3.25 show the relationship between the wave period and the damping value was consistent throughout. The damping value was greatest at T= 1.0 s. The damping values decreased with time since initial mixing. The damping value decreased significantly between 1 and 4 hours after mixing. The damping value decreased slightly from 4 to 25 hours and then increased slightly from 25 to 29 hours. In Figure 3.25 we can draw two different observations. The first observation was that the damping increased with increasing the wave period and decreased again as found in Nagai *et al.* (1984), Sakakiyama and Bijker (1989), Zhang and Zhao (1999), Hu and Wai (2001), Hsu *et al.* (2013) among others, and this was explained in detailed in the previous sections of the relationship of damping and wave period which related to the rate of work done in the bottom. The second observation shows that after 29 hours the damping slightly increases again which lead us to a question of why does this increase occur.

To answer this question, we did a similar test to look at the relationship between the damping value and the time of mixing but for a longer time. We stirred the mud for 20 minutes at 9 am and ran the wavemaker at 10 am with input data h= 44 cm, S= 2 cm, T= 1 s, for 2 minutes. Then we repeated the test twice more

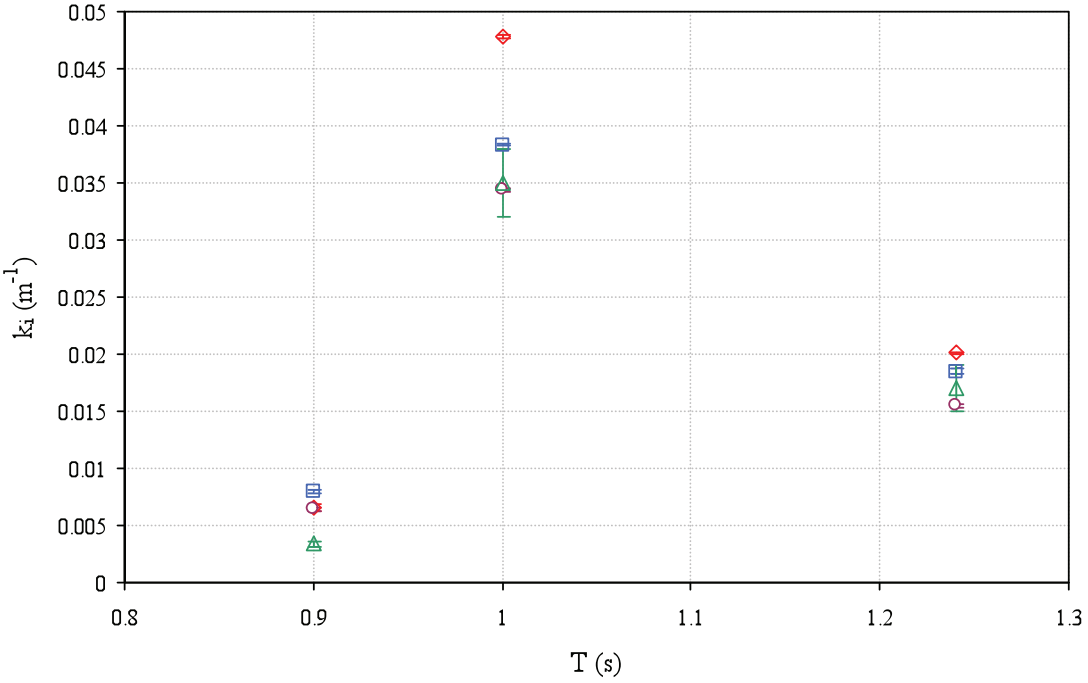

Figure 3.25: Damping value versus time of stir-up the mud with input data (h= 44 cm, S= 2 cm and T= 1 s) and varying wave period after one hour of mixing the mud (◊), 4 hours (□), 25 hours (○)and 29 hours (△))

.

and averaged the resulting damping value for the three runs. Between each run we allowed the tank to settle for 5 minutes then we measured the damping value. After 5 hours we repeated this procedure and measured the damping value. We repeated this procedure each day for the next three days without re-stirring the mud. Then we waited 2.5 days and then ran the wavemaker one final time and measured the damping value. Figure 3.26 shows the damping value relative to time. It is observed that the damping value has its maximum value at the beginning of the test then it decreases with time generally till it reached k_i= 0.315 m^{-1}. After 25 hours we see a

slight increase in the damping value.

At 29 hours the damping value increase by 10%. Between 29 and 53 hours the damping value is almost constant. Finally, after 2.5 days with no testing we measured the damping value which is after 125 hours of the initial mixing we see that the damping value decrease (8%) which is almost the same value of the 25 hours. The same results were observed in Nouri (2013). He measured the damping value by using a shake table test with a layer of the same mud. Figure 3.27 shows the relation of the lutocline (d_2) the mud depth versus time (t). When we stir up the mud the mud layer is mixed with water and its becomes a mixture. With time, the mud starts to consolidate and the lutocline decreases with time. Density samples were also taken at each time step and the results shows that the density increases with time because of the consolidation process see Figure 3.28.

The results were compared with the viscous fluid model of Dalrymple and Liu (1978) by using the viscosity parameter of the mud from Nouri (2013) and the results shows that the maximum attenuation coefficient occurrs at the 29 hours, which explains the increasing in the attenuation coefficient at this time in lab. Dalrymple and Liu (1978) found that the maximum damping rates occur when the thickness of mud layer is equal to the thickness of water layer and what explain the increase in damping at 29 hours. What we can conclude from these experiments is that the consolidation of mud and the mud density plays an important factor with the attenuation.

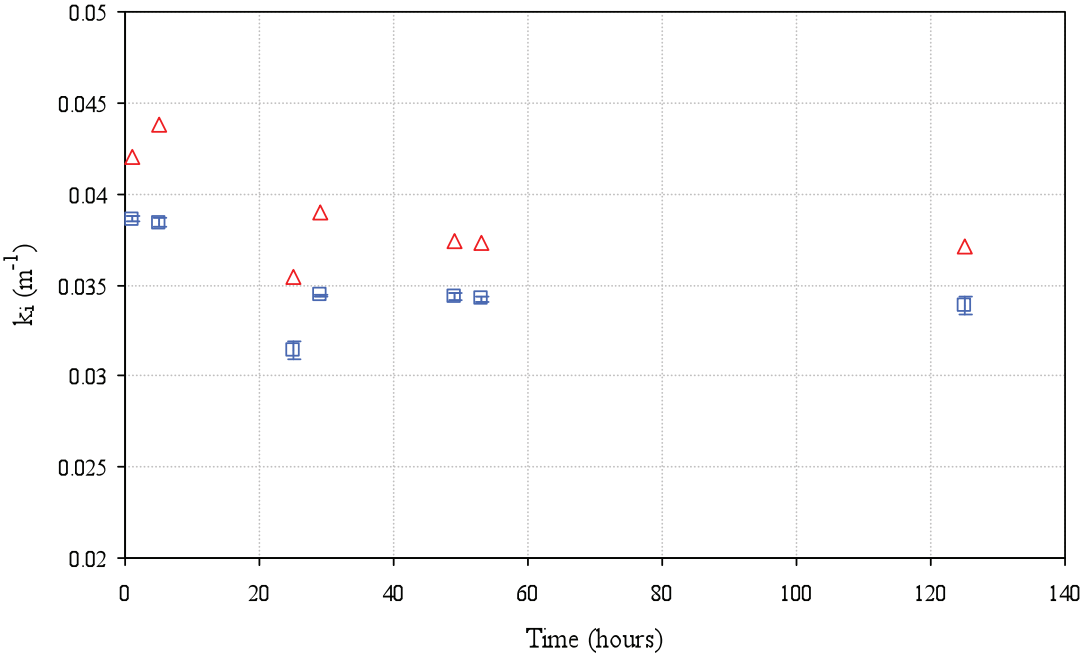

Figure 3.26: Damping value versus time of stir-up the mud with input data (h= 44 cm, S= 2 cm and T= 1 s)) for the days (09/19/12-09/21/12 and 09/24/12) Experimental data ((□); (Dalrymple and Liu, 1987) (△))

.

3.7.4 Damping in shallow water

When water wave propagate over a mud bottom in shallow water, we expect high energy dissipation. Elgar and Raubenheimer (2008) used a numerical model of wave propagating over a mud layer to study frequency and depth effects on energy dissipation. They focused on the Louisiana continental shelf for their study. They found that shallower waters increased dissipation. These results were compared with field observations of Winterwerp *et al.* (2007) and were consistent with laboratory studies of two layer fluid systems Gade (1958) and Kaihatu *et al.* (2007). In this

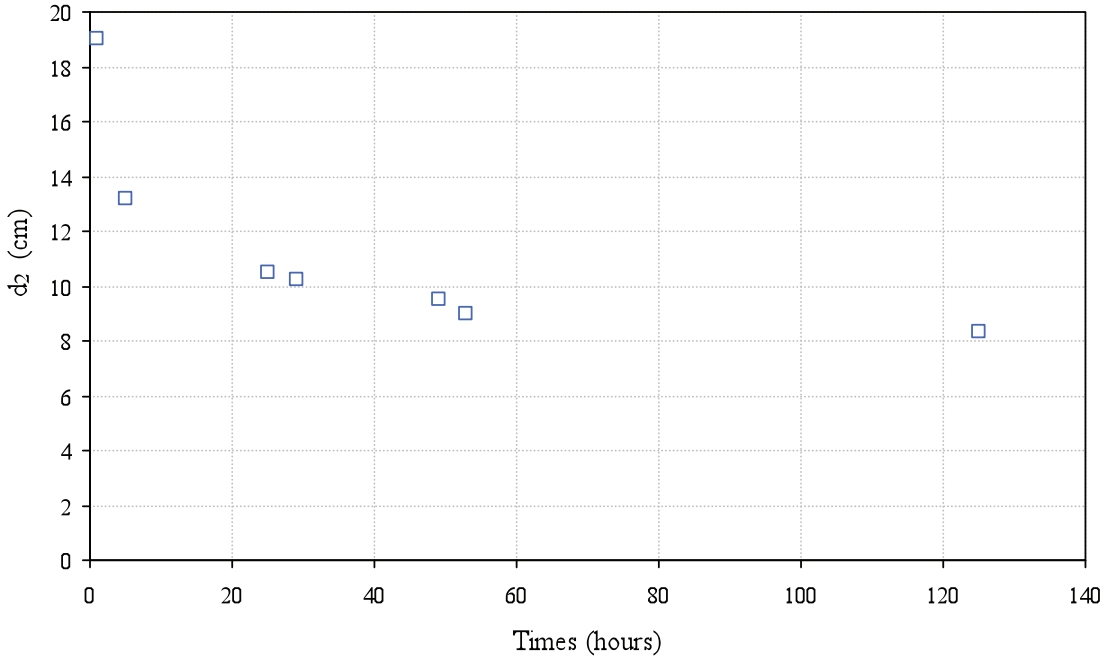

Figure 3.27: Lutocline (d_2) versus time of stir up the mud with input data (h= 44 cm, S= 2 cm and T= 1 s) for the days (09/19/12-09/21/12 and 09/24/12).

.

section, a series of monochromatic wave tank experiments will test the effect wave characteristics on damping in shallow water.

To produce high damping values, the water depth was lowered in order to run tests at shallow depths. We tested with water levels at 21 cm, 25 cm, and 30 cm. The first test was at water level equal to 21 cm where the mud was manually mixed for 20 minutes and allowed to settle until reaching d_2=12 cm.

This test (with three repition) used ten different wave periods (T= 0.7, 0.8, 0.9, 1, 1.1, 1.2, 1.4, 1.6, 1.8, 2, 3 seconds). We then calculated the average attenuation

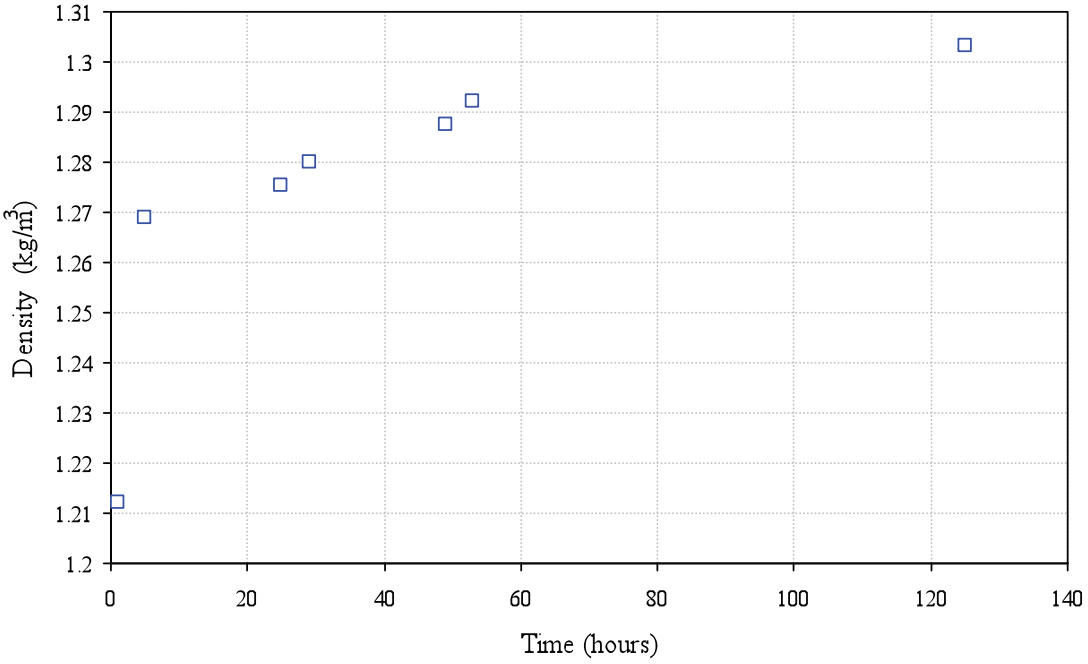

Figure 3.28: Density (ρ) versus time of stir up the mud with input data (h= 44 cm, S= 2 cm and T= 1 s) for the days (09/19/12-09/21/12 and 09/24/12).

.

coefficient. Results show that for wave periods less than 1 s and greater than 2 s, the waves started to break down at early stage. As a result, the attenuation coefficient cannot be measured. On the other hand, for tests with wave periods between 1 and 2 s, high attenuation coefficients were observed (k_i=0.045-0.22) m^{-1}. The attenuation coefficient starts to increase when the wave period was increased until reaching its peak at (T=1.2 s) and starting to decrease.

This test was repeated with a water depth equal to 25 cm and similar results were observed, but the attenuation coefficient is less than for the water depth 21 cm.

Increasing the water depth to 30 cm and running the wavemaker with various wave periods (T= 0.7, 0.8, 0.9, 1, 1.1, 1.2, 1.4, 1.6, 1.8, 2, 3 seconds). Shows the same relationship that had been observed with both water depth= 21 cm and 25 cm, but the attenuation coefficients are smaller than for tests with water depth equal to 21 and 25 cm. Figure 3.29 shows the results of the attenuation coefficients with varying wave periods and neglecting the results for wave periods= 0.7, 0.8, 0.9 s due to the seiching existence in the tank. The experimental data were compared with MacPherson (1980) model and by using the viscous and elastic parameters from Nouri (2013), the results shows a good agreement for wave periods 1.2-2 s.

Experiments showed three aspects involving damping in shallow water. First, in shallow water, the relationship between damping and wave period increases until it reaches a peak and then it decreases. Second, as the water depth increases, the damping effect decreases, meaning that deeper water has less of an effect the damping. Third, compared with MacPherson (1980) viscoelastic model, we found relative agreement on 1.2 s and throughout the rest of the Figure 3.29.

3.8 Conclusions

There are four primary findings of interest. First, for the wave amplitude, this study found that damping increases with increase wave amplitude as did Yamamoto and Schuckman (1984) and Soltanpour *et al.* (2010). Also we found damping decreases

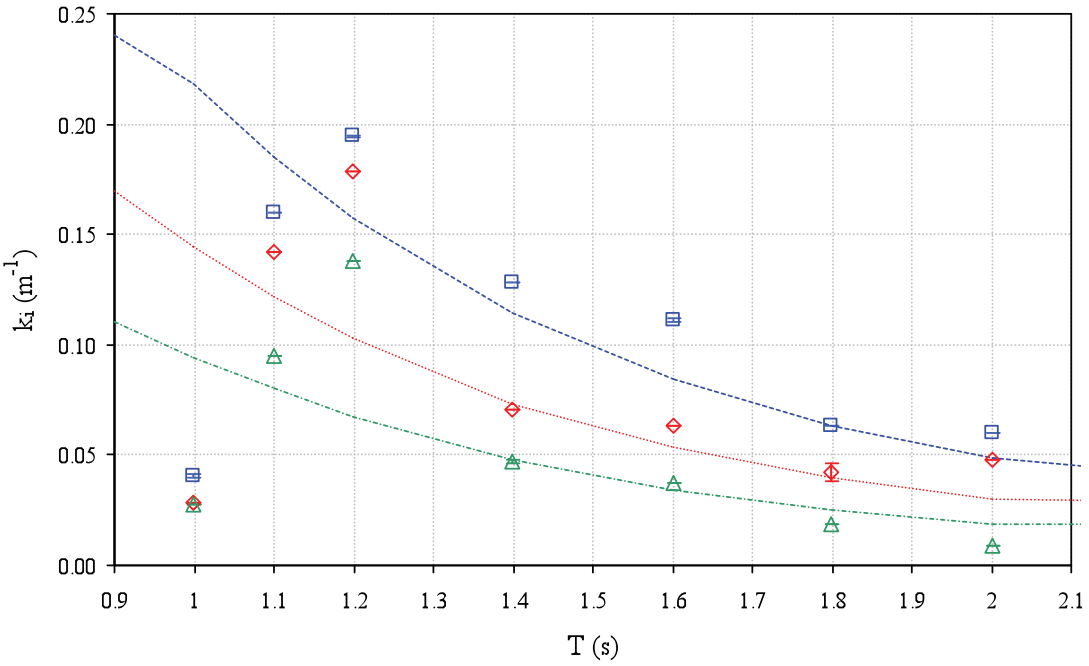

Figure 3.29: Attenuation coefficient versus wave period with input data (S= 2) and varying water depths (h= 21 cm (□), h= 25 cm (◊), h= 30 cm (△), the dash lines are the (MacPherson, 1980) model for h= 21 cm (—-),h= 25 cm (——) and h= 30 cm (—-).

with increase wave amplitude similar to (Nagai *et al.*, 1984; Sakakiyama and Bijker, 1989) and this behavior depends on the rate of work done in the bottom. The rate of work depends on the difference in phase shift between the bottom pressure and vertical velocity.

The second observation is the relationship between damping and wave period. The results shows that the damping increased until it reached a peak ($T = 1.2$ s) and then decreased. It also was related to the rate of work done in the bottom. These results shows agreements with Tsuruya and Nakano (1987), Sakakiyama and Bijker

(1989), Zhang and Zhao (1999) and Hsu *et al.* (2013).

The third, the mud history and mud consolidation plays a role in damping. Our results show that damping for softer mud with low density is large. In addition, for harder mud with high density, the damping is small. We conclude that the mud consolidation can effect the damping and as the mud get denser the damping will decrease.

Finally, we examine damping in shallow water with different wave periods and water depths. We observed high damping value in shallow water (k_i= 0.2 m^{-1}) and we conclude that as the water depth increases, the damping effect decreases. Our results were compared with theoretical model MacPherson (1980) with good agreements.

The most important factor that effect the damping is the variation in mud properties. There was difficulty assuming the properties of mud and rheological behavior of mud. With better understanding of the various potential results, based on these tests, there will be a clearer vision about the behavior of mud.

Chapter 4

Damping in deep water

4.1 Introduction

For a single wave train propagating in deep water over mud, we expect there will be no damping. However, Sheremet and Stone (2003) observed damping of short waves over mud in deep water. In this chapter, we will examine a possibile model for this wave damping. Two short waves were created in deep water with slightly different frequencies, which form a wave group with its associated nonlinear bound long waves. At second order, the bound long waves consist of a long wave with a frequency given by difference of the two deep water wave and a frequency with short wave with a frequency equal to the sum of the short waves frequencies. We examine the difference frequency long bound wave and the possibility of its interaction with the bottom. In particular, we will demonstrate that the length of the difference frequency

bound wave can be long enough such that the bound long wave is in intermediate or shallow water, therefore exerting pressure in the bottom.

4.2 Damping in deep water

Water waves propagating over mud bottom in deep water do not exert a bottom pressure that could lead to energy dissipate. However, testing deep water waves experimentally in the wave tank can give measurable damping coefficients. Initially it would seem that deep water waves should not be affected by the presence of the bottom. However, there are one consideration that need to be made before even beginning to look at more complicated mechanisms. The consideration involves the deep water region definition itself. The bottom pressure from linear wave theory is at $kh{=}\pi$, the value of $1/\cosh kh$ is 0.086. Therefore, according to linear theory at $kh{=}\pi$, the pressures at the bottom under a deep water wave are about 9% of their maximum values. These are surprising large values and calls into question the use of the deep water limit of $kh{=}\pi$. A better deep water limit is perhaps 1.5π.

In this chapter we want to show that in deep water damping could exist due to the wave-mud interaction. To prove this result, two short waves will be generated in the wavemaker that satisfied the deep water conditions. Testing each individule wave train showed no damping values. The idea here is these two short waves will combine to form wave group, which will be associated with long bound wave. The bound or

the wave group length will be long enough to feel the bottom and will cause the wave to dissipate energy.

In our study, the two short waves tests will be generated to great a wave group. These short waves will be examined by three different types depending of the ration of amplitudes of the two short waves. First test will be by generating to waves with (a_2/a_1) is equal to 1. The second test will be on generating two short waves with (a_2/a_1) is equal to 1.1. The third tests will be generating two short waves with (a_2/a_1) is equal to 0.5. For all of the three different types in tests, the wave attenuation will be examined and evaluated.

Theoretically, assume a simple wave group pattern formed by the addition of two waves of equal height travelling in the same direction, but with slight different frequencies and therefore different wave length or wave numbers. For these two waves, one wave moves faster that the other, thus occur regions where the wave add constructively and other regions where the waves add destructively. This gives a wave group pattern or amplitude modulated (beat) pattern. Consider two waves:

$$\eta_1 = \frac{H}{2}\cos(k_1 x - \sigma_1 t) \tag{4.1}$$

$$\eta_2 = \frac{H}{2}\cos(k_2 x - \sigma_2 t) \tag{4.2}$$

The total water surface is obtained by superimposing these waves. After some trigonometric identities we get:

$$\eta = \eta_1 + \eta_2 \tag{4.3}$$

$$\eta = H\cos(kx - \sigma t)\cos(\frac{\Delta k}{2}x - \frac{\Delta\sigma}{2}t) \tag{4.4}$$

$$\eta = H\cos(kx - \sigma t)\cos(\frac{1}{2}\Delta k(x - C_g t)) \tag{4.5}$$

where Δk and $\Delta\sigma$ are the differences in wave numbers and frequencies, C_g is group velocity, k is the wave number and σ is the wave frequency. See Figure (4.1).

4.3 Instrumentation

In these experiments, six capacitance gages and a density sampler device were used.

4.3.1 Wave gages

In this experiments, wave amplitude were measured by using six capacitance wave gages made by Akamina Technologies (model AWP-24-2). The wave amplitude gages were calibrated before each test series of experiments to assure that measurements were not subject to errors. The gages were located at stations 373, 554, 707, 861, 1003 and 1092 cm downstream of the wavemaker.

4.3.2 Density sampler

After each experiment, measurements of mud density were taken at various times throughout the study. Samples of mud were taken by using a density sampler built

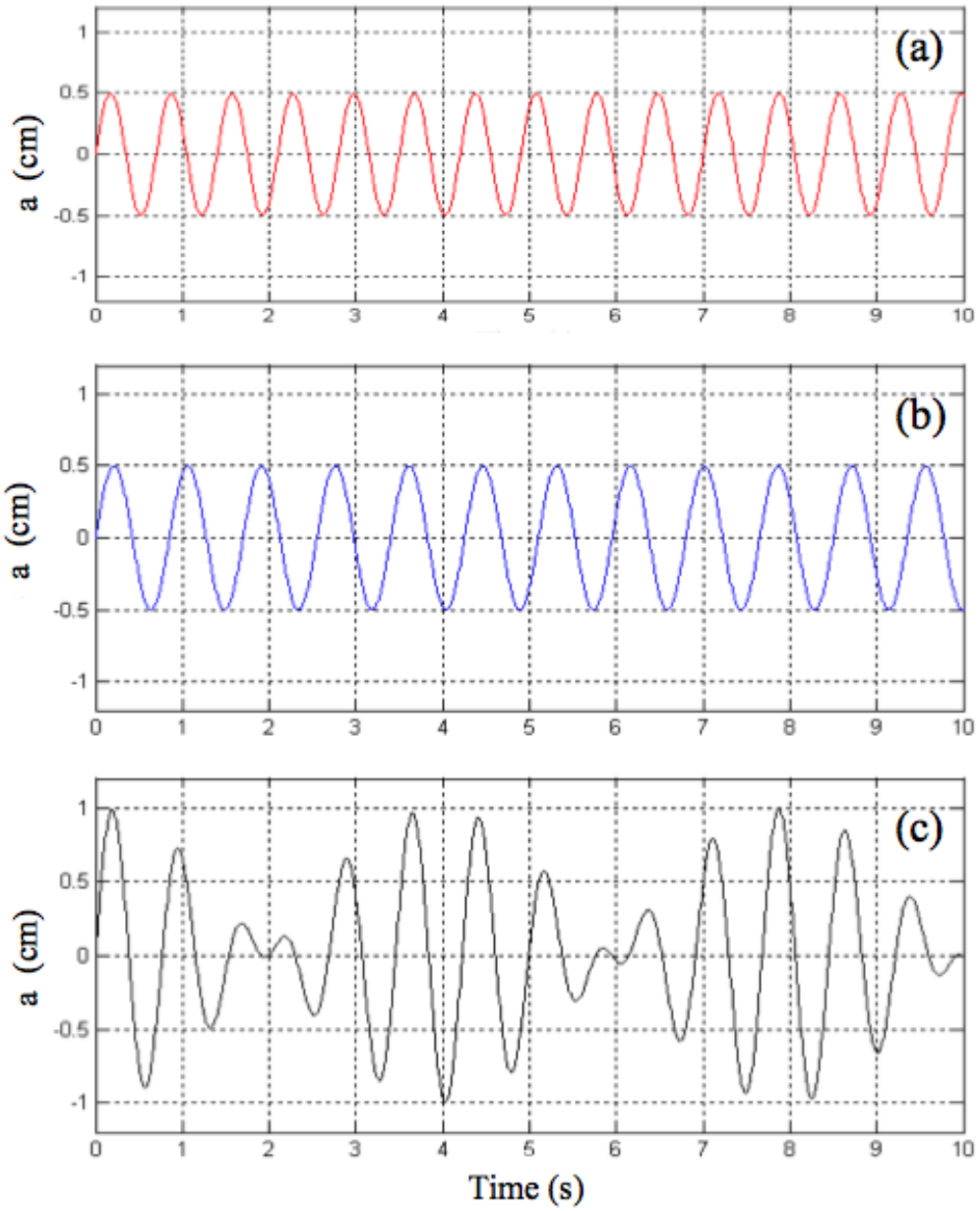

Figure 4.1: The wave amplitude (cm) versus time (s). (a) First wave σ=10.47s^{-1} and k_i=0.0012 m^{-1}, (b) Second wave σ=9.67s^{-1} and k_i=0.00092 m^{-1}, (c) The superimposed two waves T_{beat}=7.85 s and $\Delta\sigma$= 0.8 s^{-1}.

by Eric Maxeiner. This mud device has been made of a cylindrical tube open at both ends. This horizontal cylindrical tube has a circular rubber covers at both ends that can be closed exactly. After each test, samples were taken at the surface of the mud bottom.

Figure 4.2: The density sampler used to collect mud from the bottom of the tank.

4.4 Methodology

The experiments were performed in Coastal Engineering Laboratory wave tank using a commercial kaolinite mixed with water by using a 60 gallon barrel (see Figure 4.3) for all the tests to provide a well mixed suspension. Before any experiment, the mud was stirred by rake for 20 minutes to fully mix the mud throughout the water column, then allowing the mud to settle. When the lutocline, which is which is the

interface between the clear water and the fluid mud reached 12 cm, the wavemaker was started. Wave groups were created by superimposing two short waves of different frequencies in deep water that when they superimpose they create a beat frequency is long wave.

Tests have been conducted varying on the wave amplitude and wave periods of the two incident short waves. The wave amplitudes of the two short wave trains were varied such that their ratio of amplitudes (a_2/a_1) was equal to 0.5, 1, 1.1. Also the wave periods of the two short waves were varing, such as the first group (T_1=0.6 & T_2=0.65), second group (T_1=0.6 & T_2=0.63) and the third group (T_1=0.62 & T_2=0.66). Each wave group tests will be tested with each ration of amplitude. Each test was run for six minutes. The water surface elevation was measured in each test at six stations by using the capacitance gages and the amount of energy dissipation was calculated at each gage.

4.4.1 3D wave velocity measurements

In each experiment in this chapter, 3D water velocity was measured by using Nortek Vectrino velocimeter. The Vectrino is a high resolution acoustic velocimeter that measures the 3D water velocity and the turbulence. The device consists of a titanium probe with 4 transducers (see Figure 4.4) and it is connected to the PC by cable.

The acoustic transducers are submerged and it is stable during the experiments.

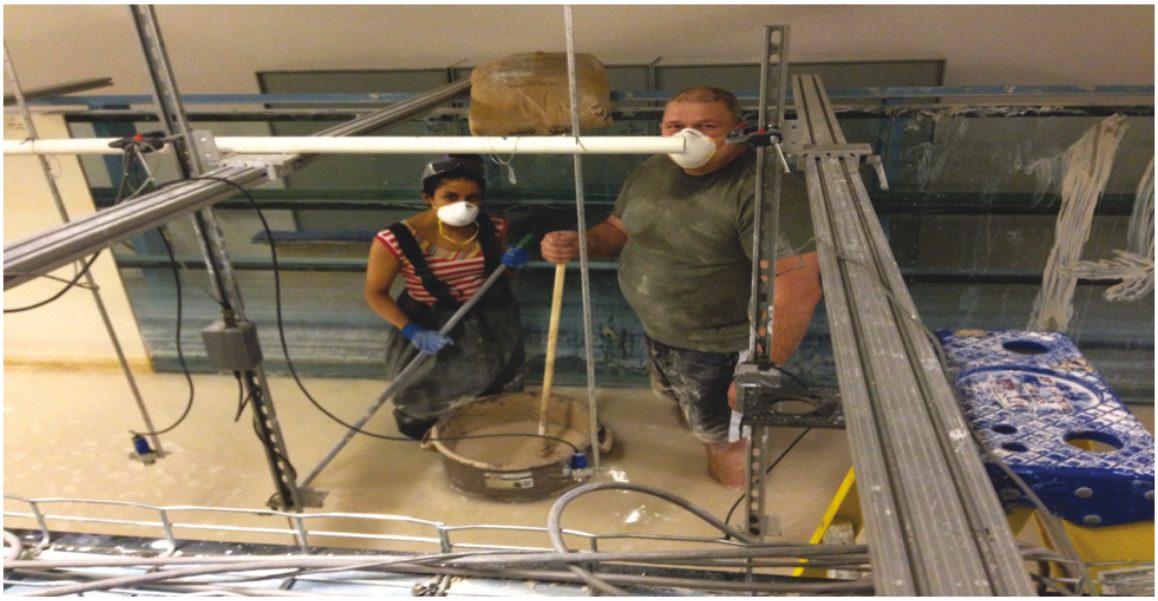

Figure 4.3: The mud is mixed manually by using a 60 gallons barrel to create a well water-mud mixture.

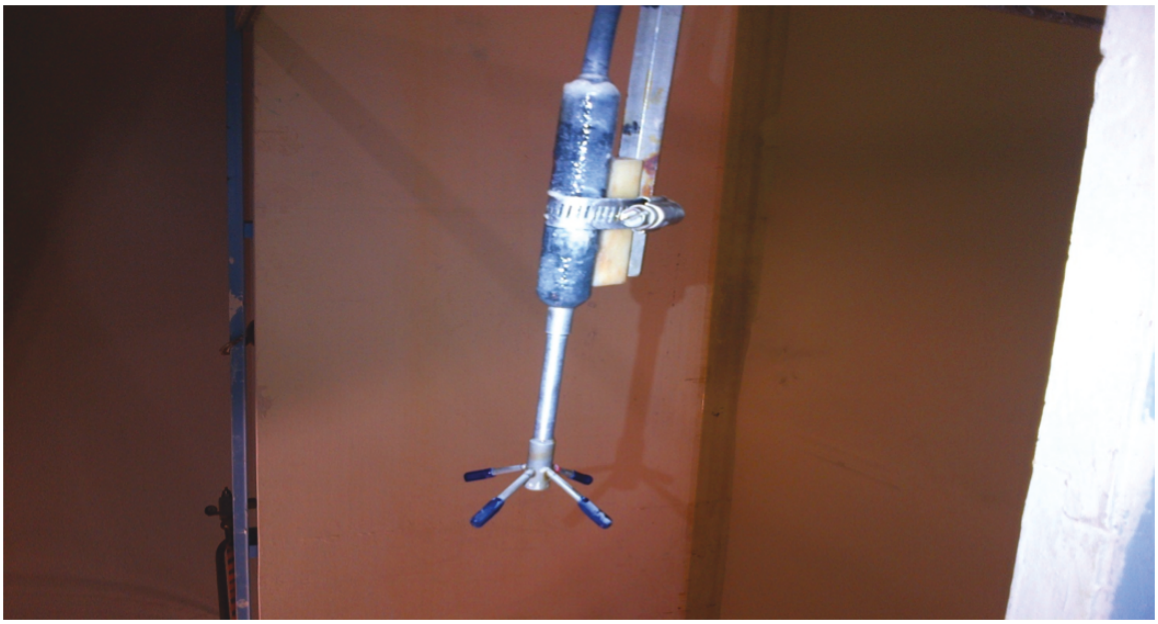

Figure 4.4: The Vectrino acoustic velocimeter probe which is made of titanium and consists of one end with 4 transducers covered with epoxy to measure 3D water velocity and the turbulence of the water wave.

Vectrino software is used to read the experimental data, which are saved as binary files*.dat. For more information about the Vectrino visit (www.nortek-as.com). In each test, the 3D water velocity is measured for 10 minutes and number of samples was 100000. The water temperature during the tests was 20 ^{0}C and the sampling rate was 200 Hz. The average velocity in each direction and the total water velocity were measured in each experiment (see Table 4.1).

4.5 Experimental Data

Prior to each wave group test, the component short waves were tested individually and the attenuation coefficient calculated. Then the components were added to do the wave group test. All the tests were replicated three times and the average taken. Due to the limitation of the wave tank dimension, we could not conduct a wide range of beat frequencies. Table 4.2 shows all the input parameters for each test.

Table 4.2: Parameters of experimental tests of monochromatic and bi-chromatic waves over mud.

Test	Stroke (S_1) (cm)	Period (T_1) (s)	Stroke (S_2) (cm)	Period (T_2) (s)	Water depth (h) (cm)	Lutocline depth (d_2) (cm)	Mud Density (kg/m^3)
1	2	0.6	2	0.65	44	12	1291

Table 4.2 Parameters of experimental tests (see full caption on previous page)

Test	Stroke (S_1) (cm)	Period (T_1) (s)	Stroke (S_2) (cm)	Period (T_2) (s)	Water depth (h) (cm)	Lutocline depth (d_2) (cm)	Mud Density (kg/m^3)
2	2	0.6	0	0	44	12	1291
3	2	0.65	0	0	44	12	1291
4	2	0.6	2.2	0.65	44	12	1301
5	2.2	0.65	0	0	44	12	1301
6	2	0.6	1	0.65	44	12	1288
7	1	0.65	0	0	44	12	1288
8	2	0.6	2	0.63	44	12	1294
9	2	0.6	0	0	44	12	1294
10	2	0.63	0	0	44	12	1294
11	2	0.6	2.2	0.63	44	12	1303
12	2.2	0.63	0	0	44	12	1303
13	2	0.6	1	0.63	44	12	1249
14	1	0.63	0	0	44	12	1249
15	2	0.62	2	0.66	44	12	1311
16	2	0.6	0	0	44	12	1311
17	2	0.66	0	0	44	12	1311

Table 4.2 Parameters of experimental tests (see full caption on previous page)

Test	Stroke (S_1) (cm)	Period (T_1) (s)	Stroke (S_2) (cm)	Period (T_2) (s)	Water depth (h) (cm)	Lutocline depth (d_2) (cm)	Mud Density (kg/m^3)
18	2	0.62	2.2	0.66	44	12	1299
19	2.2	0.66	0	0	44	12	1299
20	2	0.62	1	0.66	44	12	1301
21	1	0.66	0	0	44	12	1301

4.6 Method (Analysis)

4.6.1 Power Spectrum Density Method (PSD)

The first method was the Power Spectrum Density method (PSD), this method is well known in statistical signal processes analysis for time series and has been used to measure the power of signal or wave distributed over a given frequency domain (See Figure 4.5). By calculating the area under the power spectrum density, the amount of energy in this spectrum is calculated at each sensor along the wave tank.

Table 4.1: Velocity Parameters of experimental tests of monochromatic and bichromatic waves over mud.

Test	Stroke (S_1) (cm)	Period (T_1) (s)	Stroke (S_2) (cm)	Period (T_2) (s)	Water depth (h) (cm)	Average velocity in x-direction (x) (m/s)	Average velocity in y-direction (y) (m/s)	Average velocity in z-direction (z) (m/s)
1	2	0.6	2	0.65	44	6.51E-06	-3.52E-05	-1.75E-04
8	2	0.6	2.2	0.65	44	3.15E-06	-2.55E-05	-2.18E-04
15	2	0.6	1	0.65	44	5.75E-06	-4.38E-05	-1.45E-04
4	2	0.6	2	0.63	44	6.45E-06	-3.74E-05	-1.94E-04
11	2	0.6	2.2	0.63	44	3.98E-06	-2.28E-05	-2.19E-04
18	2	0.6	1	0.63	44	5.25E-06	-4.96E-05	-1.45E-04
6	2	0.62	2	0.66	44	6.62E-06	-3.12E-05	-1.17E-04
13	2	0.62	2.2	0.66	44	3.72E-06	-2.85E-05	-2.77E-04
20	2	0.62	1	0.66	44	5.97E-06	-4.76E-05	-1.65E-04

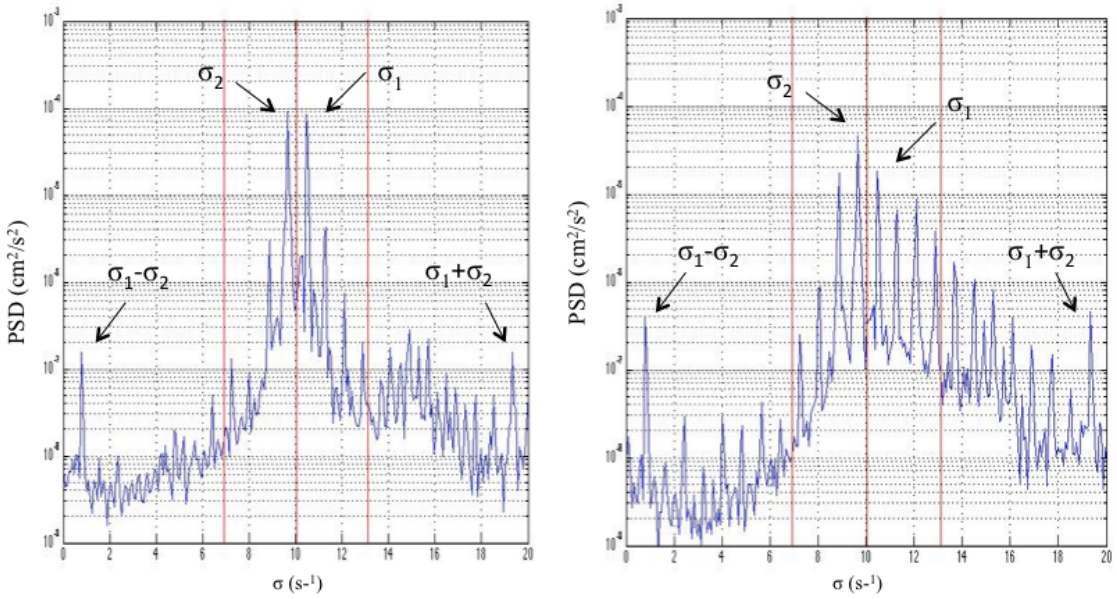

Figure 4.5: The power spectral density of the experiment #1 with water depth= 44 cm and mud depth 12 cm, with two short waves (S=2 cm, T_1=0.6 s and S=2 cm , T_2=0.65 s) for test #1 (130922_S2_T0p6_ S2_T0p65_run1.txt), (a) Sensor#1 (b) Sensor#6

4.6.2 The Extended Prony Method

The second method used to analyze the data is the extended Prony method. The Prony method was developed by Gaspard Riche de Prony in 1795 (Prony, 1795) to estimate the amplitudes and frequencies of a discrete sum of anharmonic sinusoidal signals. It is a common method that can be used to extract useful information such as frequency, amplitude and damping value of waves in a given composite signal. In our analysis we used the extended Prony method (Kay and Marple, 1981) that estimates the frequencies and amplitudes by using the eigenanalysis method described in Smyth (2000). The analysis here uses the S-plus software package. We shall describe the

method in detail here.

The objective of the method is to extract information of a time sequence of the form

$$f(t) = \sum_{k=1}^{p} \alpha_k \sin(\sigma_k t + \varphi_k) \tag{4.6}$$

$$= \sum_{k=1}^{p} \alpha_k \sin(\sigma_k t)\cos(\varphi_k) + \alpha_k \cos(\sigma_k t)\sin(\varphi_k) \tag{4.7}$$

By writing

$$\sin(\sigma_k t) = \frac{e^{i\sigma_k t} - e^{-i\sigma_k t}}{2i} \tag{4.8}$$

$$\cos(\sigma_k t) = \frac{e^{i\sigma_k t} + e^{-i\sigma_k t}}{2} \tag{4.9}$$

we have

$$f(t) = \sum_{k=1}^{p} \left(\frac{\alpha_k}{2i}\cos\varphi_k + \frac{\alpha_k}{2}\sin\varphi_k\right) e^{i\sigma_k t} + \left(-\frac{\alpha_k}{2i}\cos\varphi_k + \frac{\alpha_k}{2}\sin\varphi_k\right) e^{-i\sigma_k t} \tag{4.10}$$

Introduce

$$\sigma_k = -\sigma_{k-p} \qquad \text{for } k = p+1, \cdots, 2p, \tag{4.11}$$

$$\widetilde{\alpha}_k = \tfrac{\alpha_k}{2i}\cos\varphi_k + \tfrac{\alpha_k}{2}\sin\varphi_k \qquad \text{for } k = 1, \cdots, p, \tag{4.12}$$

$$\widetilde{\alpha}_k = -\tfrac{\alpha_{k-p}}{2i}\cos\varphi_{k-p} + \tfrac{\alpha_{k-p}}{2}\sin\varphi_{k-p} \quad \text{for } k = p+1, \cdots, 2p. \tag{4.13}$$

We can simply write

$$f(t) = \sum_{k=1}^{2p} \widetilde{\alpha}_k e^{i\sigma_k t} \tag{4.14}$$

This signal is real if and only if

$$f(t) = f^*(t) \Longleftrightarrow \sum_{k=1}^{2p} \widetilde{\alpha}_k e^{i\sigma_k t} = \sum_{k=1}^{2p} \widetilde{\alpha}_k^* e^{-i\sigma_k t} \Longleftrightarrow \widetilde{\alpha}_k = \widetilde{\alpha}_{k-p}^* \quad \text{for } k = p+1, \cdots, 2p. \tag{4.15}$$

For any n distinct point, there exists a unique interpolating polynomial (up to a constant multiplier). Then given $n = 2p$ "modes" $e^{i\sigma_1}, \cdots, e^{i\sigma_{2p}}$, one can find an order $2p$ interpolating polynomial $C(z)$ such that $C(z_k) = 0$ for $z_k = e^{i\omega_k}$ and $k = 1, \cdots, n$. In particular, one can define a polynomial of order $2p$

$$C(z) = (z - e^{i\sigma_1})(z - e^{i\sigma_2}) \cdots (z - e^{i\sigma_{2p}}) \tag{4.16}$$

If the signal is real, then the frequencies σ_k's appear in pairs and the roots of $C(z)$ are complex conjugate pairs, which dictates that the coefficients of the polynomial are real. In Gaspard Riche's paper, he define such a function to be

$$C(z) = c_1 + c_2 z + \cdots + c_{2p+1} z^{2p} \tag{4.17}$$

which is the same as (4.16) up to a constant. We will use Gaspard Riche's notation for the sake of consistency. Now observe that, for any k, $e^{i\sigma_k}$ solves the equation

$$c_1 + c_2 z + \cdots + c_{2p+1} z^{2p} = 0 \tag{4.18}$$

that is

$$c_1 + c_2 e^{i\sigma_k} + \cdots + c_{2p+1} e^{i\sigma_k (2p)} = 0 \tag{4.19}$$

Multiply both sides by $\widetilde{\alpha}_k e^{i\sigma_k t}$, we have

$$c_1\widetilde{\alpha}_k e^{i\sigma_k t} + c_2\widetilde{\alpha}_k e^{i\sigma_k(t+1)} + \cdots + c_{2p+1}\widetilde{\alpha}_k e^{i\sigma_k(t+2p)} = 0 \tag{4.20}$$

Sum over $k = 1, \cdots, 2p$, we have

$$c_1 \sum_{k=1}^{2p} \widetilde{\alpha}_k e^{i\sigma_k t} + c_2 \sum_{k=1}^{2p} \widetilde{\alpha}_k e^{i\sigma_k(t+1)} + \cdots + c_{2p+1} \sum_{k=1}^{2p} \widetilde{\alpha}_k e^{i\sigma_k(t+2p)} = 0 \tag{4.21}$$

i.e.,

$$c_1 f(t) + ... + c_{2p+1} f(t+2p) = 0. \tag{4.22}$$

Hence $f(t)$ solves the difference equation

$$c_1 f(t) + ... + c_{2p+1} f(t+2p) = 0 \tag{4.23}$$

where the $2p$ roots of $C(z) = c_1 + c_2 z + \cdots + c_{2p+1} z^{2p}$ is given by $\exp(i\sigma_1), \cdots, \exp(i\sigma_{2p})$.

Hence the method works like this: one needs to find $\mathbf{c} = (c_1, \cdots, c_{2p})^T$ first, then finding the roots of $C(z)$ gives the relevant $2p$ frequencies (if the signal is real, these frequencies come in pairs). If the $2p$ roots are $z_1, \cdots, z_{2p}$, then the $2p$ frequencies are such that $z_j = \exp(i\sigma_j)$ for $j = 1, \cdots, 2p$. Then to find $\widetilde{\alpha}$ is essentially a least squares problem and the original α_k and φ_k in (4.6) is easily solved from (4.12). Note from the n data point $y_1, \cdots, y_n$, we have (without noise)

$$\begin{aligned} y_1 &= \widetilde{\alpha}_1 e^{i\sigma_1} + \cdots + \widetilde{\alpha}_{2p} e^{i\sigma_{2p}} \\ &\cdots \\ y_n &= \widetilde{\alpha}_1 e^{in\sigma_1} + \cdots + \widetilde{\alpha}_{2p} e^{in\sigma_{2p}} \end{aligned} \tag{4.24}$$

These linear equations may not have solutions when $n > 2p$. To find $\widetilde{\alpha}_1, \cdots, \widetilde{\alpha}_{2p}$, one can use the least squares method such that the line determined by $y = \widetilde{\alpha}_1 x_1 + \cdots + \widetilde{\alpha}_{2p} x_{2p}$ passes through the n data points $(e^{i\omega_1}, \cdots, e^{i\sigma_{2p}}, y_1), \cdots, (e^{in\sigma_1}, \cdots, e^{in\sigma_{2p}}, y_n)$ such that the sum of the distance squared of the n points to the line is minimized.

How to find $\mathbf{c}$? Note if our observed signal $y_t = f(t)$, it will solve equation (4.23). Hence, if we have n data points $y_1, \cdots, y_n$, we have $n - 2p$ equations

$$c_1 y_1 + \cdots + c_{2p+1} y_{2p+1} = 0 \tag{4.25}$$

$$c_1 y_2 + \cdots + c_{2p+1} y_{2p+2} = 0 \tag{4.26}$$

$$\cdots \tag{4.27}$$

$$c_1 y_{n-2p} + \cdots + c_{2p+1} y_n = 0 \tag{4.28}$$

We can write this in matrix form $Y\mathbf{c} = \mathbf{0}$ with

$$Y = \begin{pmatrix} y_1 & y_2 & \cdots & y_{2p+1} \\ y_2 & y_3 & \cdots & y_{2p+2} \\ \cdots & \cdots & \cdots & \cdots \\ y_{n-2p} & y_{n-2p+1} & \cdots & y_n \end{pmatrix}$$

However, since the signal will in general comprises noises, we want to find $\mathbf{c}$ such that $Y\mathbf{c}/\|\mathbf{c}\|$ is close to 0 in a certain sense for certain norm $\|\cdot\|$. There are different choices of the norm, which gives different methods. One is the so-called Pisarenko's method, which can be written as

$$\min_{\|\mathbf{c}\|_2=1} \mathbf{c}^* B \mathbf{c} \quad \text{with } B = \frac{1}{n} Y^* Y. \tag{4.29}$$

Here $\mathbf{c^*Bc} = \frac{\mathbf{1}}{\mathbf{n}}\|\mathbf{Yc}\|_\mathbf{2}^\mathbf{2}$ and $\|c\|_2 = \sqrt{c_1^2 + \cdots + c_{2p+1}^2}$. That is we are minimizing $\|Y\mathbf{c}\|_\mathbf{2}/\|\mathbf{c}\|_\mathbf{2}$. Kay and Marple (1981) propose the extended Prony method that uses a different scaling constraint c_{2p+1}, which can be written as

$$\min_{c_{2p+1}=1} \mathbf{c^*Bc} \quad \text{with } B = \frac{1}{n}Y^*Y. \tag{4.30}$$

Kahn *et al.*, (1992) have examined the asymptotic efficiencies of the two method and concluded the extended Prony method is preferable for large noise.

The output is in the form

$$f(t) = \mu + \alpha_1 \cos(\sigma_1 t) + \beta_1 \sin(\sigma_1 t) + \cdots + \alpha_k \cos(\sigma_k t) + \beta_k \sin(\sigma_k t) \tag{4.31}$$

where μ a the constant, σ_i i= 1, 2,...k, are the estimated frequencies, and α_i and β_i are the wave amplitude. Figure 4.6 shows the results of the fitted line of the extended Prony method with an experimental data for test#1 and sensor #1 of the water surface elevation versus the time series for two short waves ($S = 2$ cm, $\sigma_1 = 10.47s^{-1}$ and $S = 2$ cm, $\sigma_2 = 9.67s^{-1}$), water depth 44 cm and mud depth 12 cm, by using Smyth (2000) model.

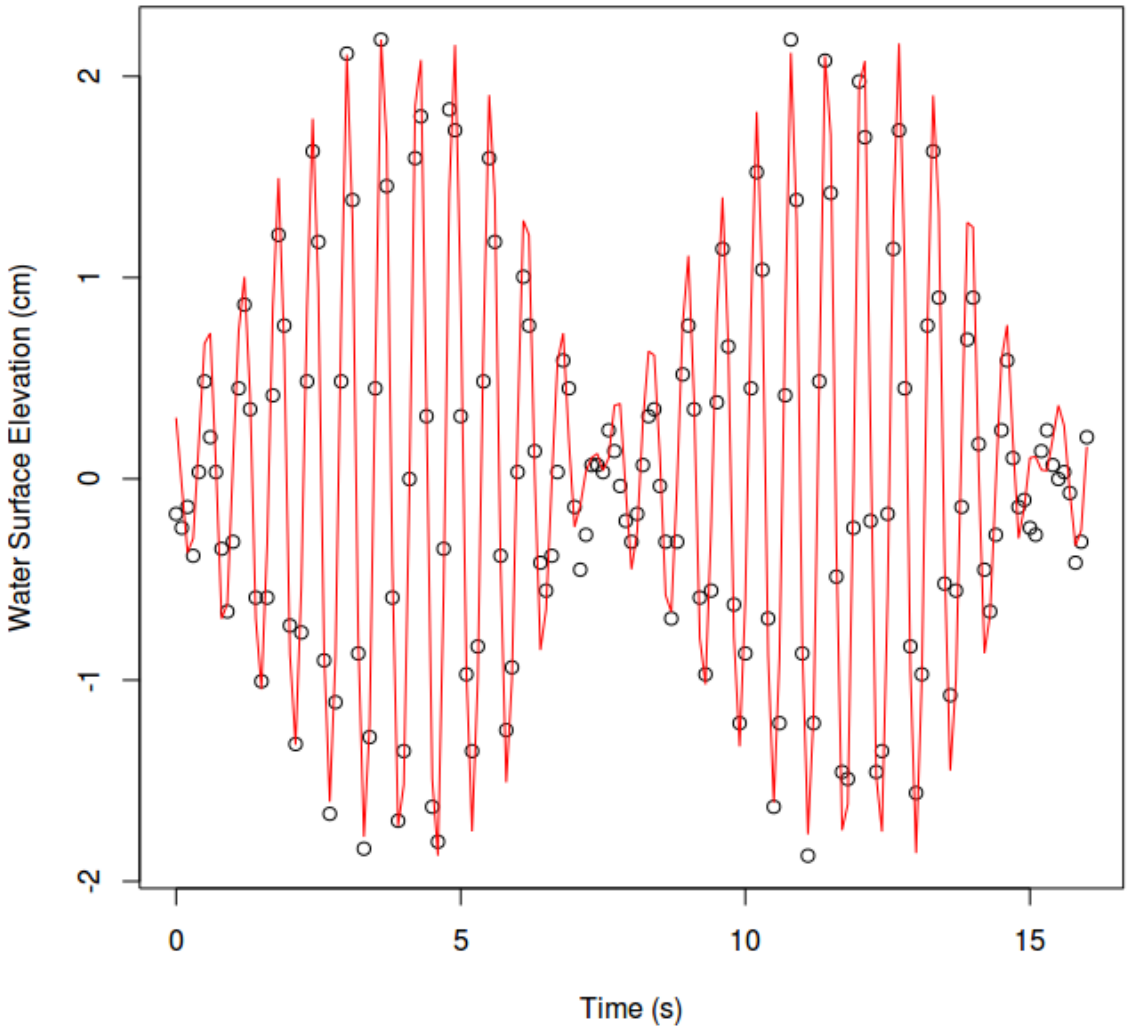

Figure 4.6: Experimental data of the water surface elevation versus the time series ($\circ$) and the fitted line is the solution by using the extended Prony method for test#1 and sensor#1 with water depth 44 cm and mud depth 12 cm, with two short waves ($S = 2$ cm, $\sigma_1 = 10.47s^{-1}$ and $S = 2$ cm , $\sigma_2 = 9.67s^{-1}$).The horizontal axis is time in seconds and the vertical axis is water surface elevation.

After using the Prony method, the results will estimate the amplitude of each two short wave components and also for the sum and difference long waves. These amplitudes will be plotted versus sensors location and the exponential fitted line will

be the damping value.

4.7 Results and discussion

The results for monochromatic individual short wave trains in deep water show no damping (Test# 2, 3 5, 7, 9, 10, 12, 14, 16). For the tests of bi-chromatic waves, the results in this paper are presented in two groups varying with the ratio of amplitude and wave periods. The three ratios which were used are (a_2/a_1) is equal to 0.5, 1, 1.1 and the wave period of the two short waves are (T_1=0.6 & T_2=0.65), (T_1=0.6 & T_2=0.63) and (T_1=0.62 & T_2=0.66). The results include the extended Prony method that will estimate the amplitude at each sensor for different frequencies.

4.7.1 Power Spectrum Density Method (PSD)

The first general method for analysis the wave group was calculating to total amount of energy in the spectrum by using the Power Spectral Density method (PSD). The total amount of energy in the spectrum was calculated in each gage and also the energy associated with the peak area, which is defined as the energy contained in the area between the two frequencies and was compared with the total amount of energy of all tests. It observed from the results that the total amount of energy decreased along the tank but the energy in the peak area dissipated more energy as it is observed in Figure (4.7-4.9), which shows the results of the tests with waves with

(a_2/a_1) is equal to 1 and Figure (4.10-4.12), which shows the results of tests with two waves with (a_2/a_1) is equal to 1.1. For tests with (a_2/a_1) are equal to 0.5 (Figures 4.13-4.15), the total amount of energy is almost in the peak region and shows that the energy is dissipating in sensors along the tank.

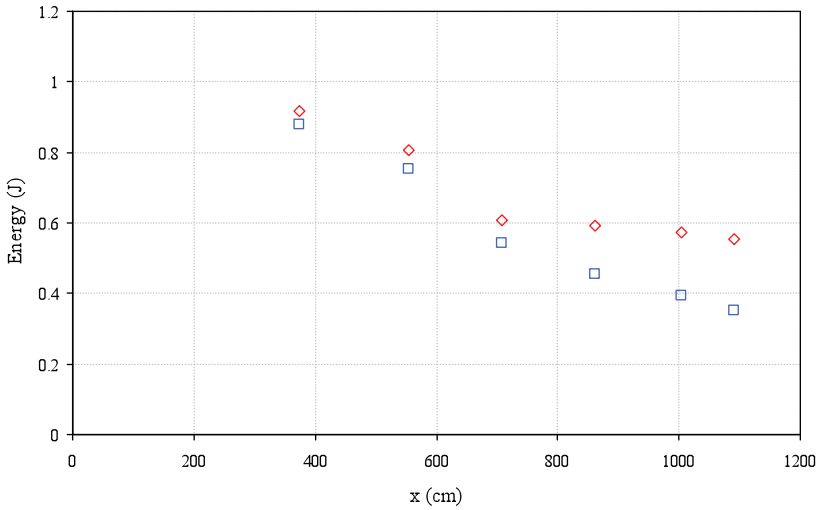

Figure 4.7: The amount of energy of the wave group at a distance from the wave maker (x) by using power spectral density method for test#1 with water depth= 44 cm and mud depth 12 cm, with two short waves (S=2 cm, , σ_1= 10.47 s^{-1} and S=2 cm , σ_2= 9.67 s^{-1}). The total amount of energy in the full experiment (◊), The amount of the energy in the range of the peak (□).

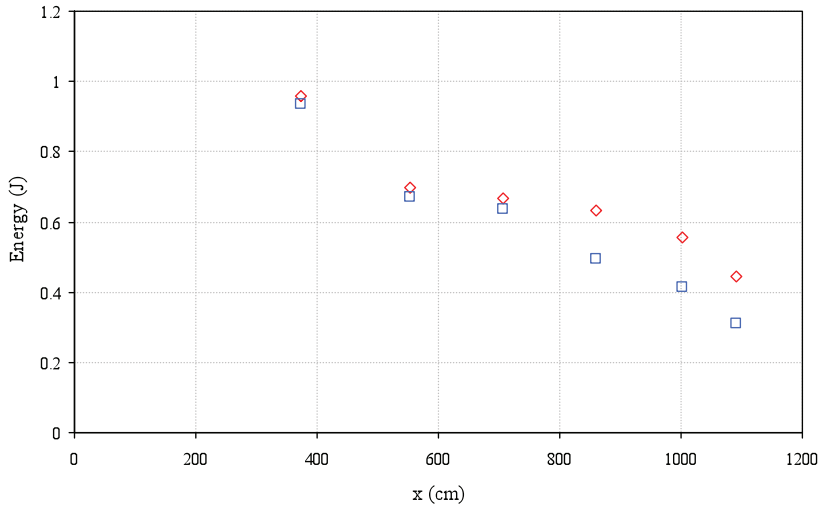

Figure 4.8: The amount of energy of the wave group at a distance from the wave maker (x) by using power spectral density method for test#8 with water depth= 44 cm and mud depth 12 cm, with two short waves (S=2 cm, , σ_1= 10.47 s^{-1} and S=2 cm , σ_2= 9.97 s^{-1}). The total amount of energy in the full experiment (◊), The amount of the energy in the range of the peak.

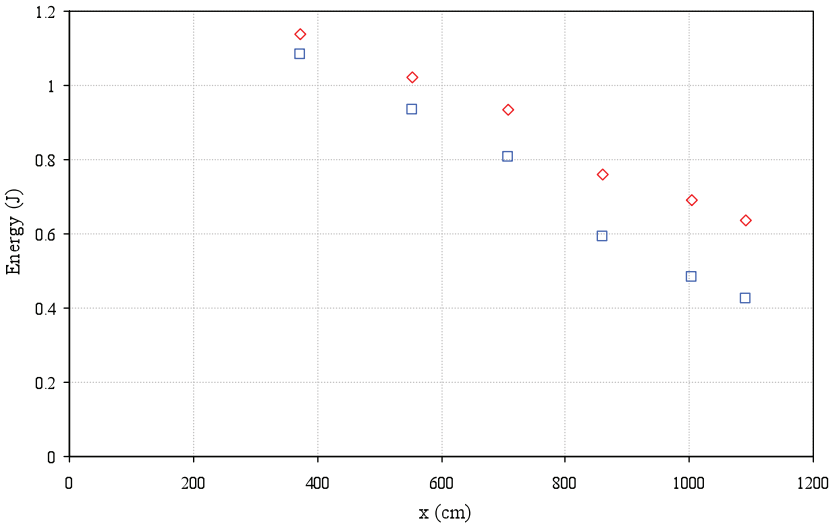

Figure 4.9: The amount of energy of the wave group at a distance from the wave maker (x) by using power spectral density method for test#15 with water depth= 44 cm and mud depth 12 cm, with two short waves (S=2 cm, , σ_1= 10.13 s^{-1} and S=2 cm , σ_2= 9.52 s^{-1}). The total amount of energy in the full experiment (◊), The amount of the energy in the range of the peak (□).

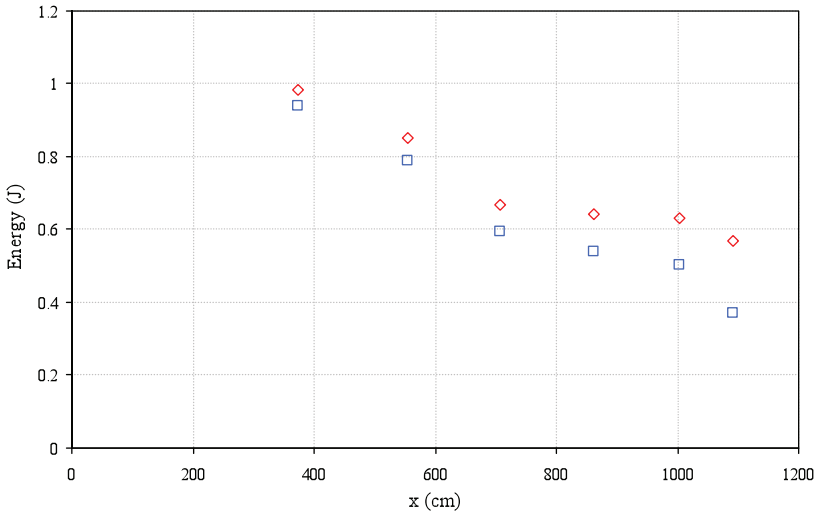

Figure 4.10: The amount of energy of the wave group at a distance from the wave maker (x) by using power spectral density method for test#4 with water depth= 44 cm and mud depth 12 cm, with two short waves (S=2 cm, , σ_1= 10.47 s^{-1} and S=2.2 cm , σ_2= 9.67 s^{-1}). The total amount of energy in the full experiment (◊), The amount of the energy in the range of the peak (□).

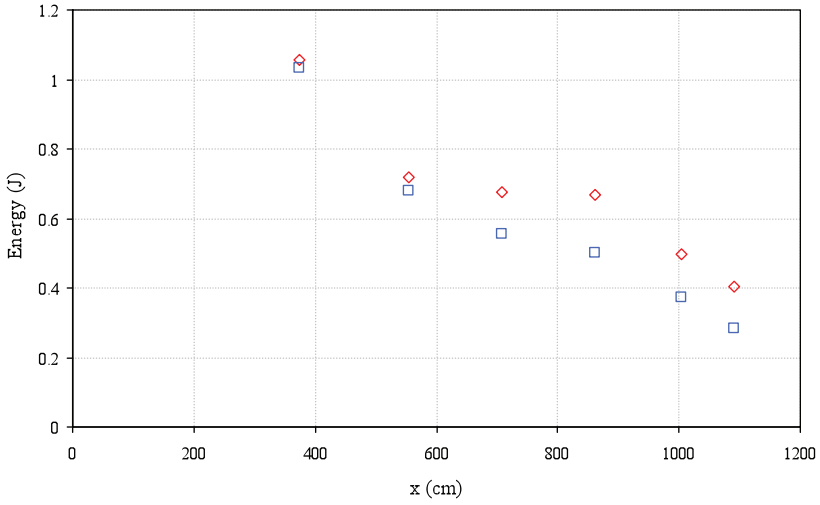

Figure 4.11: The amount of energy of the wave group at a distance from the wave maker (x) by using power spectral density method for test#11 with water depth= 44 cm and mud depth 12 cm, with two short waves (S=2 cm, , σ_1= 10.47 s^{-1} and S=2.2 cm , σ_2= 9.97 s^{-1}). The total amount of energy in the full experiment (◊), The amount of the energy in the range of the peak (□).

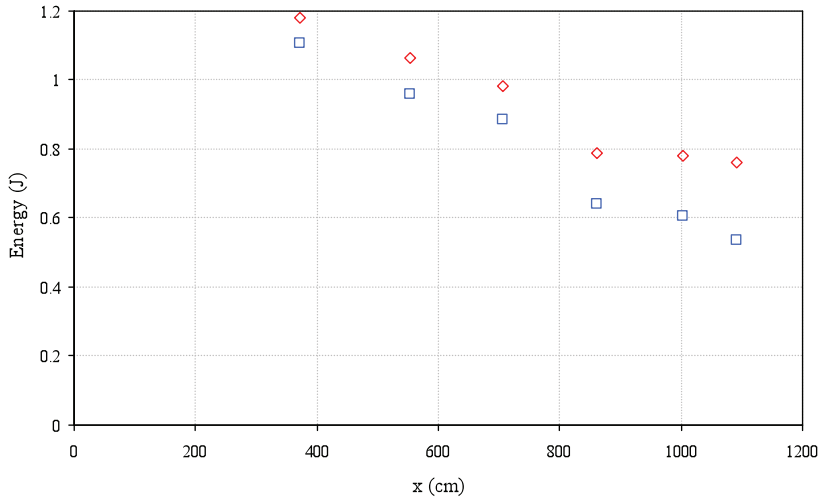

Figure 4.12: The amount of energy of the wave group at a distance from the wave maker (x) by using power spectral density method for test#18 with water depth= 44 cm and mud depth 12 cm, with two short waves (S=2 cm, , σ_1= 10.13 s^{-1} and S=2.2 cm , σ_2= 9.52 s^{-1}). The total amount of energy in the full experiment (◊), The amount of the energy in the range of the peak.

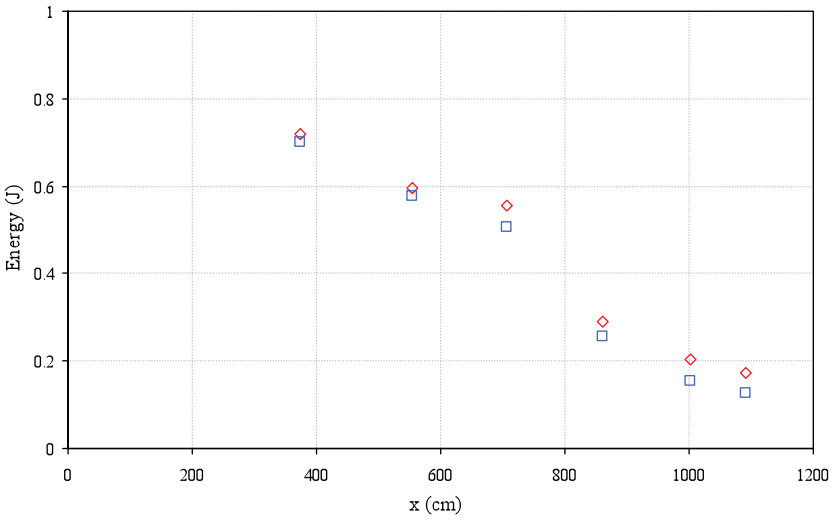

Figure 4.13: The amount of energy of the wave group at a distance from the wave maker (x) by using power spectral density method for test#6 with water depth= 44 cm and mud depth 12 cm, with two short waves (S=2 cm, , σ_1= 10.47 s^{-1} and S=1 cm , σ_2= 9.67 s^{-1}). The total amount of energy in the full experiment (◊), The amount of the energy in the range of the peak (□).

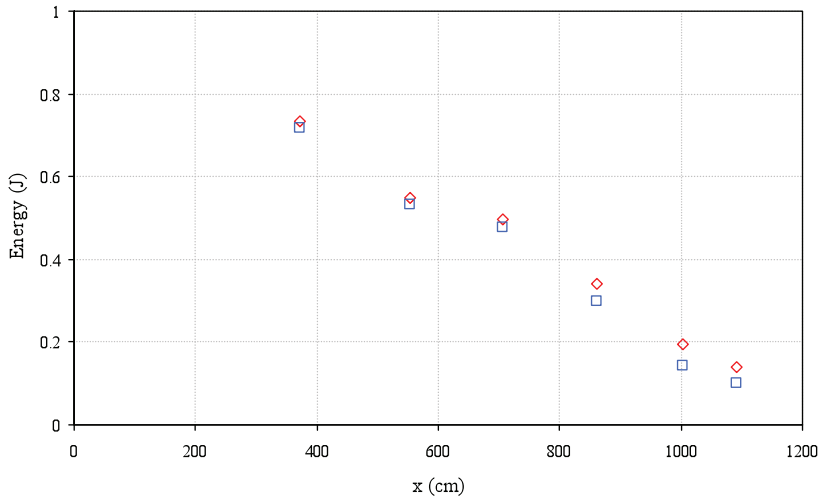

Figure 4.14: The amount of energy of the wave group at a distance from the wave maker (x) by using power spectral density method for test#13 with water depth= 44 cm and mud depth 12 cm, with two short waves (S=2 cm, , σ_1= 10.47 s^{-1} and S=1 cm , σ_2= 9.97 s^{-1}). The total amount of energy in the full experiment (◊), The amount of the energy in the range of the peak (□).

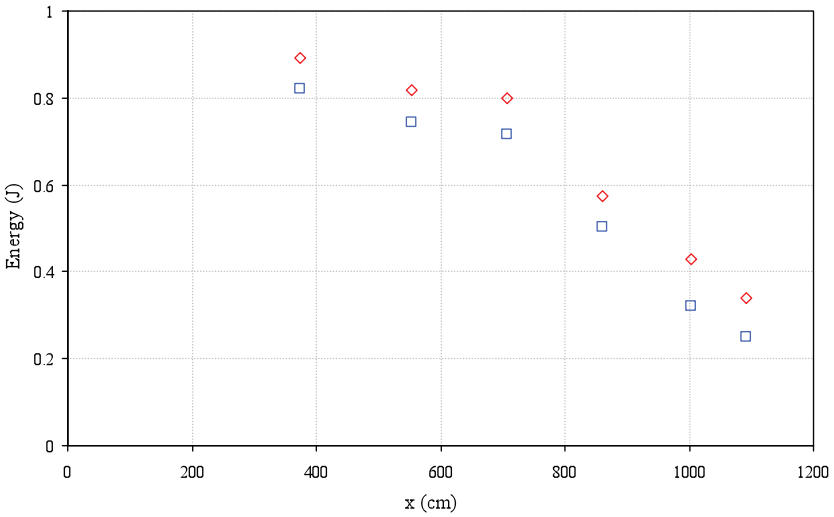

Figure 4.15: The amount of energy of the wave group at a distance from the wave maker (x) by using power spectral density method for test#20 with water depth= 44 cm and mud depth 12 cm, with two short waves (S=2 cm, , σ_1= 10.13 s^{-1} and S=1 cm , σ_2= 9.52 s^{-1}). The total amount of energy in the full experiment (◊), The amount of the energy in the range of the peak (□).

The percentage of the energy in the peak region has been calculated to show that the energy dissipation from sensor one to sensor six. For the test in Figure 4.16 the percentage of the total amount of energy was (96%) at sensor one and decreases (94.2%) at sensor two, (89.55%) at sensor 3, (77.06%) sensor 4, (68.48%) at sensor 5, and (63.77%) at sensor 6. For Figure 4.17, the percentage of the total amount of energy at sensor 1 is (97.66%), which then dropped at sensor 6 (70.2%). For Figure 4.18, the percentage of the total amount of energy at sensor 1 is (95.14%), which then dropped at sensor 6 (66.76%). For Figure 4.19, the percentage of the total amount of energy at sensor 1 is (95.53%), which then dropped at sensor 6 (65.05%). For Figure 4.20, the percentage of the total amount of energy at sensor 1 is (97.84%), which then dropped at sensor 6 (70.60%). For Figure 4.21, the percentage of the total amount of energy at sensor 1 is (93.64%), which then dropped at sensor 6 (70.83%). For Figure 4.22, the percentage of the total amount of energy at sensor 1 is (97.50%), which then dropped at sensor 6 (73.39%). For Figure 4.23, the percentage of the total amount of energy at sensor 1 is (98.02%), which then dropped at sensor 6 (72.87%). For Figure 4.24, the percentage of the total amount of energy at sensor 1 is (92.08%), which then dropped at sensor 6 (74.17%). In conclusion, it is observed for all tests at shown in Figures (4.16-4.24) that most of the energy is dissipated along the tank.

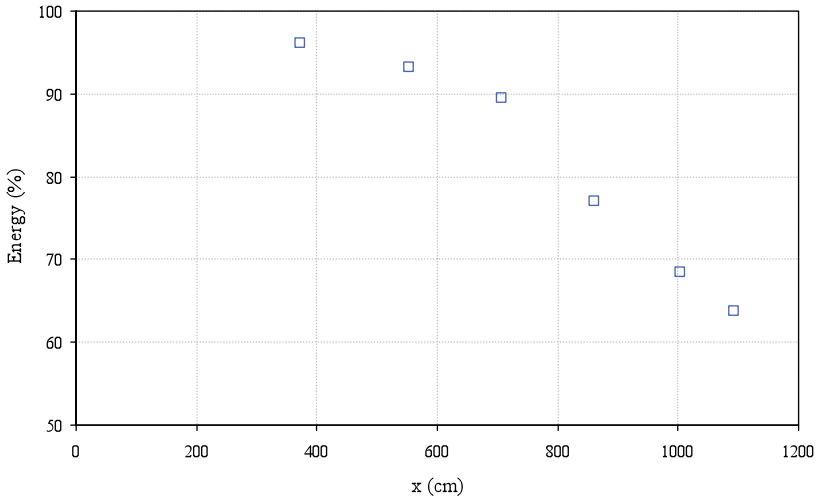

Figure 4.16: The percentage amount of energy of the wave group on the peak region at each sensor by using power spectral density method for test#1 with water depth= 44 cm and mud depth 12 cm, with two short waves (S=2 cm, , σ_1= 10.47 s^{-1} and S=2 cm , σ_2= 9.67 s^{-1}).

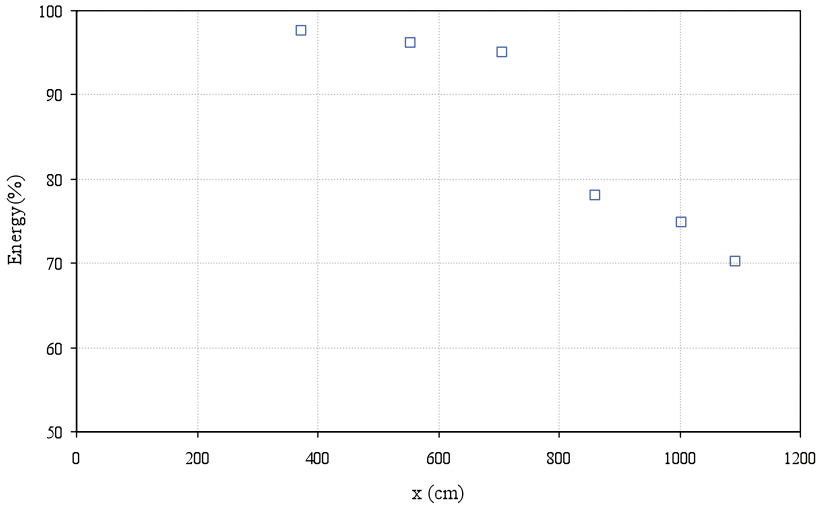

Figure 4.17: The percentage amount of energy of the wave group on the peak region at each sensor by using power spectral density method for test#8 with water depth= 44 cm and mud depth 12 cm, with two short waves (S=2 cm, , σ_1= 10.47 s^{-1} and S=2 cm , σ_2= 9.97 s^{-1}).

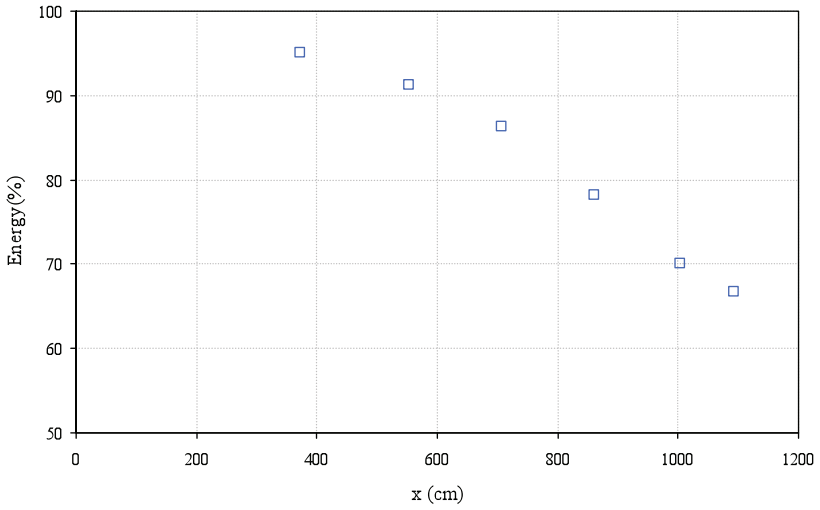

Figure 4.18: The percentage amount of energy of the wave group on the peak region at each sensor by using power spectral density method for test#15 with water depth= 44 cm and mud depth 12 cm, with two short waves (S=2 cm, , σ_1= 10.13 s^{-1} and S=2 cm , σ_2= 9.52 s^{-1}).

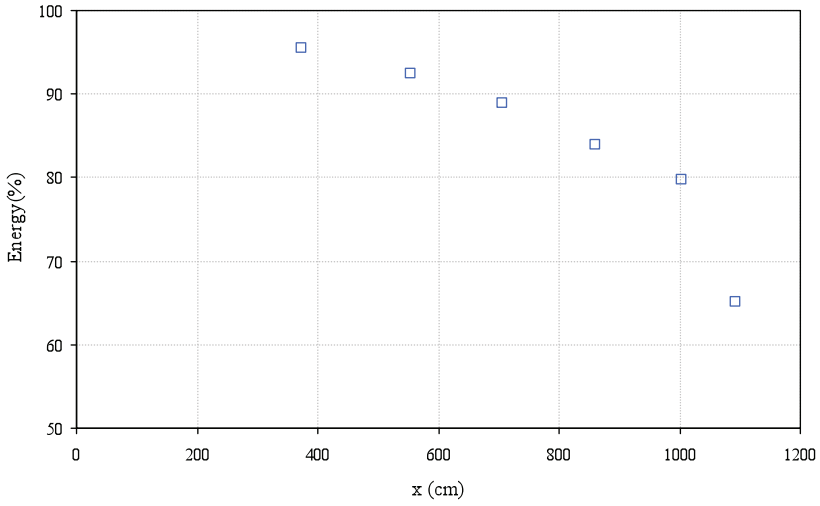

Figure 4.19: The percentage amount of energy of the wave group on the peak region at each sensor by using power spectral density method for test#4 with water depth= 44 cm and mud depth 12 cm, with two short waves (S=2 cm, , σ_1= 10.47 s^{-1} and S=2.2 cm , σ_2= 9.67 s^{-1}).

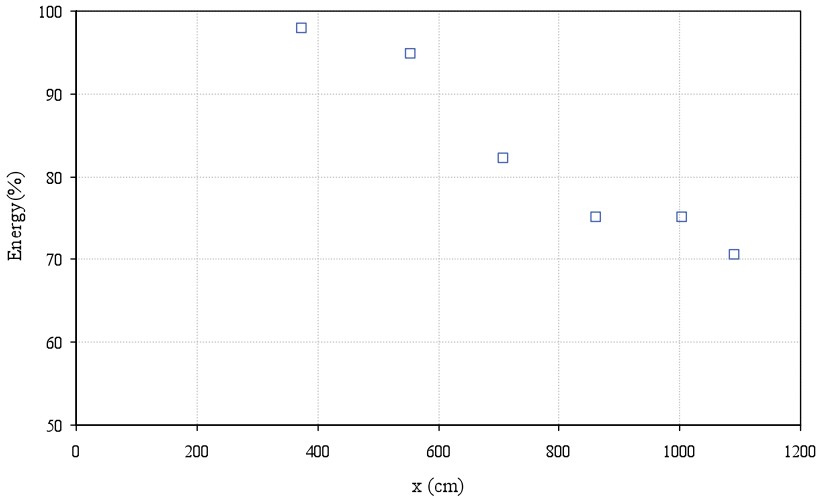

Figure 4.20: The percentage amount of energy of the wave group on the peak region at each sensor by using power spectral density method for test#11 with water depth= 44 cm and mud depth 12 cm, with two short waves (S=2 cm, , σ_1= 10.47 s^{-1} and S=2.2 cm , σ_2= 9.97 s^{-1}).

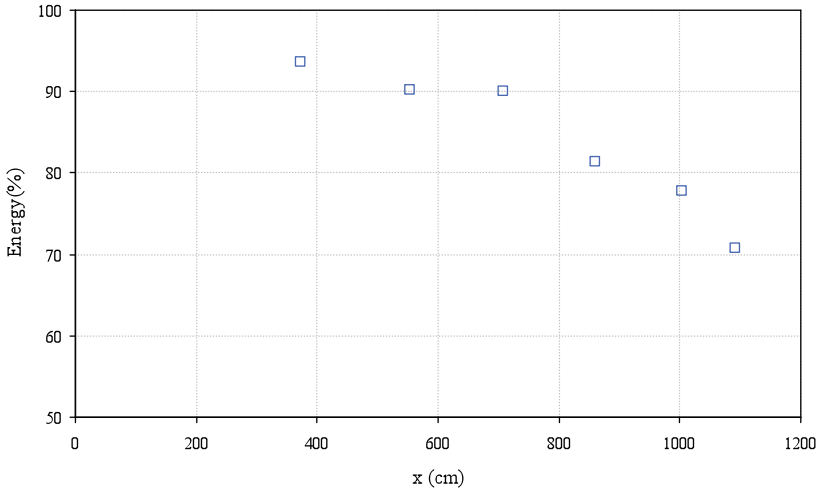

Figure 4.21: The percentage amount of energy of the wave group on the peak region at each sensor by using power spectral density method for test#18 with water depth= 44 cm and mud depth 12 cm, with two short waves (S=2 cm, , σ_1= 10.13 s^{-1} and S=2.2 cm , σ_2= 9.52 s^{-1}).

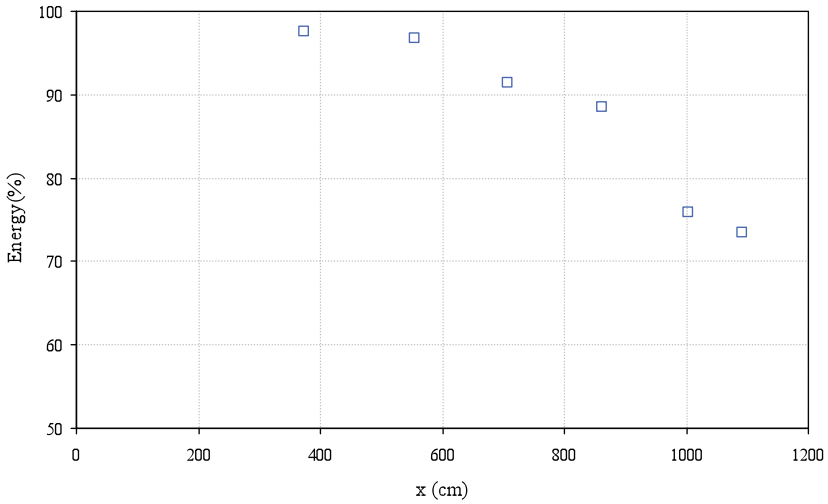

Figure 4.22: The percentage amount of energy of the wave group on the peak region at each sensor by using power spectral density method for test#6 with water depth= 44 cm and mud depth 12 cm, with two short waves (S=2 cm, , σ_1= 10.47 s^{-1} and S=1 cm , σ_2= 9.67 s^{-1}).

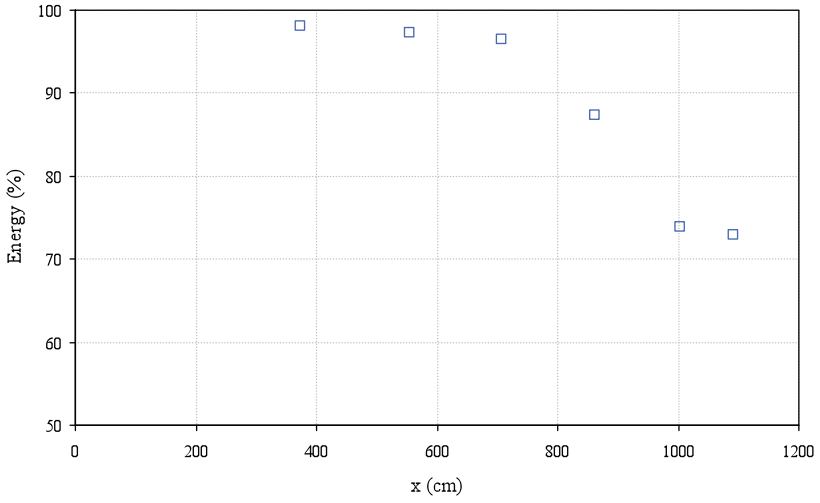

Figure 4.23: The percentage amount of energy of the wave group on the peak region at each sensor by using power spectral density method for test#13 with water depth= 44 cm and mud depth 12 cm, with two short waves (S=2 cm, , σ_1= 10.47 s^{-1} and S=1 cm , σ_2= 9.97 s^{-1}).

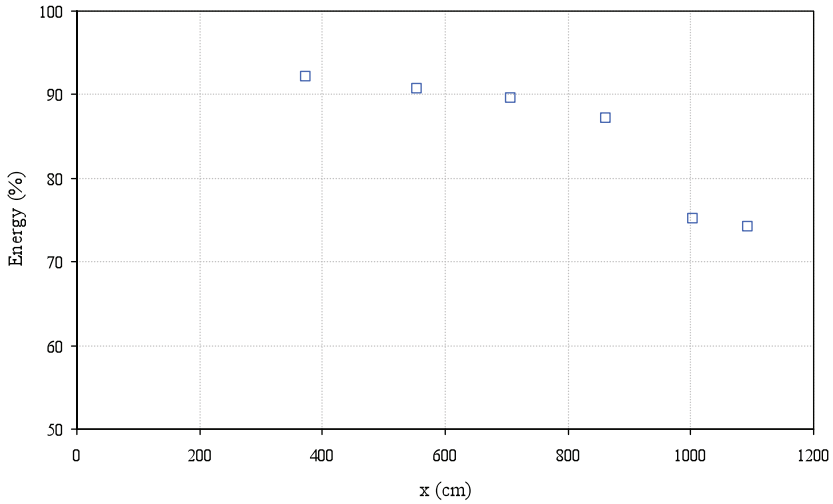

Figure 4.24: The percentage amount of energy of the wave group on the peak region at each sensor by using power spectral density method for test#20 with water depth= 44 cm and mud depth 12 cm, with two short waves (S=2 cm, , σ_1= 10.13 s^{-1} and S=1 cm , σ_2= 9.52 s^{-1}).

In summary, the Power Spectral Density method (PSD) shows the rate of energy is dissipating along the tank for all our experiments. It also calculates the percentage of loss of energy in each sensor. We want to look at the problem in more details and we want to know at each frequency what is the behavior and characteristic of the individual wave.

4.7.2 The Extended Prony Method

The second method in this chapter to analysis the wave group will be the Pronys method. Pronys method will help to zoom in at the problem and will explain more details about each frequency in the wave group and track the amplitude coefficient at each sensor for all experiments. The method extracts the frequencies in each wave

group and estimates the wave amplitude, phase and damping for each wave. Figure (4.25-4.27) presents the results of extended Prony's method for waves with (a_2/a_1) are equal to 1. It is observed that the wave amplitude decay with distance along the tank. In test with frequencies ($\sigma_1 = 10.47$ s^{-1}, $\sigma_2 = 9.67$ s^{-1}) wave amplitude for each frequency decayed with time but in the wave with lower frequency ($\sigma_2 = 9.67$ s^{-1}) more than the higher frequency ($\sigma_1 = 10.47$ s^{-1}). This observation was also found in tests with frequencies ($\sigma_1 = 10.47$ s^{-1}, $\sigma_2 = 9.97$ s^{-1}) and ($\sigma_1 = 10.13$ s^{-1}, $\sigma_2 = 9.52$ s^{-1}) but the difference in decay in test ($\sigma_1 = 10.47$ s^{-1}, $\sigma_2 = 9.97$ s^{-1}) is less that ($\sigma_1 = 10.47$ s^{-1}, $\sigma_2 = 9.67$ s^{-1}) and it is almost the same in test ($\sigma_1 = 10.13$ s^{-1}, $\sigma_2 = 9.52$ s^{-1}).

Comparing the two tests with similar $\sigma_1 = 10.47$ s^{-1} and different σ_2, we found that the wave with $\sigma_2 = 9.67$ s^{-1} and $\sigma_2 = 9.97$ s^{-1} showed low damping. Also it observed that amplitude of the different of frequency (σ_1-σ_2) shows a strong damping while the sum of frequency (σ_1+σ_2) gives low damping values becuase the waves are short. Figure (4.28-4.30) presents the same tests but with (a_2/a_1) is equal to 1.1. The result shows almost the same as in tests with $a_2/a_1 = 1$. Interestingly, tests with $a_2/a_1 = 0.5$ shows that the bigger wave dies faster than smaller wave (see Figure 4.31-4.33).

From Prony's method we measured the damping rate for each indivitual wave. The experimens showed high damping values compared to the Power Spectrum Density method (PSD). Prony's method proved that waves propagating over mud bottom in

deep water caused the energy to dissipate. These waves have been tested individually and showed high damping.

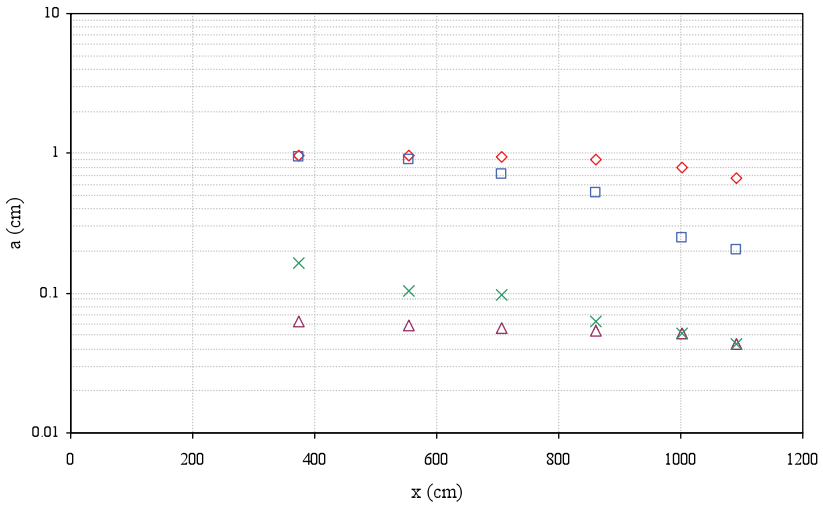

Figure 4.25: The wave amplitude at a distance from the wave maker (x) by using Prony method for test#1 with water depth= 44 cm and mud depth 12 cm, with two short waves (S=2 cm, σ_1= 10.47 s^{-1} and S=2 cm , σ_2= 9.67 s^{-1}) $\sigma_1(\Diamond)$, $\sigma_2(\square)$, $\sigma_1+\sigma_2(\triangle)$ and σ_1-$\sigma_2(\times)$.

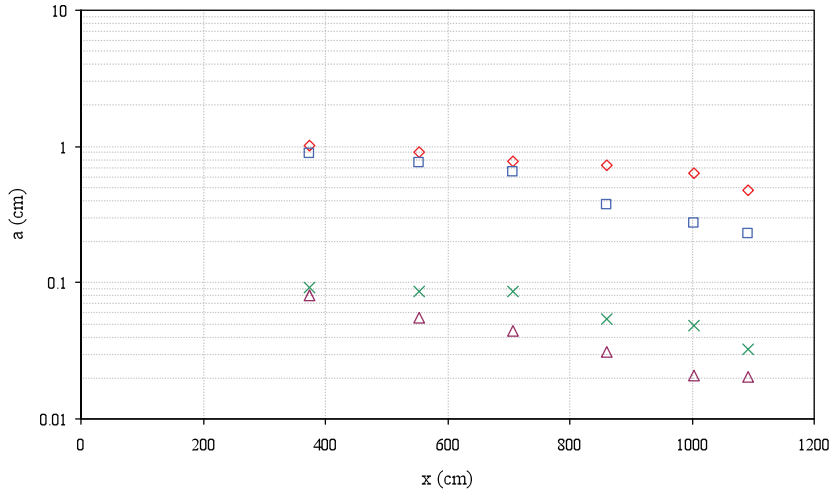

Figure 4.26: The wave amplitude at a distance from the wave maker (x) by using Prony method for test#8 with water depth= 44 cm and mud depth 12 cm, with two short waves (S=2 cm, σ_1= 10.47 s^{-1} and S=2 cm , σ_2= 9.97 s^{-1}) $\sigma_1(\Diamond)$, $\sigma_2(\square)$, $\sigma_1+\sigma_2(\triangle)$ and σ_1-$\sigma_2(\times)$.

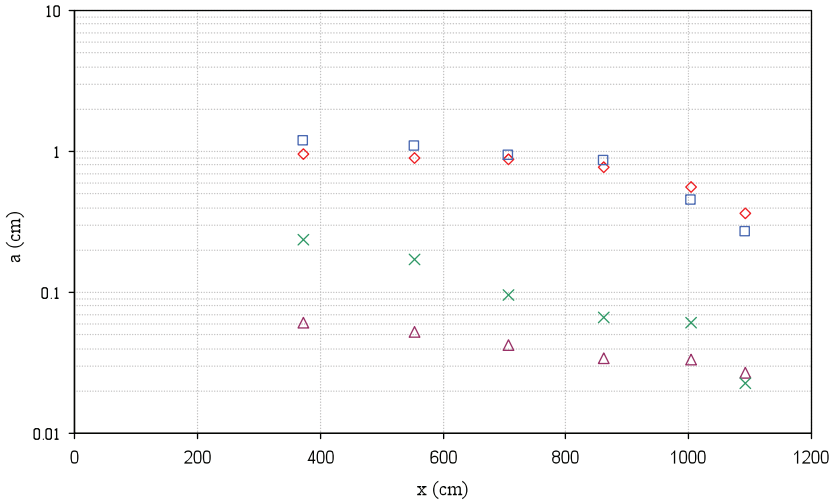

Figure 4.27: The wave amplitude at a distance from the wave maker (x) by using Prony method for test#15 with water depth= 44 cm and mud depth 12 cm, with two short waves (S=2 cm, σ_1= 10.13 s^{-1} and S=2 cm , σ_2= 9.52 s^{-1}) $\sigma_1(\Diamond)$, $\sigma_2(\square)$,$\sigma_1+\sigma_2(\triangle)$ and σ_1-$\sigma_2(\times)$.

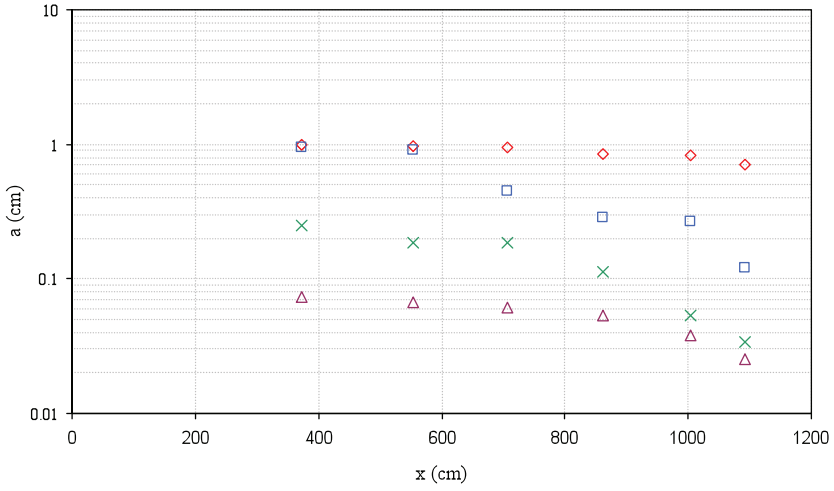

Figure 4.28: The wave amplitude at a distance from the wave maker (x) by using Prony method for test#4 with water depth= 44 cm and mud depth 12 cm, with two short waves (S=2 cm, σ_1= 10.47 s^{-1} and S=2.2 cm , σ_2= 9.67 s^{-1}) $\sigma_1(\Diamond)$, $\sigma_2(\square)$, $\sigma_1+\sigma_2(\triangle)$ and σ_1-$\sigma_2(\times)$.

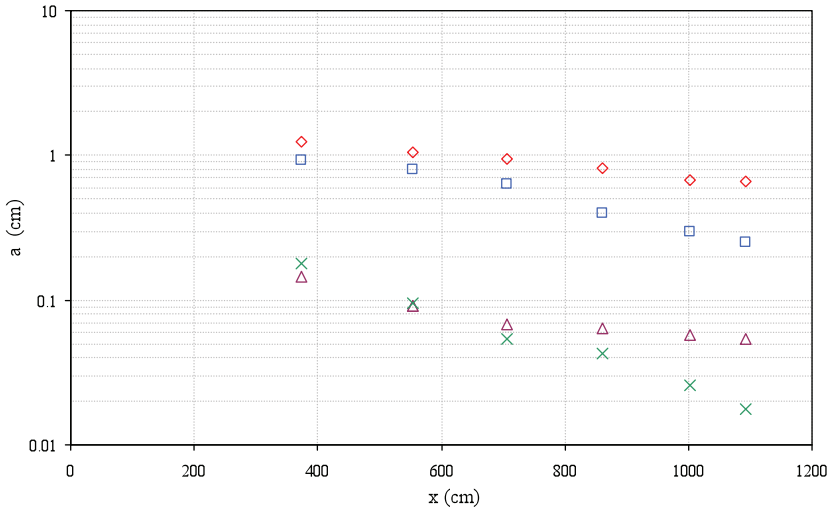

Figure 4.29: The wave amplitude at a distance from the wave maker (x) by using Prony method for test#11 with water depth= 44 cm and mud depth 12 cm, with two short waves (S=2 cm, σ_1= 10.47 s^{-1} and S=2.2 cm , σ_2= 9.97 s^{-1}) $\sigma_1(\Diamond)$, $\sigma_2(\square)$, $\sigma_1+\sigma_2(\triangle)$ and σ_1-$\sigma_2(\times)$.

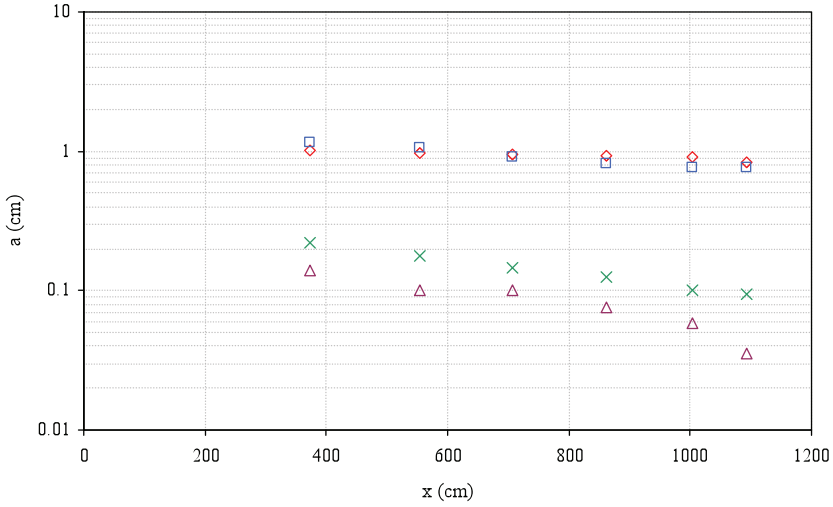

Figure 4.30: The wave amplitude at a distance from the wave maker (x) by using Prony method for test#18 with water depth= 44 cm and mud depth 12 cm, with two short waves (S=2 cm, σ_1= 10.13 s^{-1} and S=2.2 cm , σ_2= 9.52 s^{-1}) $\sigma_1(\Diamond)$, $\sigma_2(\square)$, $\sigma_1+\sigma_2(\triangle)$ and σ_1-$\sigma_2(\times)$.

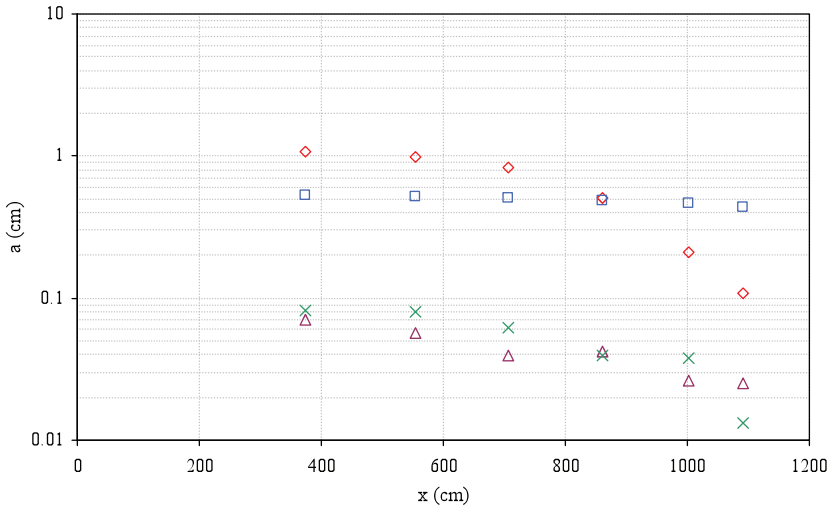

Figure 4.31: The wave amplitude at a distance from the wave maker (x) by using Prony method for test#6 with water depth= 44 cm and mud depth 12 cm, with two short waves (S=2 cm, σ_1= 10.47 s^{-1} and S=1 cm , σ_2= 9.67 s^{-1}) $\sigma_1(\Diamond)$, $\sigma_2(\square)$, $\sigma_1+\sigma_2(\triangle)$ and σ_1-$\sigma_2(\times)$.

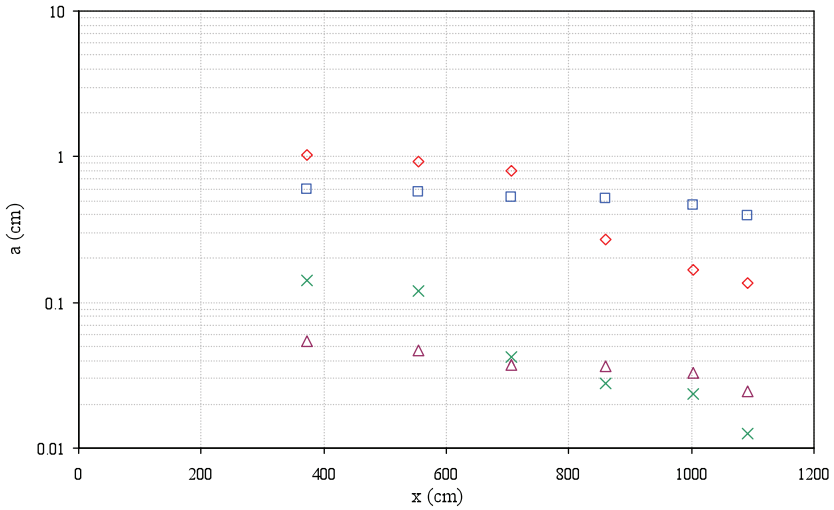

Figure 4.32: The wave amplitude at a distance from the wave maker (x) by using Prony method for test#13 with water depth= 44 cm and mud depth 12 cm, with two short waves (S=2 cm, σ_1= 10.47 s^{-1} and S=1 cm , σ_2= 9.97 s^{-1}) $\sigma_1(\Diamond)$, $\sigma_2(\square)$, $\sigma_1+\sigma_2(\triangle)$ and σ_1-$\sigma_2(\times)$.

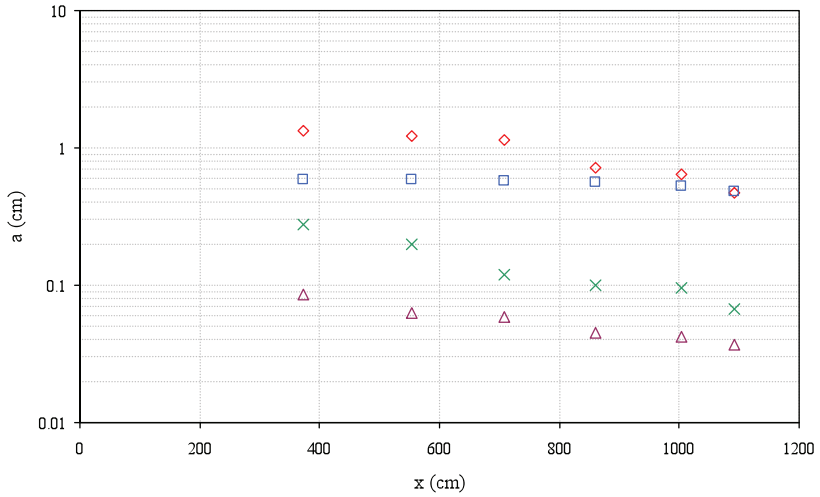

Figure 4.33: The wave amplitude at a distance from the wave maker (x) by using Prony method for test#20 with water depth= 44 cm and mud depth 12 cm, with two short waves (S=2 cm, σ_1= 10.13 s^{-1} and S=1 cm , σ_2= 9.52 s^{-1}) $\sigma_1(\Diamond)$, $\sigma_2(\square)$, $\sigma_1+\sigma_2(\triangle)$ and σ_1-$\sigma_2(\times)$.

By using the Prony's method all the damping values were measured for the frequencies (σ_1, σ_2, σ_1-σ_2, and $\sigma_1+\sigma_2$) and were summarized in Table 4.3.

We show from Table 4.3 the attenuation coefficient for all the wave group tests for the frequencies (σ_1, σ_2, σ_1-σ_2, and $\sigma_1+\sigma_2$) by using Prony's method.

Now we want to test the long bound wave in a theoretical model since it caused the damping. Since the long bound wave exerts pressure the bottom, we will use a model for single wave train, but with the characteristics of the bound long wave. We want to look at the long bound wave and compare the measured attenuation coefficients with the visco-elastic model of MacPherson (1980) and the viscous model of Dalrymple and Liu (1978). For the visco-elastic model we used the the viscosity, elasticity and density parameters of mud from Nouri (2013). The water density=

Table 4.3: Experimental attenuation coefficients for all the wave group tests by using Prony method for the frequencies (σ_1, σ_2, σ_1-σ_2, and σ_1+σ_2) and coefficient of determination for all the data.

Test #	Stroke (S_1) (cm)	Period (T_1) (s)	Stroke (S_2) (cm)	Period (T_2) (s)	Water depth (h) (cm)	k_i for σ_1 (m^{-1})	k_i for σ_2 (m^{-1})	k_i for σ_1-σ_2 (m^{-1})	k_i for σ_1+σ_2 (m^{-1})	R^2
1	2	0.6	2	0.65	44	0.015	0.013	0.031	0.002	0.957
4	2	0.6	2.2	0.65	44	0.010	0.017	0.028	0.003	0.988
6	2	0.6	1	0.65	44	0.012	0.012	0.022	0.008	0.988
8	2	0.6	2	0.63	44	0.011	0.011	0.021	0.007	0.956
11	2	0.6	2.2	0.63	44	0.010	0.012	0.031	0.009	0.890
13	2	0.6	1	0.63	44	0.011	0.015	0.024	0.001	0.988
15	2	0.62	2	0.66	44	0.012	0.014	0.029	0.004	0.988
18	2	0.62	2.2	0.66	44	0.010	0.012	0.019	0.002	0.928
20	2	0.62	1	0.66	44	0.009	0.015	0.024	0.001	0.977

1000 (kg/m^3), water depth 0.44 m, upper fluid kinematic viscosity = 1*10^{-6} (m^2/s), mud density= 1300 (kg/m^3), lower fluid (mud) kinematic viscosity= 0.006281 (m^2/s), the mud elasticity= 82.97 pa, the mud viscosity= 421.66 pa. For the viscous model the viscosity= 421.66 pa. Table 4.4 shows the attenuation coefficient for the Prony method, visco-elastic model and viscous model for the long bound wave.

The attenuation coefficient results in Table 4.4 shows that visco-elastic model applied to the bound long wave agrees pretty well with the measured data. However, with the viscous model, the results shows much lower attenuation values compared with Prony method.

4.8 Conclusions

In this chapter, a series of experiments were conducted in a wave tank to examine the damping of waves in deep water. The individual short wave in deep water showed no damping because the wave pressure does not extend to the bottom. However, wave groups, which are two waves superimposed and creates a long bound wave that has a length long enough to extend the wave pressure to the bottom and cause the energy to dissipate. The experiment tests described the energy dissipation of wave groups in deep water. Three types of tests were used to measure the energy dissipation. These types were grouped by the ratio of amplitudes of the two short waves (a_2/a_1) is equal to 0.5, 1, 1.1.

Table 4.4: The measured and calculated attenuation coefficients for the bound long wave of all the wave group tests by using Prony method, MacPherson (1980) and Dalrymple and Liu (1978).

Test #	k_i for σ_1-σ_2 (m^{-1}) Prony method	k_i for σ_1-σ_2 (m^{-1}) MacPherson (1980)	k_i for σ_1-σ_2 (m^{-1}) Dalrymple and Liu (1978)
1	0.031	0.023	0.002
4	0.028	0.028	0.002
6	0.022	0.015	0.001
8	0.021	0.025	0.002
11	0.031	0.027	0.002
13	0.024	0.017	0.001
15	0.029	0.025	0.002
18	0.019	0.022	0.002
20	0.019	0.016	0.001

The tests were analyzed by two methods to determine the energy loss. The first method was the Power Spectrum Density method (PSD), which calculates the amount of energy in the spectrum along the tank. The results showed that the energy dissipated along the tank and showed high damping values. From this method we were able to measure the damping for the total waves in the group. To look at the damping for each individual wave, the second method to analyze the data was the extended Prony method. This method extracts the frequencies from the signals and measured the amplitude of each wave. The results showed that the amplitude is decreased along the tank which means that the energy is dissipated due the wave pressure that extended to the bottom which caused by the long bound waves that associated with the wave groups. High damping rates were observed compared to the Power Spectrum Density method.

Finally, measured the attenuation coefficient by using Prony method and the results showed that the long bound wave have high attenuation coefficient. We also compared the attenuation coefficient for th bound long wave of Prony method with the viscous and visco-elastic models. The results showed that visco-elastic model works pretty well with the measured data than the viscous model.

Chapter 5

The non-linear interaction between two wave trains in deep water

5.1 Introduction

Longuet-Higgins and Stewart (1960) have first carried out a systematic nonlinear evaluation of two wave trains travelling in the same direction using the Stokes' method of approximation to second order. They calculated the change in wavelength and amplitude arising from non-linear interactions between the two wave trains. Using this, they concluded that the contraction of the particles in longer wave causes the change in wave length of short waves on the crests of longer waves.

Longuet-Higgins (1950) studied the relationship of the second order bound long wave pressure variations and 'microseisms', which are faint earth tremor caused by

water waves. He derived the expression of the bottom pressure variation for two short wave train with the same wavelength and propagating in the exactly opposite direction. He concluded that microseisms are caused by the pressure variation of the standing surface water waves, even in deep water. In this chapter, we carry out the same calculation using Stokes' method of approximation to the second order, for any two wave trains propagating at arbitrary angles with respect to the coordinate direction, determining the bottom pressure and bottom horizontal velocity.

Phillips (1960) also studied the non-linear interactions between pairs of intersecting gravity wave trains of arbitrary wavelength and direction on surface of deep water waves. He examined in detail the dynamical interactions between pairs and triads of wave components with different wavelengths and directions. He applied the Fourier-Stieltjes transform of surface displacement to study the energy transfer that occurs between waves. He rigorously developed the basic equations governing the surface displacement for deep water waves to third order. He concluded that even though the tertiary interactions among wave components contain algebraically small perturbation terms in comparison to secondary interactions, they have a more profound dynamical effect because of resonant wave numbers with amplitude growing with time. Subsequently, Longuet-Higgins and Stewart (1962) also studied the second-order currents and changes in mean surface level caused by gravity waves of non-uniform amplitude and interpreted the effects in terms of radiation stresses in waves.

5.2 Determination of wave profile

Here the interaction of two waves derived by the Stokes method Stokes (1847), which is based on potentail flow is presented. The motion in a real fluid does not remain irrotational after it is generated from rest, and a second-order vorticity penetrates the interior Longuet-Higgins (1953). Since, we shall be concerned only with the oscillatory part of the motion, it is therefore sufficient to assume that velocity can be represented as gradient of scalar potential ϕ. Longuet-Higgins and Stewart (1960) have evaluated the interaction between two waves propagating in the same direction using the Stokes wave theory to second order and perturbation expansion. The second order surface elevation, $\eta^{(2)}$, for the case of infinte depth is given in equation (5.1). We now apply the same method to evaluate the surface elevation due to interaction of two waves propagating at some arbitrary angle with each other.

$$\eta^{(2)} = -\frac{1}{2}a_1^2 k_1 \sin 2\psi_1 - \frac{1}{2}a_2^2 k_2 \sin 2\psi_2 - a_1 a_2 \left(k_1 \cos\psi_1 \cos\psi_2 - k_2 \sin\psi_1 \sin\psi_2\right) \quad (5.1)$$

5.2.1 Infinite Depth

The fluid described using the rectangular axes of x, y, z, and are defined as follows: the x-axis is horizontal to the mean surface, xy- plane is horizontal, and coinciding with fluid surface in equilibrium and z-axis is vertically upwards (Figure 5.1). The velocity vector, pressure, density and surface elevation are denoted by u, p, ρ and η respectively.

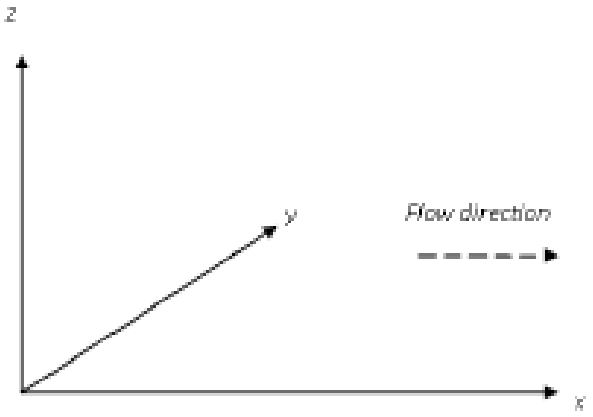

Figure 5.1: Orientation of axes and the direction of flow.

With the assumption of irrotational motion and an incompressible fluid a velocity potential exists

$$u = \nabla\phi \tag{5.2}$$

and it is governed by

$$\nabla^2\phi = 0 \tag{5.3}$$

The unsteady Bernoulli equation is given as:

$$\frac{p}{\rho} + gz + \frac{1}{2}|u|^2 + \frac{\partial\phi}{\partial t} = 0 \tag{5.4}$$

The dynamic and kinematic surface boundary conditions are given by

$$\left(\frac{p_0}{\rho} + gz + \frac{1}{2}|u|^2 + \frac{\partial\phi}{\partial t}\right)_{z=\eta} = 0 \tag{5.5}$$

$$\left(\frac{\partial \eta}{\partial t} - \frac{\partial \phi}{\partial t} + \frac{\partial \phi}{\partial x}\frac{\partial \eta}{\partial x} + \frac{\partial \phi}{\partial y}\frac{\partial \eta}{\partial y}\right)_{z=\eta} = 0 \tag{5.6}$$

and for infinite depth,

$$\lim_{z\to-\infty} \nabla\phi = 0 \tag{5.7}$$

p_0 denotes the pressure at the free surface and is assumed to be zero (gage pressure).

Expanding these conditions at $z = \eta$ in a Taylor series about z, we get;

$$g\eta + \left(\frac{1}{2}|u|^2 + \frac{\partial \phi}{\partial t}\right)_{z=0} + \eta\left[\frac{\partial}{\partial z}\left(\frac{1}{2}|u|^2 + \frac{\partial \phi}{\partial t}\right)\right]_{z=0} + ... = 0 \tag{5.8}$$

$$\frac{\partial \eta}{\partial t} + \left(\frac{\partial \phi}{\partial x}\frac{\partial \eta}{\partial x} + \frac{\partial \phi}{\partial y}\frac{\partial \eta}{\partial y} - \frac{\partial \phi}{\partial z}\right)_{z=0} + \eta\left[\frac{\partial}{\partial z}\left(\frac{\partial \phi}{\partial x}\frac{\partial \eta}{\partial x} + \frac{\partial \phi}{\partial y}\frac{\partial \eta}{\partial y} - \frac{\partial \phi}{\partial z}\right)\right]_{z=0} + ... = 0 \tag{5.9}$$

Now assuming perturbation expansions of the form;

$$u = \epsilon u^{(1)} + \epsilon^2 u^{(2)} + ... \tag{5.10}$$

$$\phi = \epsilon \phi^{(1)} + \epsilon^2 \phi^{(2)} + ... \tag{5.11}$$

$$\eta = \epsilon \eta^{(1)} + \epsilon^2 \eta^{(2)} + ... \tag{5.12}$$

$$\frac{p}{\rho} + gz = \epsilon p^{(1)} + \epsilon^2 p^{(2)} + ... \tag{5.13}$$

where ϵ is a small parameter and substituting the above expansions in (5.1), (5.3), (5.4) and collecting the first order terms, we obtain a boundary value problem

$$u^{(1)} = \nabla\phi^{(1)} \tag{5.14}$$

$$\frac{p^{(1)}}{\rho} + \frac{\partial \phi^{(1)}}{\partial t} = 0 \tag{5.15}$$

$$\nabla^2\phi^{(1)} = 0 \tag{5.16}$$

$$\lim_{z\to-\infty}\nabla\phi^{(1)} = 0 \tag{5.17}$$

$$g\eta^{(1)} + \left(\frac{\partial\phi^{(1)}}{\partial t}\right)_{z=0} = 0, t = 0 \tag{5.18}$$

$$\frac{\partial\eta^{(1)}}{\partial t} - \left(\frac{\partial\phi^{(1)}}{\partial z}\right)_{z=0} = 0.z = 0 \tag{5.19}$$

Eliminating $\eta^{(1)}$ from equations (5.17) and (5.18) we get the linear combined free surface boundary condition;

$$\left(\frac{\partial^2\phi^{(1)}}{\partial t^2} + g\frac{\partial\phi^{(1)}}{\partial z}\right)_{z=0} = 0 \tag{5.20}$$

The solution of these equations, for two progressive surface wave trains of wave numbers k_1 and k_2 and with angles α and β to the x-axis (Figure 5.2) is

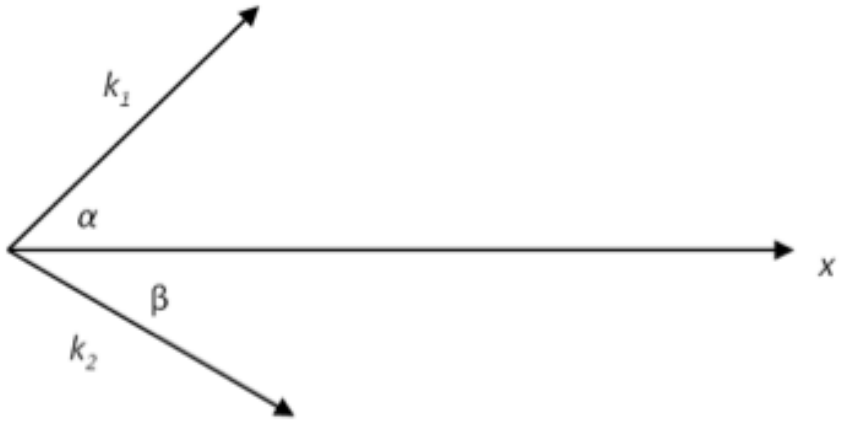

Figure 5.2: Surface waves and their direction with respect to the x-axis.

$$\begin{aligned}\phi^{(1)} &= A_1 e^{k_1 z}\cos\left(k_1 x\,\cos\alpha + k_1 y\,\sin\alpha - \sigma_1 t + \theta_1\right)\\ &\quad + A_2 e^{k_2 z}\cos\left(k_2 x\,\cos\beta + k_2 y\,\sin\beta - \sigma_2 t + \theta_2\right)\end{aligned} \tag{5.21}$$

which satisfied the Laplace equation in (5.16), where $A_1, A_{2,}\, \sigma_1, \sigma_2, k_1, k_2$ are constants θ_1 and θ_2 are the phase shift of the first and second waves. Now from equation (5.19); we get

$$\sigma_1^2 = gk_1\ ,\ \sigma_2^2 = gk_2 \tag{5.22}$$

which related each wave's angular frequency (σ) to its wave number (k). Substituting and solving the free surface elevation (5.18) yields,

$$\eta^{(1)} = a_1\sin\left(k_1 x\,\cos\alpha + k_1 y\,\sin\alpha - \sigma_1 t + \theta_1\right) + a_2\sin\left(k_2 x\,\cos\beta + k_2 y\,\sin\beta - \sigma_2 t + \theta_2\right) \tag{5.23}$$

where

$$a_1 = -\frac{A_1 k_1}{\sigma_1},\quad a_2 = -\frac{A_2 k_2}{\sigma_2} \tag{5.24}$$

where θ_1 and θ_2 are the phase shift of the first and second waves. Proceeding now to the second approximation; we get

$$u^{(2)} = \nabla\phi^{(2)} \tag{5.25}$$

$$\frac{p^{(2)}}{\rho} + \frac{1}{2}|u^{(1)^2}| + \frac{\partial\phi^{(2)}}{\partial t} = 0 \tag{5.26}$$

$$\nabla^2\phi^{(2)} = 0 \tag{5.27}$$

$$\lim_{z\to-\infty}\nabla\phi^{(2)} = 0 \tag{5.28}$$

$$g\eta^{(2)} + \left(\frac{1}{2}|u^{(1)^2}| + \frac{\partial\phi^{(2)}}{\partial t} + \eta^{(1)}\frac{\partial^2\phi^{(1)}}{\partial z\partial t}\right)_{z=0} = 0 \tag{5.29}$$

$$\frac{\partial\eta^{(2)}}{\partial t} + \left(\frac{\partial\phi^{(1)}}{\partial x}\frac{\partial\eta^{(1)}}{\partial x} + \frac{\partial\phi^{(1)}}{\partial y}\frac{\partial\eta^{(1)}}{\partial y} - \frac{\partial\phi^{(2)}}{\partial z} + \eta^{(1)}\frac{\partial^2\phi^{(1)}}{\partial z^2}\right)_{z=0} = 0 \tag{5.30}$$

Eliminating $\eta^{(2)}$from the above equations, we get the second order CFSBC;

$$\left(\frac{\partial^2\phi^{(2)}}{\partial t^2} + g\frac{\partial\phi^{(2)}}{\partial z}\right)_{z=0} = -\left[\frac{\partial}{\partial t}\left(u^{(1)^2}\right) + \eta^{(1)}\frac{\partial}{\partial z}\left(\frac{\partial^2\phi^{(1)}}{\partial t^2} + g\frac{\partial\phi^{(1)}}{\partial z}\right)\right]_{z=0} \tag{5.31}$$

Substituting the first order solution into the right hand side, the above equation simplifies to

$$\frac{\partial^2\phi^{(2)}}{\partial t^2} + g\frac{\partial\phi^{(2)}}{\partial z} = -\frac{\partial}{\partial t}\left(u^{(1)^2}\right) \tag{5.32}$$

The solution for $\phi^{(2)}$is given by ;

$$\begin{aligned}\phi^{(2)} &= (A_1A_2k_1k_2/2\sigma_2)\, e^{|\mathbf{k_1}-\mathbf{k_2}|z}\left[\left(\frac{\sigma_2-\sigma_1}{\sigma_2+\sigma_1}\right)\right. \\ &\left.(1-\cos(\alpha-\beta))\sin(\psi_1+\psi_2) - (1+\cos(\alpha-\beta))\sin(\psi_1-\psi_2)\right] + Gt\end{aligned} \tag{5.33}$$

where G is an arbitrary constant that is determined by the condition that the origin is at the mean surface level and ψ_1 and ψ_2 are as follows,

$$\psi_1 = k_1x\,\cos\alpha + k_1y\,\sin\alpha - \sigma_1t + \theta_1 \tag{5.34}$$

$$\psi_2 = k_2x\,\cos\beta + k_2y\,\sin\beta - \sigma_2t + \theta_2 \tag{5.35}$$

Substituting back in equation (5.28) we get $\eta^{(2)}$ as:

$$\begin{aligned}\eta^{(2)} &= -\frac{1}{2}a_1^2k_1\cos 2\psi_1 - \frac{1}{2}a_2^2k_2\cos 2\psi_2 \\ &\quad +\frac{1}{2}a_1a_2\big[\,(k_1\,(\cos\,(\alpha-\beta)-2)-k_2)\cos\,(\psi_1+\psi_2) \\ &\quad +(k_2-k_1\cos\,(\alpha-\beta))\cos\,(\psi_1-\psi_2)\,\big] \qquad (5.36)\end{aligned}$$

Thus if we absorb the small parameter ϵ into a_1, a_2 by writing $\epsilon = 1$, we get

$$\begin{aligned}\eta &= \left(a_1\sin\psi_1 - \frac{1}{2}a_1^2k_1\cos 2\psi_1\right) + \left(a_2\sin\psi_2 - \frac{1}{2}a_2^2k_2\cos 2\psi_2\right) \\ &\quad +\frac{1}{2}a_1a_2\big[\,(k_1\,(\cos\,(\alpha-\beta)-2)-k_2)\cos\,(\psi_1+\psi_2) \\ &\quad +(k_2-k_1\cos\,(\alpha-\beta))\cos\,(\psi_1-\psi_2)\,\big] + 0(a_1^3, a_2^3) \qquad (5.37)\end{aligned}$$

The first and second parenthetical terms in equation (5.37) are the first and second order incident wave solutions, while the a_1a_2 waves (σ_1+σ_2) and (σ_1-σ_2) are the result of the interaction. These are the sum and difference waves.

5.2.2 Finite depth

We now suppose that the water is of finite depth h and k_1h, k_2h are not necessarily much large. The bottom boundary condition is that the vertical velocity of the incident waves vanishes and is given by,

$$\left(\frac{\partial\phi}{\partial z}\right)_{z=-h} = 0 \qquad (5.38)$$

and so

$$\left(\frac{\partial\phi^{(1)}}{\partial z}\right)_{z=-h} = \left(\frac{\partial\phi^{(2)}}{\partial z}\right)_{z=-h} = 0 \qquad (5.39)$$

To have the elevation of free surface given by ;

$$\eta^{(1)} = a_1 \sin\psi_1 + a_2 \sin\psi_2 \tag{5.40}$$

in the first approximation we must have;

$$\phi^{(1)} = -\frac{a_1\sigma_1}{k_1 \sinh k_1 h}\cosh k_1 (z+h)\cos\psi_1 - \frac{a_2\sigma_2}{k_2 \sinh k_2 h}\cosh k_2 (z+h)\cos\psi_2 \tag{5.41}$$

where the dispersion relationship are:

$$\sigma_1^2 = gk_1 \tanh k_1 h \ , \ \sigma_2^2 = gk_2 \tanh k_2 h \tag{5.42}$$

The second approximation is evaluated in the same manner as before. The algebra may be simplified by omitting all nonlinear terms except those involving the product $a_1 a_2$ in which we are interested. Thus, we obtain the surface condition as follows.

$$\frac{\partial^2\phi^{(2)}}{\partial t^2} + g\frac{\partial\phi^{(2)}}{\partial z} = A\ \sin(\psi_1 - \psi_2) + B\ \sin(\psi_1 + \psi_2) \tag{5.43}$$

where

$$\begin{aligned} A &= -\frac{1}{2}a_1 a_2 \big[2\sigma_1\sigma_2\big(\sigma_1 - \sigma_2\big)\left(1 + \alpha_1\alpha_2\cos(\alpha - \beta)\right) \\ &\quad +\sigma_1^3\left(\alpha_1^2 - 1\right) - \sigma_2^3\left(\alpha_2^2 - 1\right)\big] \end{aligned} \tag{5.44}$$

$$\begin{aligned} B &= -\frac{1}{2}a_1 a_2 \big[2\sigma_1\sigma_2\big(\sigma_1 + \sigma_2\big)\left(1 - \alpha_1\alpha_2\cos(\alpha - \beta)\right) \\ &\quad -\sigma_1^3\left(\alpha_1^2 - 1\right) - \sigma_2^3\left(\alpha_2^2 - 1\right)\big] \end{aligned} \tag{5.45}$$

here

$$\alpha_1 = \coth\ k_1 h\ , \alpha_2 = \coth\ k_2 h \tag{5.46}$$

The solution of the above equation and satisfying the boundary condition (5.37) is;

$$\begin{aligned}\phi^{(2)} &= \frac{A\,\cosh\left(|\mathbf{k_1}-\mathbf{k_2}|\right)(z+h)\sin\left(\psi_1-\psi_2\right)}{-\left(\sigma_1-\sigma_2\right)^2\cosh\left(|\mathbf{k_1}-\mathbf{k_2}|\right)h\;+g\,|\mathbf{k_1}-\mathbf{k_2}|\sinh\left(|\mathbf{k_1}-\mathbf{k_2}|\right)h} \\ &+\frac{B\,\cosh\left(|\mathbf{k_1}+\mathbf{k_2}|\right)(z+h)\sin\left(\psi_1+\psi_2\right)}{-\left(\sigma_1+\sigma_2\right)^2\cosh\left(|\mathbf{k_1}+\mathbf{k_2}|\right)h\;+g\,|\mathbf{k_1}+\mathbf{k_2}|\sinh\left(|\mathbf{k_1}+\mathbf{k_2}|\right)h} \quad (5.47)\end{aligned}$$

Substituing $\phi^{(2)}$ in equation (5.28) we get;

$$g\eta^{(2)} = \frac{1}{2}a_1a_2\left[C\;\cos\left(\psi_1-\psi_2\right)-D\;\cos\left(\psi_1+\psi_2\right)\right] \quad (5.48)$$

where

$$\begin{aligned}C &= \frac{-A\left(\sigma_1-\sigma_2\right)\left(\alpha_1\alpha_2-1\right)}{\sigma_1^2\left(\alpha_1^2-1\right)-2\sigma_1\sigma_2\left(\alpha_1\alpha_2-1\right)+\sigma_2^2\left(\alpha_2^2-1\right)} \\ &+\left(\sigma_1^2+\sigma_2^2\right)-\sigma_1\sigma_2\left(\alpha_1\alpha_2\cos\left(\alpha-\beta\right)+1\right) \quad (5.49)\end{aligned}$$

$$\begin{aligned}D &= \frac{-B\left(\sigma_1+\sigma_2\right)\left(\alpha_1\alpha_2+1\right)}{\sigma_1^2\left(\alpha_1^2-1\right)-2\sigma_1\sigma_2\left(\alpha_1\alpha_2+1\right)+\sigma_2^2\left(\alpha_2^2-1\right)} \\ &+\left(\sigma_1^2+\sigma_2^2\right)+\sigma_1\sigma_2\left(1-\alpha_1\alpha_2\cos\left(\alpha-\beta\right)\right) \quad (5.50)\end{aligned}$$

Absorbing the small parameter ϵ into a_1, a_2 by writing $\epsilon = 1$, we have

$$\begin{aligned}\eta &= a_1\sin\psi_1+a_2\sin\psi_2+\frac{1}{2}\frac{a_1a_2}{g}\big[C\;\cos\left(\psi_1-\psi_2\right) \\ &-D\;\cos\left(\psi_1+\psi_2\right)\big]+0(a_1^2,a_2^2) \quad (5.51)\end{aligned}$$

We can now find the pressure at the bottom $z = -h$ for the sum and difference waves, using equation (5.26). If k_1h, k_2h are sufficiently large (deep water), then $\alpha_1 = \coth\ k_1h \to 1$, $\alpha_2 = \coth\ k_2h \to 1$ we get,

$$\begin{aligned}\frac{p^{(2)}}{\rho} &= \frac{a_1a_2\sigma_1\sigma_2\left(\sigma_1-\sigma_2\right)^2\left(1+\cos\left(\alpha-\beta\right)\right)\cos\left(\psi_1-\psi_2\right)}{\left(\sigma_1-\sigma_2\right)^2\cosh\left(|\mathbf{k_1}-\mathbf{k_2}|\,h\right)-g\,|\mathbf{k_1}-\mathbf{k_2}|\sinh\left(|\mathbf{k_1}-\mathbf{k_2}|\,h\right)} \\ &+\frac{a_1a_2\sigma_1\sigma_2\left(\sigma_1+\sigma_2\right)^2\left(1-\cos\left(\alpha-\beta\right)\right)\cos\left(\psi_1+\psi_2\right)}{\left(\sigma_1+\sigma_2\right)^2\cosh\left(|\mathbf{k_1}+\mathbf{k_2}|\,h\right)-g\,|\mathbf{k_1}+\mathbf{k_2}|\sinh\left(|\mathbf{k_1}+\mathbf{k_2}|\,h\right)} \quad (5.52)\end{aligned}$$

As can be observed from the above equation, the first term in the equation denotes the contribution due the difference waves and the second term in the equation denotes the contribution due to the sum waves at α and β equal to zero. Figure 5.3 shows the plot for variation of bottom pressure for sum and difference waves with respect to change in angle of separation between the two waves. In this case the two waves have the same amplitudes (a_1=2 cm and a_2=2 cm), the angular frequencies are (σ_1=10.47 s^{-1} and σ_2=9.67 s^{-1}) and water depth, (h=44 cm). As can be inferred from the plot, the pressure at the bottom due to the sum waves (dash line) is negligible with increase of angle of separation until 100^o and then increases significantly with increase in angle of separation till it reaches the maximum at 180^o. For the case of difference waves (solid line), the pressure at the bottom is maximum for 0^o angle of separation and decreases to zero at 22^o.

Increasing a_2 slightly, (a_2/a_1 =1.1) between the two waves and keeping the other terms constant (a_1=2 cm and a_2=2.2 cm), the angular frequencies (σ_1=10.47 s^{-1} and σ_2=9.67 s^{-1}) and water depth (h=44 cm). Figure 5.4 shows the plot for variation of bottom pressure for sum and difference waves with respect to change in angle of separation between the two waves and (a_2/a_1 =1.1). By looking at Figure (5.4), the pressure at the bottom due to the sum waves (dash line) is negligible with increase of angle of separation until 100^o and then increases significantly with increase in angle of separation till it reaches the maximum at 180^o. For the case of difference waves (solid line), the pressure at the bottom is maximum for 0^o angle of separation and decreases

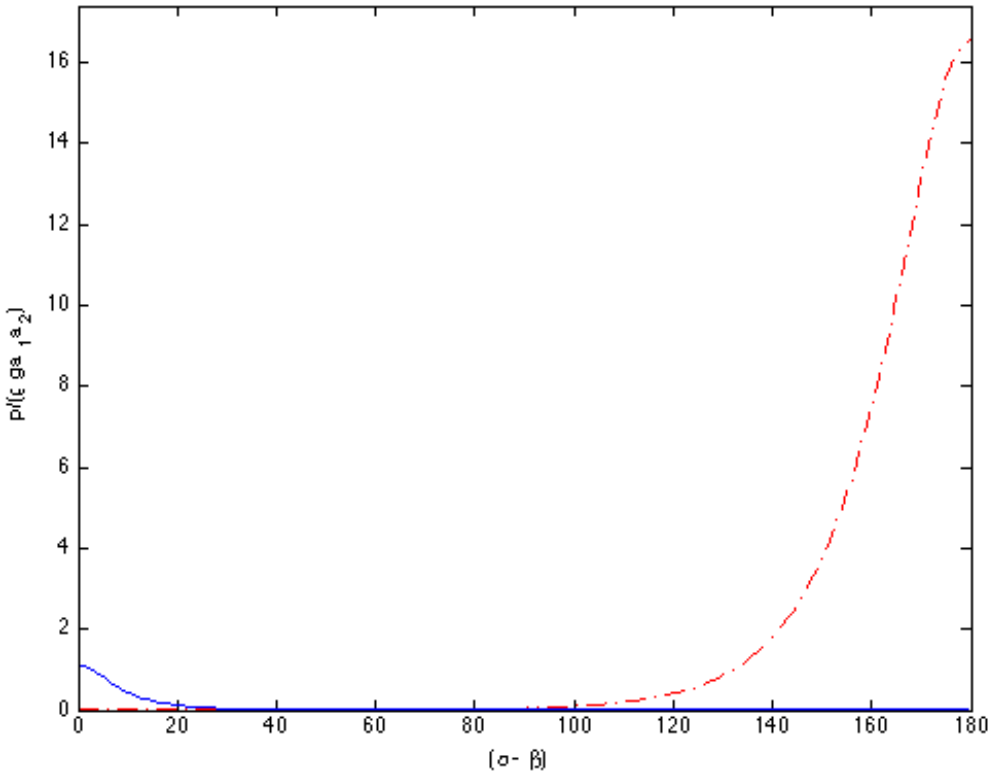

Figure 5.3: Variation of bottom pressure for sum (dash line) and difference (solid line) waves with respect to change in angle of separation between two waves (a_1=2 cm, a_2=2 cm, σ_1=10.47 s^{-1}, σ_2=9.67 s^{-1} and h=44 cm).

monotonically to zero. As we can see here that there is no changes in the results in the case (a_2/a_1 =1.1) in the two waves and we get the same results as Figure 5.3 but the there is slightly difference in the bottom pressure for sum and difference waves.

Now we want to look at the effect of (a_2/a_1 =0.5) and keeping the other terms constant (a_1 =2 cm and a_2=1 cm), the angular frequencies (σ_1=10.47 s^{-1} and σ_2=9.67 s^{-1}) and water depth (h=44 cm). Figure 5.5 shows the results of the bottom pressure due to sum and difference waves. We can observed that the bottom pressure due to

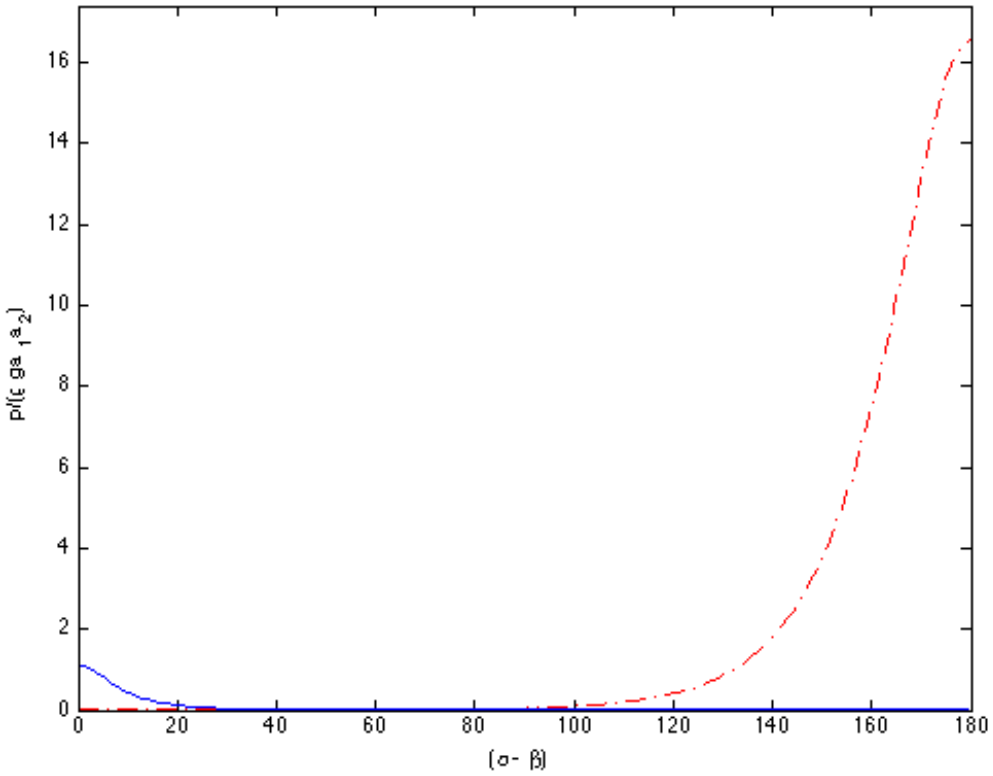

Figure 5.4: Variation of bottom pressure for sum (dash line) and difference (solid line) waves with respect to change in angle of separation between two waves (a_1=2 cm, a_2=2.2 cm, σ_1=10.47 s^{-1}, σ_2=9.67 s^{-1} and h=44 cm).

sum and difference waves is reduced to 20% than (a_2/a_1 =1)

The pressure at the bottom due to the sum waves (dash line) is negligible with increase of angle of separation until 100^o and then increases significantly with increase in angle of separation. For the case of difference waves (solid line), the pressure at the bottom is maximum for 0^o angle of separation and decreases monotonically to zero. This results are similar to the previous cases were the two waves (a_2/a_1 =1) and (a_2/a_1 =1.1). But with (a_2/a_1 =0.5), the amount of bottom pressure for the sum

and difference waves with respect to the change in angle of separation between two waves decreases.

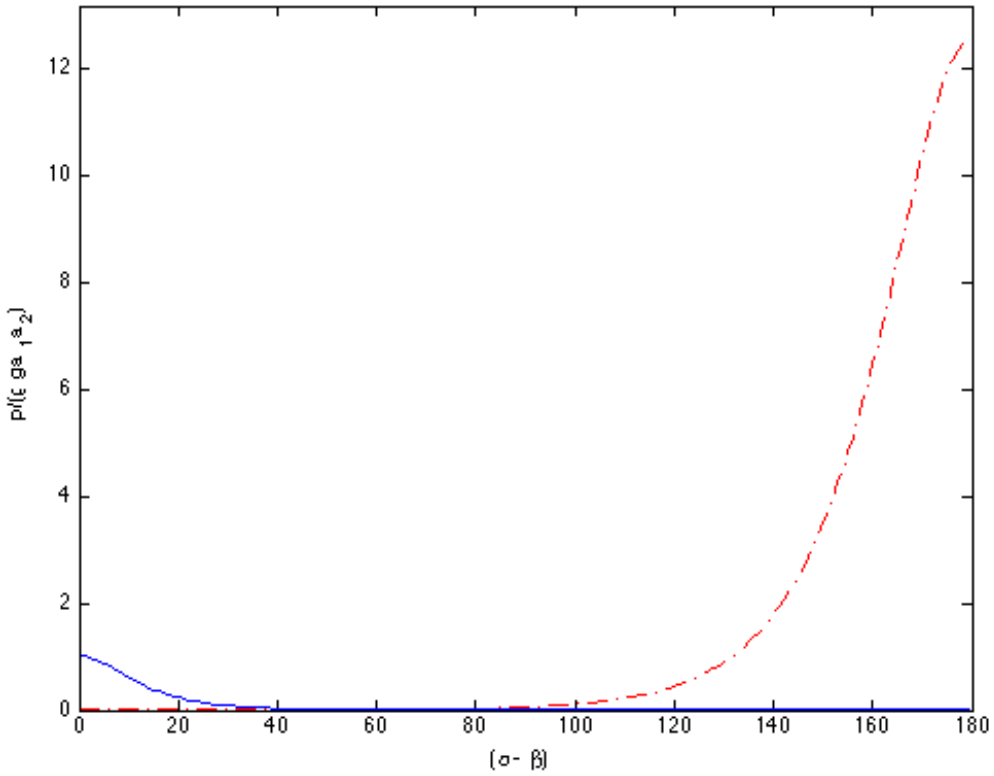

Figure 5.5: Variation of bottom pressure for sum (dash line) and difference (solid line) waves with respect to change in angle of separation between two waves (a_1=2 cm, a_2=1 cm, σ_1=10.47 s^{-1}, σ_2=9.67 s^{-1} and h=44 cm).

In conclusion, the effect of wave amplitude for two waves on the bottom pressure due to sum and difference waves with respect to change in angle of separation between waves is observed. Here we look at the effect of wave amplitude in three different cases, (a_2/a_1 =0.5, 1, 1.1) and keeping the other wave parameters constant, such as angular frequencies and water depth. For the three cases, the pressure at the bottom

due to the sum waves (dash line) is negligible with increase of angle of separation until 100^o and then increases significantly with increase in angle of separation. For the case of difference waves (solid line), the pressure at the bottom is maximum for 0^o angle of separation and decreases to zero at 22^o. We can conclude that the amount of bottom pressure due to sum and difference waves are effected by changing the wave amplitude in the three cases. In the first case were (a_2/a_1 =1), the amount of bottom pressure is higher. When (a_2/a_1 =1.1), the amount of bottom pressure is almost same as in the first case were (a_2/a_1 =1). Finally, for the third case were (a_2/a_1 =0.5), the amount of bottom pressure due to sum and difference waves is reduced to 20% than the first case were (a_2/a_1 =1).

Next we look at the effect of water depth on the bottom pressure due to sum and difference waves with respect to change in angle of separation between two waves. Going back to Figure (5.3), the two waves have the input parameters (a_1=2 cm and a_2=2 cm), the angular frequencies (σ_1=10.47 s^{-1} and σ_2=9.67 s^{-1}) and water depth (h=44 cm). As we observed from the plot, the pressure at the bottom due to the sum waves (Solid line) is negligible with increase of angle of separation until 100^o and then increases significantly with increase in angle of separation. For the case of difference waves (dash line), the pressure at the bottom is maximum for 0^o angle of separation and decreases monotonically to zero. Then we increase the water depth to 1 m instead of 44 cm and keep the other wave parameters are same. Figure (5.6) shows the results for two waves with input parameters (a_1=2 cm and a_2=2 cm), the

angular frequencies (σ_1=10.47 s^{-1} and σ_2=9.67 s^{-1}) and water depth (h=1 m). In Figure (5.6) when we increase the water depth, we observed two main things. First observation was that the amounts of bottom pressure due to sum and difference waves are decreases to 50% than the case Figure (5.6). The second observation is that the pressure at the bottom due to the sum waves (dash line) is negligible with increase of until angle of separation 140^o and then increases significantly with increase in angle of separation till it reached maximum at 18^o. For the case of difference waves (solid line), the pressure at the bottom is maximum for 0^o angle of separation and decreases faster than the shallower depth case.

In even shallower water, h=35 cm. Figure (5.7) shows the results of two waves with input parameters (a_1=2 cm and a_2=2 cm), the angular frequencies (σ_1=10.47 s^{-1} and σ_2=9.67 s^{-1}) and water depth (h=35 cm). We can observe that the pressure at the bottom due to the sum waves (dash line) is negligible with increase of angle of separation until 80^o and then increases significantly with increase in angle of separation and reaches the maximum at 180^o. For the case of difference waves (solid line), the pressure at the bottom is maximum for 0^o angle of separation and decreases monotonically to zero. Also the amount of bottom pressure due to sum and difference waves is higher that the case of water depth equal to 44 cm.

Now we want to look at the bottom pressure due to sum and difference waves for the case where the water depth goes to infinity. Figure (5.8) shows the results of two waves with input parameters (a_1=2 cm and a_2=2 cm), the angular frequencies

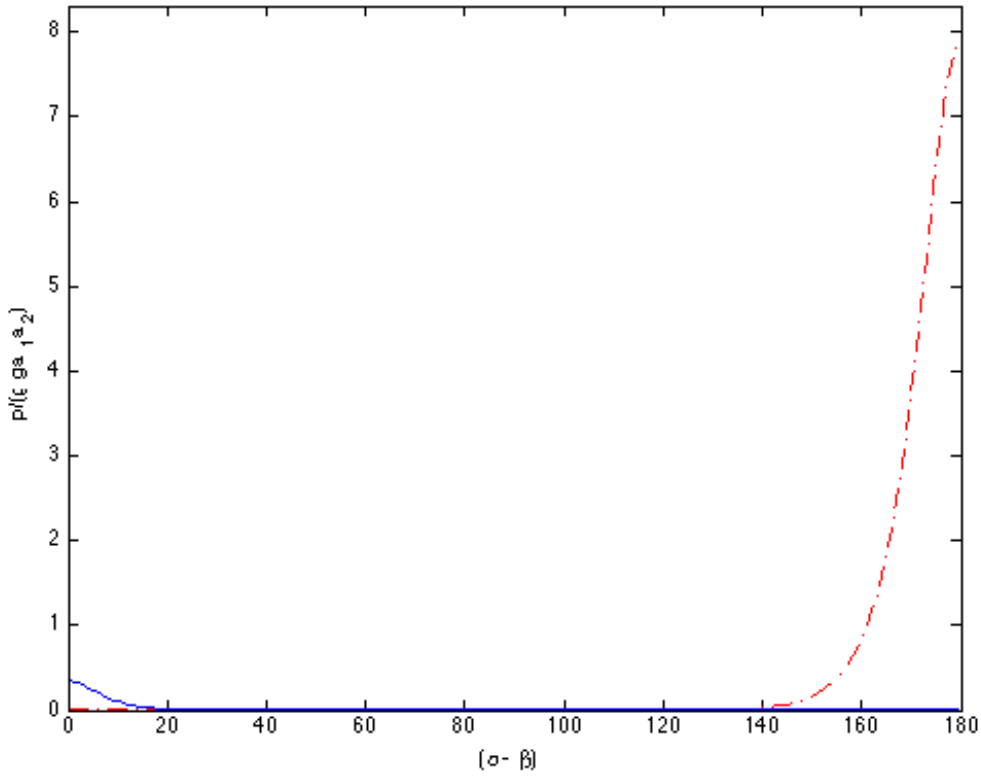

Figure 5.6: Variation of bottom pressure for sum (dash line) and difference (solid line) waves with respect to change in angle of separation between two waves (a_1=2 cm, a_2=2 cm, σ_1=10.47 s^{-1}, σ_2=9.67 s^{-1} and h=1 m).

(σ_1=10.47 s^{-1} and σ_2=9.67 s^{-1}) and water depth (h=∞). We can observe that the pressure at the bottom due to the sum waves (dash line) remains largely unaffected with increase of angle of separation until 177^o and then increases significantly with increase in angle of separation. For the case of difference waves (solid line), the pressure at the bottom is maximum for 0^o angle of separation and decreases monotonically to zero. Also the amount of bottom pressure due to sum and difference waves is almost equal to zero and does not feel the bottom which too small in comparing it with the

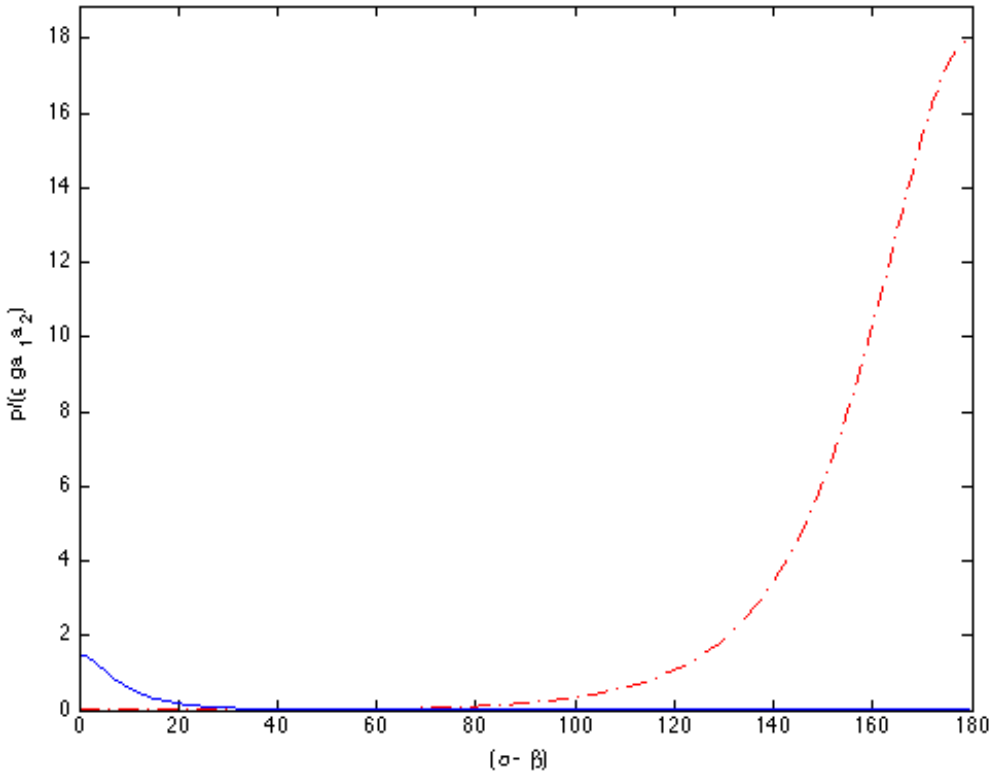

Figure 5.7: Variation of bottom pressure for sum (dash line) and difference (solid line) waves with respect to change in angle of separation between two waves (a_1 =2 cm, a_2=2 cm, σ_1=10.47 s^{-1}, σ_2=9.67 s^{-1} and h=35 cm).

case of water depth equal to 44 cm.

In conclusion, the effect of water depth on the bottom pressure due to sum and difference waves with respect to change in angle of separation between the two waves is critical. We showed from Figure(5.3,5.6,5.7,5.8) that with increasing of the water depth, the pressure at the bottom due to the sum waves (dash line) is negligible with increase of angle of separation and then increases significantly with increase in angle of separation. The amount of bottom pressure increase significantly with increase

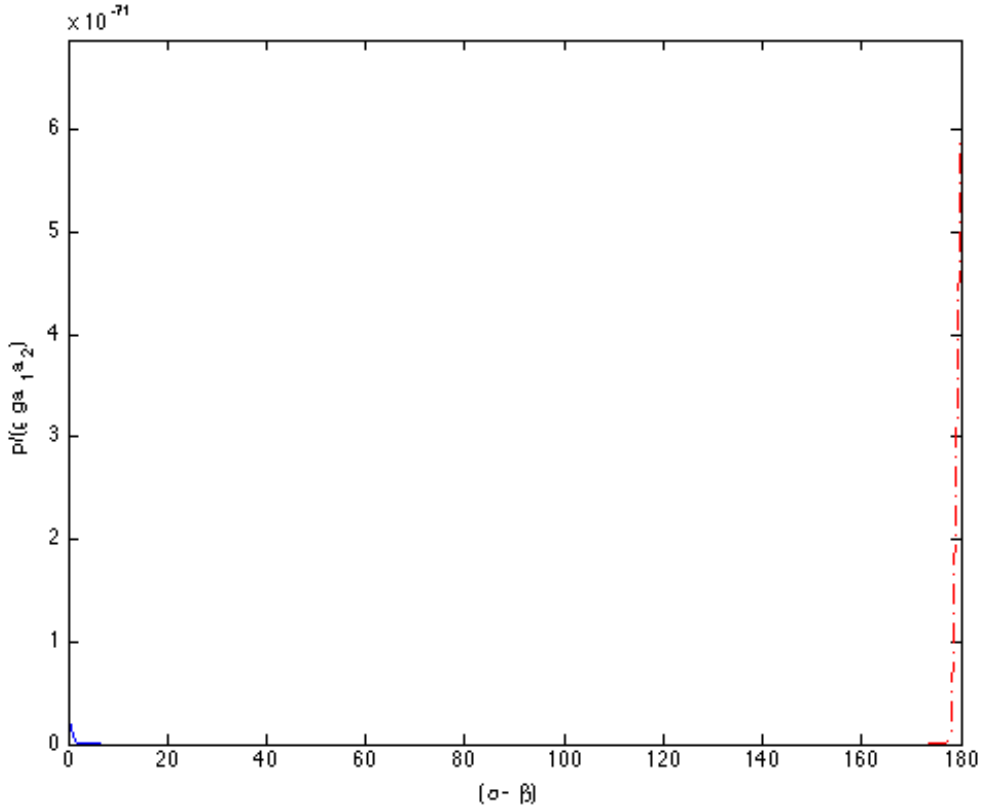

Figure 5.8: Variation of bottom pressure for sum (dash line) and difference (solid line) waves with respect to change in angle of separation between two waves (a_1 =2 cm, a_2=2 cm, σ_1=10.47 s^{-1}, σ_2=9.67 s^{-1} and h= ∞).

of angle of separation but differ with water depth. As the water depth increase the bottom pressure increase with increase the angle of separation. For the case of difference waves (solid line), the pressure at the bottom is maximum for 0^o angle of separation and decreases monotonically to zero. The minimum here is differing. As the water depth increase the minimum of angle of separation decrease.

Finally, the effect of the change in the difference of angular frequencies ($\Delta\sigma$) between the two waves on the bottom pressure is also an important factor to be

studied. Figure (5.3) shows the results of two waves with input parameters (a_1=2 cm and a_2=2 cm), the angular frequencies (σ_1=10.47 s^{-1} and σ_2=9.67 s^{-1}) and water depth (h=44 cm). The difference in angular frequencies between the two waves ($\Delta\sigma$)= 0.8 s^{-1}. Now we want to predict the bottom pressure for the sum and difference wave and by repeating the same input parameters of Figure (5.3) and decreasing the difference in angular frequencies ($\Delta\sigma$)= 0.5 s^{-1}.

Figure (5.9) shows the results of two waves with input parameters (a_1=2 cm and a_2=2 cm), the angular frequencies (σ_1=10.47 s^{-1} and σ_2=9.97 s^{-1}) and water depth (h=44 cm). We can observe that the pressure at the bottom due to the sum waves (dash line) is negligible with increase of angle of separation until 100^o and then increases significantly with increase in angle of separation. For the case of difference waves (solid line), the pressure at the bottom is maximum for 0^o angle of separation and decreases monotonically to zero. Also, we can observe that the amount of the bottom pressure is increases with decreases the difference of the angular frequencies ($\Delta\sigma$) between the two waves.

Moreover, by repeating the same input parameters of Figure (5.3) and increasing the difference in angular frequencies between the two waves ($\Delta\sigma$)= 1.5 s^{-1} we predict the bottom pressure for the sum and difference waves. Figure (5.10) shows the results of two waves with input parameters (a_1=2 cm and a_2=2 cm), the angular frequencies (σ_1=10.47 s^{-1} and σ_2=8.975 s^{-1}) and water depth (h=44 cm). We can observe that the pressure at the bottom due to the sum waves (dash line) is negligible with increase

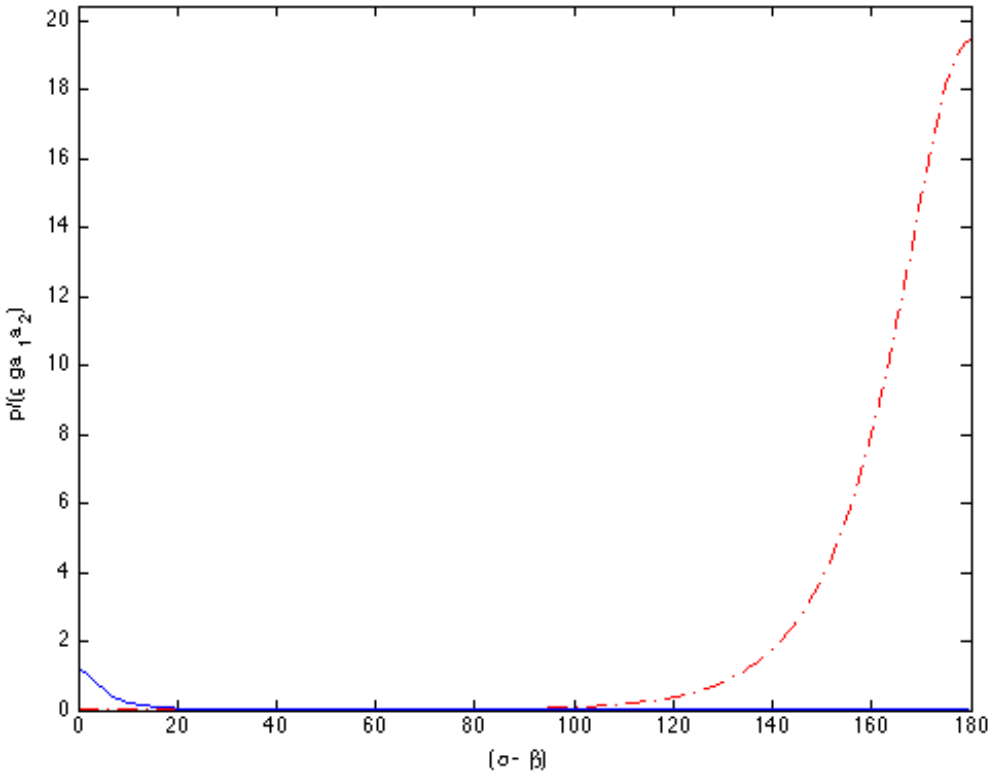

Figure 5.9: Variation of bottom pressure for sum (dash line) and difference (solid line) waves with respect to change in angle of separation between two waves (a_1 =2 cm, a_2=2 cm, σ_1=10.47 s^{-1}, σ_2=9.97 s^{-1} and h=44 cm).

of angle of separation until 80^o and then increases significantly with increase in angle of separation. For the case of difference waves (solid line), the pressure at the bottom is maximum for 0^o angle of separation and decreases monotonically to zero. Also, we can observe that the amount of the bottom pressure is decreases with increase the difference of the angular frequencies ($\Delta\sigma$) between the two waves.

In conclusion, the effect of the change in the difference of angular frequencies between the two waves is critical. As we can see from Figures (5.4,5.9,5.10), that

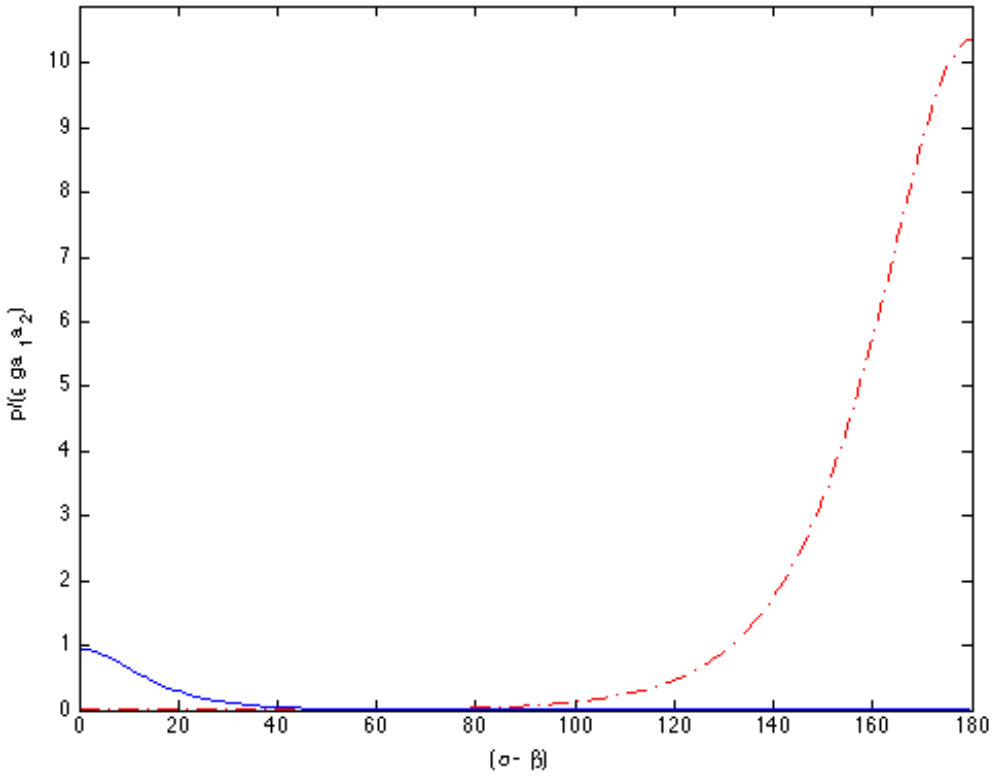

Figure 5.10: Variation of bottom pressure for sum (dash line) and difference (solid line) waves with respect to change in angle of separation between two waves (a_1 =2 cm, a_2=2 cm, σ_1=10.47 s^{-1}, σ_2=8.975 s^{-1} and h=44 cm).

the change in the difference between the angular frequencies ($\Delta\sigma$) can really effect the amount of bottom pressure for the sum and difference waves and the change of angle of separation. We can conclude that with increasing the difference in angular frequencies between the two waves ($\Delta\sigma$), two parameters will be effected. First, if we increase the difference in angular frequencies between the two waves ($\Delta\sigma$), the amount of bottom pressure will decrease.

Second we can observed that the pressure at the bottom due to the sum waves

(dash line) is negligible with increase of angle of separation and start to increase significantly with increase in the angle of separation in an earlier stage when the difference in angular frequencies between the two waves ($\Delta\sigma$) is small. And in the case were the difference in angular frequencies between the two waves ($\Delta\sigma$) is large, the pressure at the bottom due to the sum waves (dash line) is negligible with increase of angle of separation and start to increase significantly with increase in the angle of separation at a late stage. Now for the case of difference waves (dash line), the pressure at the bottom is maximum for 0^o angle of separation and decreases monotonically to zero. The minimum here is differ and effected by the difference in angular frequencies between the two waves ($\Delta\sigma$). We observed that the minimum increase with increase the difference in angular frequencies between the two waves ($\Delta\sigma$).

Now we predict the pressure on the bottom due to sum waves and difference for the experimental data obtained and presented in chapter 4. These results are presented in Table 5.1.

The first order and second order approximations for the horizontal velocities can be determined from equations (5.14) and (5.25) respectively. Substituting we get,

$$\begin{aligned}\mathbf{u}^{(1)} &= \frac{\sigma_1 a_1}{\sinh k_1 h}\big[\cos\alpha\cosh k_1(z+h)\sin\psi_1\mathbf{i} + \sin\alpha\cosh k_1(z+h)\sin\psi_1\mathbf{j} \\ &\quad - \sinh k_1(z+h)\cos\psi_1\mathbf{k}\big] + \frac{\sigma_2 a_2}{\sinh k_2 h}\big[\cos\beta\cosh k_2(z+h)\sin\psi_2\mathbf{i} \\ &\quad + \sin\beta\cosh k_2(z+h)\sin\psi_2\mathbf{j} - \sinh k_2(z+h)\cos\psi_2\mathbf{k}\big]\end{aligned} \tag{5.53}$$

Table 5.1: The predict pressure at the bottom due to sum waves and difference for the experimental data obtained and presented in chapter 4.

Test	(S_1) (cm)	(T_1) (s)	(S_2) (cm)	(T_2) (s)	(h) (cm)	(d_2) (cm)	(ρ) (kg/m^3)	Sum $(\frac{p}{\varrho})$ (cm^2/s^2)	Difference $(\frac{p}{\varrho})$ (cm^2/s^2)	Total $(\frac{p}{\varrho})$ (cm^2/s^2)
1	2	0.6	2	0.65	44	12	1291	0	43.629	43.629
2	2	0.6	2	0.63	44	12	1301	0	45.651	45.651
3	2	0.62	2	0.66	44	12	1288	0	45.309	45.309
4	2	0.6	2.2	0.65	44	12	1294	0	47.992	47.992
5	2	0.6	2.2	0.63	44	12	1303	0	50.216	50.216
6	2	0.62	2.2	0.66	44	12	1249	0	49.84	49.84
7	2	0.6	1	0.65	44	12	1311	0	21.815	21.815
8	2	0.6	1	0.63	44	12	1299	0	22.825	22.825
9	2	0.62	1	0.66	44	12	1301	0	22.654	22.654

$$
\begin{aligned}
\mathbf{u}^{(2)} = & \frac{A\cosh|\mathbf{k}_1-\mathbf{k}_2|(z+h)\cos(\psi_1-\psi_2)}{-(\sigma_1-\sigma_2)^2\cosh|\mathbf{k}_1-\mathbf{k}_2|h-g|\mathbf{k}_1-\mathbf{k}_2|\sinh|\mathbf{k}_1-\mathbf{k}_2|h} \\
& [(k_1\cos\alpha-k_2\cos\beta)\mathbf{i}+(k_1\sin\alpha-k_2\sin\beta)\mathbf{j}] \\
& +\frac{B\cosh|\mathbf{k}_1+\mathbf{k}_2|(z+h)\cos(\psi_1+\psi_2)}{-(\sigma_1+\sigma_2)^2\cosh|\mathbf{k}_1+\mathbf{k}_2|h-g|\mathbf{k}_1+\mathbf{k}_2|\sinh|\mathbf{k}_1+\mathbf{k}_2|h} \\
& [(k_1\cos\alpha+k_2\cos\beta)\mathbf{i}+(k_1\sin\alpha+k_2\sin\beta)\mathbf{j}] \\
& +\frac{A|\mathbf{k}_1-\mathbf{k}_2|\sinh|\mathbf{k}_1-\mathbf{k}_2|(z+h)\cos(\psi_1-\psi_2)}{-(\sigma_1-\sigma_2)^2\cosh|\mathbf{k}_1-\mathbf{k}_2|h-g|\mathbf{k}_1-\mathbf{k}_2|\sinh|\mathbf{k}_1-\mathbf{k}_2|h}\mathbf{k} \\
& +\frac{B|\mathbf{k}_1+\mathbf{k}_2|\sinh|\mathbf{k}_1+\mathbf{k}_2|(z+h)\cos(\psi_1+\psi_2)}{-(\sigma_1+\sigma_2)^2\cosh|\mathbf{k}_1+\mathbf{k}_2|h-g|\mathbf{k}_1+\mathbf{k}_2|\sinh|\mathbf{k}_1+\mathbf{k}_2|h}\mathbf{k}
\end{aligned}
\tag{5.54}
$$

where the velocity vectors are defined in Figure 5.11

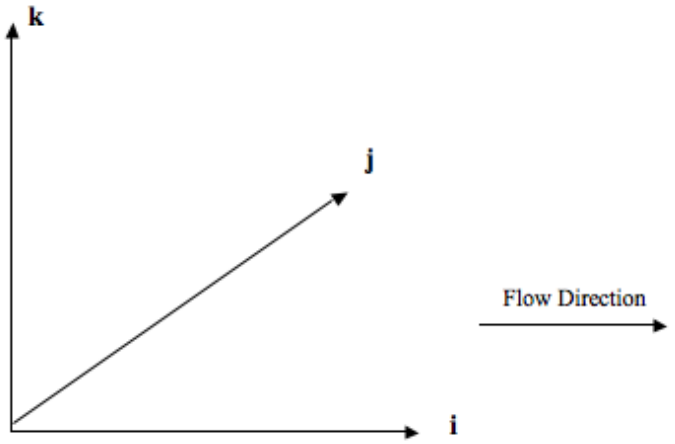

Figure 5.11: Orientation of the velocity vectors and the flow direction.

For $\alpha = 0, \beta = 0$ and substituting the values of A and B, we get:

$$\begin{aligned}\mathbf{u}^{(2)} &= \frac{2a_1a_2\sigma_1\sigma_2\left(\sigma_1-\sigma_2\right)\left(k_1-k_2\right)\cos\left(\psi_1-\psi_2\right)}{\left(\sigma_1-\sigma_2\right)^2\cosh\left|\mathbf{k}_1-\mathbf{k}_2\right|h+g\left|\mathbf{k}_1-\mathbf{k}_2\right|\sinh\left|\mathbf{k}_1-\mathbf{k}_2\right|h} \\ &\quad \left[\cosh\left|\mathbf{k}_1-\mathbf{k}_2\right|\left(z+h\right)\mathbf{i}+\sinh\left|\mathbf{k}_1-\mathbf{k}_2\right|\left(z+h\right)\mathbf{k}\right]\end{aligned} \tag{5.55}$$

Figures (5.12, 5.13, 5.14) shows the velocities measurements for two wave propagating with 0^o angles, at the surface, certain depth and at the bottom in the x-axis (solid line), y-axis (dash-dot-line) and in z-axis ($\circ$). We can observe from the figures that the velocity in the x-axis is maximum at the surface and decrease with an increase in the depth. By looking at Figure (5.12) and (5.14), the velocity in x-axis dropped by 75% at the bottom. In y-axis, the velocity is always zero since our angle for the two waves is 0^o. Finally, the velocity in z-direction at surface is maximum and equal to the velocity in the x-axis and it decrease with increase the depth untill it reaches zero at the bottom.

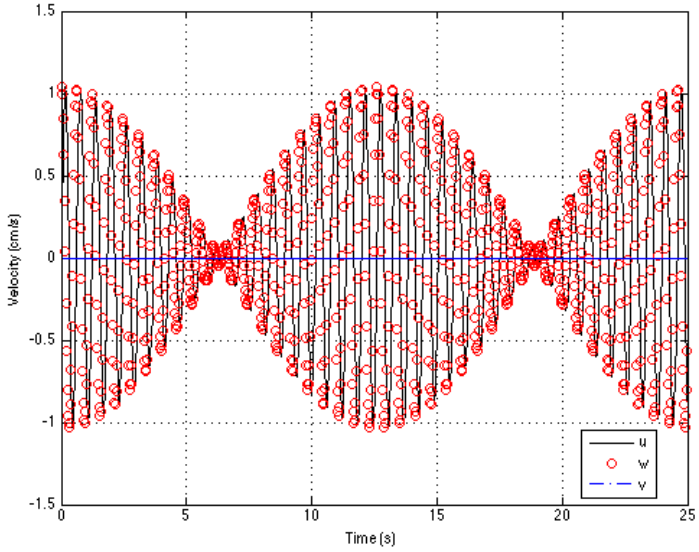

Figure 5.12: The velocity measurements in the x-axis (solid line), y-axis (dash-dot line) and z-axis (∘) at the surface for two waves propagating 0 angle (a_1 =2 cm, a_2=2 cm, σ_1=10.47 s^{-1}, σ_2=9.97 s^{-1} and h=0 cm).

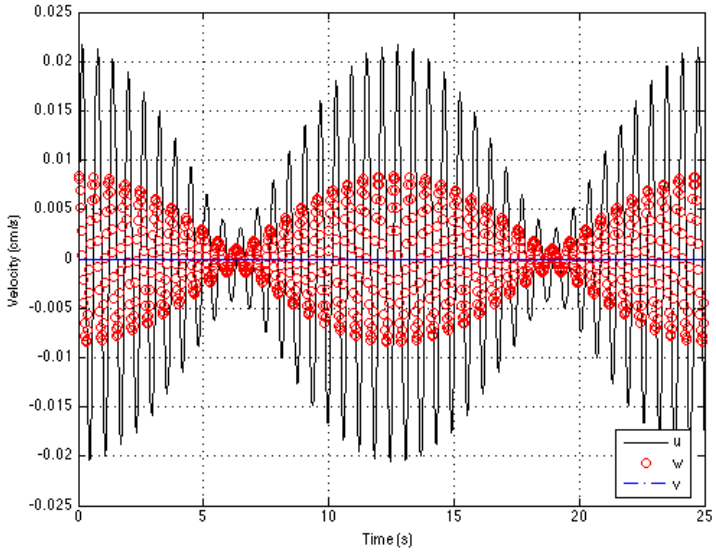

Figure 5.13: The velocity measurements in the x-axis (solid line), y-axis (dash-dot line) and z-axis (∘) at a certain for two waves propagating 0 angle (a_1 =2 cm, a_2=2 cm, σ_1=10.47 s^{-1}, σ_2=9.97 s^{-1} and h=30 cm).

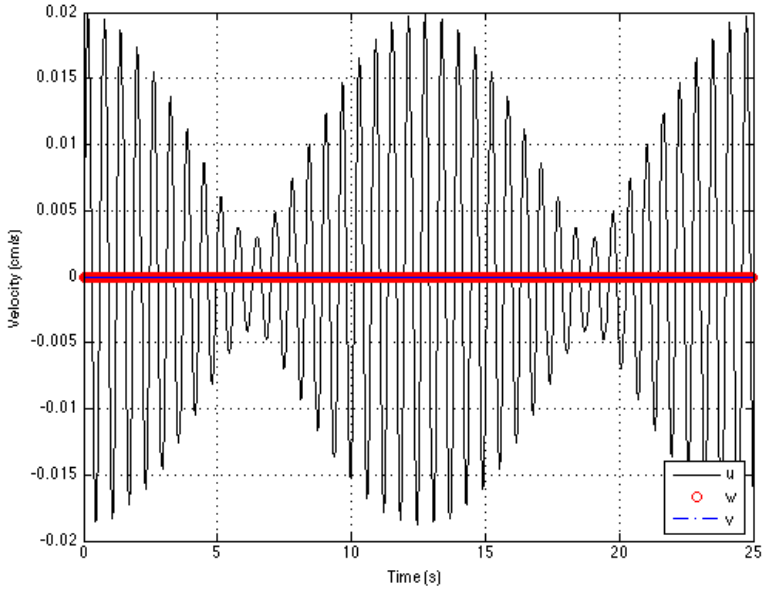

Figure 5.14: The velocity measurements in the x-axis (blue), y-axis (green) and z-axis (red) at the bottom for two waves propagating 0 angle (a_1 =2 cm, a_2=2 cm, σ_1=10.47 s^{-1}, σ_2=9.97 s^{-1} and h=44 cm).

Now we would think to measure the rate of work at the bottom since it is directly proportional to damping rate. Our developed theory is valid only for single water layer without mud bottom and we showed the effect of the difference waves on the pressure at the bottom with different waves parameters. Since we are interested in this study in water waves over muddy bottom and the interaction between them that cause the energy to dissipate, we will use the visco-elastic model of MacPherson (1980) to measure the rate of work at the bottom for difference waves. Using the visco-elastic model and the viscosity and elasticity parameters of mud from Nouri (2013), the rate of work is calculated for the difference waves versus difference in wave period of the two short waves. The other wave parameters such as water depth,

mud depth, water density and mud density kept constant.

The theoretical rates of work measurement are compared with the experimental data of the bi-chromatic waves in chapter four. Figure (5.15) shows the results of the rate of work measured theoretically and experimentally. The theoretical measurements shows increase until it reaches peak then decrease with respect of the differents of wave periods. Also the experimental data from chapter four shows a good agreement with theoretical data.

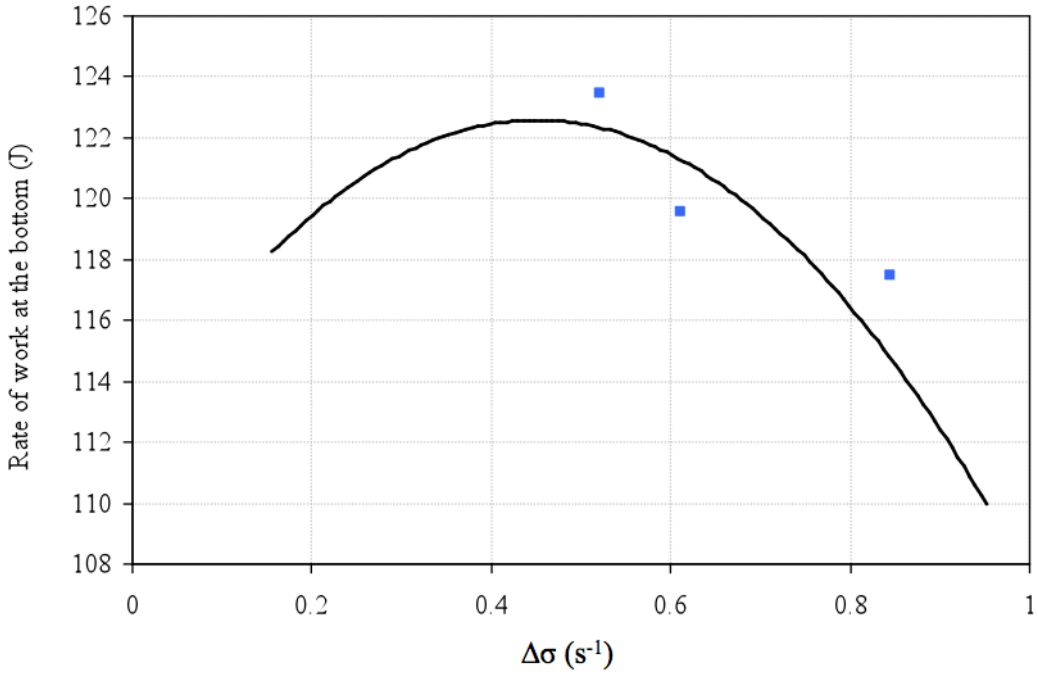

Figure 5.15: Rate of work done at the bottom by using MacPherson 1980) viscoelastic model versus the difference wave group length for the long bound wave (d_2=12 cm, h=44 cm, G'=421.6 pa, G"=82.97 pa, ρ_1= 1000 kg/m^3, ρ_2= 1307 kg/m^3).(solid line) MacPherson model and (■) Experimental data from chapter five.

Finally, we calculated the water surface elevation (η) theoretically by using equa-

Table 5.2: Predicted water surface elevation from theory for all wave group tests compared with Prony method.

Test #	Stroke (S_1) (cm)	Period (T_1) (s)	Stroke (S_2) (cm)	Period (T_2) (s)	Water depth (h) (cm)	η theory (cm)	η Prony (cm)
1	2	0.6	2	0.65	44	1.185	1.011
4	2	0.6	2.2	0.65	44	1.303	1.093
6	2	0.6	1	0.65	44	0.592	0.413
8	2	0.6	2	0.63	44	1.228	1.081
11	2	0.6	2.2	0.63	44	1.351	1.126
13	2	0.6	1	0.63	44	0.614	0.465
15	2	0.62	2	0.66	44	1.129	1.088
18	2	0.62	2.2	0.66	44	1.242	1.105
20	2	0.62	1	0.66	44	0.565	0.397

tion (5.51) at (α) and (β) equal to zero. The results were compared with the water surface elevation for the experiments in chapter four by using Prony method see Table 5.2. We can observe from Table 5.2 that the water surface elevation in Prony method is lower than the theoretical.

5.3 Conclusion

In this chapter, we developed the expressions for surface elevation due to propagation of two waves interacting at arbitrary angles using the Stokes waves theory to second order and perturbation expansion for both finite depth and infinite depth cases. We also derived the contribution of sum waves and difference waves to the pressure at the bottom for the finite depth case with respect of angle of separation.

We conclude that the wave parameters such as wave amplitude, water depth and the difference in angular frequencies between the two waves ($\Delta\sigma$) affects the amount of the bottom pressure due to sum and difference waves. We tested the effect of the wave amplitude for three cases (a_2/a_1 = 0.5, 1, 1.1). We found that for the cases (a_2/a_1 =1, 1.1), the amount of bottom pressure due to sum and different wave is higher that that the case (a_2/a_1 =0.5) but the amount of angle of separation remain the same in all cases.

We also conclude that the water depth is critical on the bottom pressure and vary with angle of separation of the two waves. The bottom pressure increase due to sum and different waves as the water depth decrease and the amount of angle of separation increase as depth increase. The difference in angular frequencies between the two waves ($\Delta\sigma$) has also been predicted. We conclude the amount of bottom pressure is increases with decrease the difference in angular frequencies between the two waves ($\Delta\sigma$). Moreover, the angle of separation for the two wave due to the sum and difference waves is differ.

We also predict the bottom pressure due to sum and different waves for different test cases in experiments conducted and presented in chapter 4 were the two waves propagating with 0 degree. Also, we derive the expression for the velocity due to two waves propagating with arbitrary angles. We predict the velocity of two wave interacting with arbitrary angles at the surface, certain depth and at the bottom.

Moreover, we used the visco-eastic model of MacPherson (1980) to measure the rate of work done on the bottom with varying wave periods since our theory is valid for the case of water layer only. The results show that the rate of work increases with increases in the wave periods until it peaks and then decreases. Also we measured the rate of work at the bottom for our experimental data in chapter 4 and the results showed good agreement with theory.

Finally, we predict the water surface elevation (η) from theory when (α) and (β) equal to zero and compared the results with the water surface elevation for the experiments in chapter four by using Prony method. the results showed that the water surface elevation in Prony method is lower the theoretical.

Chapter 6

Conclusion and future works

Waves propagating over a muddy bottom dissipate energy. Previous studies showed that the attenuation coefficient of the waves depends on the wave parameters and the rheological properties. In this study the attenuation coefficient for a series of monochromatic waves were tested in wave tank by generating waves with different wave height, wave period and water depth. Also we looked at the effect of mud history on the wave attenuation. This study showed that the attenuation coefficient can increase and decrease with varying wave parameters.

One surprising result is that previous studies showed two different conclusions. Some studies showed that the wave attenuation coefficient increased with an increase in the wave height. On the other hand, other studies showed that the attenuation coefficient decreased with increasing wave height. Interestingly, we found that both results are true and we showed that the attenuation coefficient depends on the rate

of work done in the bottom and mainly on the difference in phase shift between the bottom pressure and the vertical velocity.

Moreover, several experiments were conducted to examine the effect of wave period on the attenuation coefficient. These tests were conducted with different water depths and the results showed that the wave attenuation coefficient increased with increased the wave period until it reached the peak and then decreased and they are realted to the rate or work at the bottom. These tests were compared with the visco-elastic model and showed a good agreement. Finally, we looked at the effect of the mud history and we found that the attenuation coefficient decreased with time since stir up the mud until it reached the 29 hours the attenuation coefficient with increase again.

Short waves propagating over mud bottom can not dissipate energy, but field experiments showed that short waves dissipated energy in deep water. A series of bi-chromatic waves were conducted in the wave tank to evaluate the energy dissipation over mud bottom in deep water. Generating two waves with slightly different wave periods and amplitude created wave groups in the lab. The bound long wave associated with the wave group will be long enough to extend the pressure to the bottom and cause the energy to dissipate. Several experiments were conducted in the laboratory with different wave parameters such as wave period and wave height.

These tests were first analysis by the using the power spectrum density (PSD) method and we calculated the energy along the tank, which shows that its decreasing.

The second method to analyze these data was by using Pronys method, which is a statistical method used to extract information from the sum of sinusoidal signals, such as, the wave frequencies, wave amplitudes and the phase. By using Pronys method, the result showed that the energy is dissipating along the tank and it varies depending on the wave parameters. The tests are limited due to the size of the wave tank but this will encourage researchers to conduct more tests and look at the effect of wave groups on the attenuation coefficient in deep water.

Theoretically, we derive the expression for the water surface elevation and the bottom pressure or two waves interacting with slightly different frequencies coming with arbitrary angles. Here we used the Stokes wave theory upto the second order and perturbation expansion for both finite and infinite depths. We used this expression to predict the bottom pressure and velocities values for our experimental tests of the wave group that were conducted in the wave tank laboratory. We also predict the rate of work done on bottom by using the visco elastic model and compare the results with our experimental data of the bi-chromatic waves in chapter 4 and the results shows good agreements.

For the past four years working in the field of water-mud interaction and by reviewing the previous work that has been done in this area, I believe that there are more interesting areas to look as future work. Problems such as lacking of rheological properties for our experiments and also the limitation of tests due the wave tank size did not help us to understand more about the mud behavior. For deep water cases

I would like to run tests at greater depth. Also running tests with different mud densities and mud types will really contribute in understanding the realation between water and mud.

Rheology is also an important factor that effects the damping value. Rheometers can measure rheological variables of mud samples such as density, stress, strain, viscosity and viscoelastic properties that can effect the damping value. I would like to examine the effect of these additional mud properties on the damping rate. Looking into other studies that focus on shear stress values for different amplitudes and frequencies, which can be related to the mud depth and possibly an effective mud depth.

In addition, I used the visco-elastic model to compare my experimental data. Of particular interest would be using different models such as visco-plastic and visco-ealstic-plastic model to clarify the water-mud interaction mechanism. Theoretical models are a good source for comparison and prediction of the experimental data to understand the interaction mechanics of water waves and muddy bottom. Therefor using different types of models is a good idea to understand the behavior of mud.

Mathematically, we derive in chapter five the expression for the water surface elevation by using Stokes theory to second order perturbation expansion for one layer model without mud to show the effect of the nonlinear wave on the pressure at the bottom. As future work, I would think to extent the visco-elastic model by MacPherson (1980), which is a two layer model with mud bottom using the same

technique in chapter five. Extending MacPherson (1980) model by using Stoke's theory to second order perturbation expansion will provide more realistic expression for the pressure at the bottom and the damping rate.

Other aspects of the study could be the irregular wave damping (spectral waves). Examining the energy transfer from one frequency range to another will be an interesting area to study.

Since I will be a civil engineering professor in Kuwait University specializing in coastal engineering, I will continue my career in this area by building a coastal laboratory in Kuwait University and conducting experimental tests that will help to understand the water-mud interaction. Also I am planning to work as a team with the geotechnical engineers in the civil engineering department to study and test the rheological properties of mud and sediments.

Moreover, since Kuwait has a muddy coastal region; I am thinking to do some field experiments to compare these tests with the theoretical and numerical models. Things like conducting experiments with different mud type since I used only kaolinite, using different types of theoretical models such as elastic and visco-plastic will give great information about the mud-water interaction. Also I would like to extend my theoretical work in the nonlinear interaction of two wave in deep water by adding muddy bottom.

Finally, since I was working in water-mud interaction, I'd like to extend my work as a coastal engineer to look at the coastal hazards problems in muddy beach in short

and long terms. Problems such as storms, floods, tsumani and erosion are really very important and can effect the coastal area.

Appendix A

Data for 256 experiments that were taken in Johns Hopkins Coastal Engineering Laboratory.

Table A.1: Data for 256 experiments that were taken during the time 2/4/2011 8/4/2011 2011 in Johns Hopkins Coastal Engineering Laboratory.Where S=Stroke, T=Wave Period (s), a= Wave amplitude (m)), L= Wave length (m), k_r= Real part wave number (m^{-1}), k_i= Attenuation coefficient (m^{-1}), h= total water depth (m), d_1= Water layer thickness (m), d_2= Mud thickness (lutocline height) (m).

Test	Date	S	T (s)	h (m)	a (m)	d_1 (m)	d_2 (m)	L (m)	k_r (m^{-1})	ka	kh	k_i (m^{-1})	Comments
1	2/4/2011	1.0	1.30	0.54	0.011	0.127	0.413	2.357	2.664	0.031	1.439	0.029	-
2	2/4/2011	0.8	1.30	0.54	0.008	0.127	0.413	2.357	2.664	0.022	1.439	0.013	-
3	2/4/2011	1.5	1.30	0.54	0.019	0.127	0.413	2.357	2.664	0.051	1.439	0.029	-
4	2/4/2011	2.0	1.30	0.54	0.027	0.127	0.413	2.357	2.664	0.072	1.439	0.024	-
5	2/4/2011	2.5	1.30	0.54	0.035	0.127	0.413	2.357	2.664	0.092	1.439	0.031	-
6	2/4/2011	3.0	1.30	0.54	0.042	0.140	0.400	2.357	2.664	0.113	1.439	0.028	-
7	2/4/2011	4.0	1.30	0.54	0.058	0.140	0.400	2.357	2.664	0.154	1.439	0.012	-
8	2/8/2011	1.2	0.85	0.54	0.015	0.102	0.438	1.123	5.592	0.081	3.020	0.003	-
9	2/8/2011	0.8	0.85	0.54	0.008	0.102	0.438	1.123	5.592	0.047	3.020	0.011	-
10	2/8/2011	1.6	0.85	0.54	0.021	0.102	0.438	1.123	5.592	0.116	3.020	0.003	-
11	2/8/2011	1.0	0.85	0.54	0.011	0.102	0.438	1.123	5.592	0.064	3.020	0.018	-
12	2/8/2011	1.4	0.85	0.54	0.018	0.102	0.438	1.123	5.592	0.099	3.020	0.004	-
13	2/8/2011	2.0	1.30	0.54	0.027	0.102	0.438	2.358	2.663	0.072	1.438	0.025	-
14	2/8/2011	3.0	1.30	0.54	0.042	0.102	0.438	2.358	2.663	0.113	1.438	0.030	-
15	2/8/2011	1.0	1.30	0.54	0.011	0.102	0.438	2.358	2.663	0.031	1.438	0.038	-
16	3/9/2011	2.0	1.00	0.44	0.027	0.116	0.324	1.488	4.220	0.113	1.857	0.052	-
17	3/9/2011	1.4	0.70	0.44	0.018	0.116	0.324	0.764	8.220	0.145	3.617	0.026	longitudinal seiche
18	3/9/2011	1.3	0.67	0.44	0.016	0.116	0.324	0.700	8.971	0.144	3.947 0.011	-	
19	3/9/2011	1.5	0.73	0.44	0.019	0.116	0.324	0.830	7.566	0.145	3.329	-	large scatter, try smaller stroke

Data for 256 experiments that were taken during the time 2/4/2011 8/4/2011 2011 in Johns Hopkins Coastal Engineering Laboratory.

Test	Date	S	T (s)	h (m)	a (m)	d_2 (m)	d_1 (m)	L (m)	k_r (m^{-1})	ka	kh	k_i (m^{-1})	Comments
20	3/9/2011	1.4	0.73	0.44	0.018	0.116	0.324	0.833	7.539	0.133	3.317	-	small scatter
21	3/9/2011	1.7	0.80	0.44	0.022	0.116	0.324	0.992	6.331	0.141	2.785	-	large scatter
22	3/9/2011	1.9	0.90	0.44	0.025	0.116	0.324	1.236	5.081	0.129	2.236	0.070	-
23	3/9/2011	1.9	0.95	0.44	0.025	0.116	0.324	1.362	4.611	0.117	2.029	0.056	-
24	3/9/2011	1.8	0.88	0.44	0.024	0.116	0.324	1.187	5.291	0.126	2.328	0.043	-
25	3/9/2011	1.9	0.92	0.44	0.025	0.116	0.324	1.286	4.883	0.124	2.149	0.063	-
26	3/9/2011	1.9	0.96	0.44	0.025	0.116	0.324	1.387	4.528	0.115	1.992	0.051	-
27	3/9/2011	1.8	0.86	0.44	0.024	0.116	0.324	1.137	5.523	0.131	2.430	0.043	-
28	3/9/2011	1.8	0.89	0.44	0.024	0.116	0.324	1.212	5.182	0.123	2.280	0.055	-
29	3/9/2011	2.0	1.05	0.44	0.027	0.116	0.324	1.614	3.891	0.105	1.712	0.049	-
30	3/9/2011	2.0	1.10	0.44	0.027	0.116	0.324	1.739	3.611	0.097	1.589	0.062	small longitudinal seiche
31	3/9/2011	2.2	1.15	0.44	0.030	0.116	0.324	1.863	3.371	0.101	1.483	0.060	clear longitudinal seiche
32	3/9/2011	2.3	1.20	0.44	0.031	0.116	0.324	1.987	3.161	0.099	1.391	0.063	-
33	3/9/2011	2.0	1.07	0.44	0.027	0.116	0.324	1.664	3.774	0.101	1.661	0.060	-
34	3/9/2011	2.0	1.03	0.44	0.027	0.116	0.324	1.563	4.018	0.108	1.768	0.046	-
35	3/9/2011	2.0	1.00	0.44	0.027	0.116	0.324	1.488	4.220	0.113	1.857	0.049	Checking repeatability
36	3/10/2011	2.0	1.00	0.44	0.027	0.108	0.332	1.488	4.220	0.113	1.857	0.037	Checking repeatability
37	3/10/2011	1.9	0.90	0.44	0.025	0.106	0.334	1.236	5.081	0.129	2.236	0.055	-
38	3/10/2011	1.4	0.70	0.44	0.018	0.106	0.334	0.764	8.220	0.145	3.617	0.023	-
39	3/10/2011	2.0	1.10	0.44	0.027	0.106	0.334	1.739	3.611	0.097	1.589	0.045	-

Data for 256 experiments that were taken during the time 2/4/2011 8/4/2011 2011 in Johns Hopkins Coastal Engineering Laboratory.

Test	Date	S	T (s)	h (m)	a (m)	d_2 (m)	d_1 (m)	L (m)	k_r (m^{-1})	ka	kh	k_i (m^{-1})	Comments
40	3/10/2011	1.1	0.90	0.44	0.013	0.106	0.334	1.236	5.081	0.066	2.236	0.044	-
41	3/10/2011	2.3	0.90	0.44	0.031	0.106	0.334	1.236	5.081	0.160	2.236	0.061	-
42	3/10/2011	0.7	0.90	0.44	0.007	0.106	0.334	1.236	5.081	0.035	2.236	0.037	-
43	3/10/2011	1.5	0.90	0.44	0.019	0.106	0.334	1.236	5.081	0.097	2.236	0.052	-
44	3/10/2011	1.9	0.90	0.44	0.025	0.106	0.334	1.236	5.081	0.129	2.236	0.057	-
45	3/10/2011	2.7	0.90	0.44	0.038	0.106	0.334	1.236	5.081	0.191	2.236	0.056	-
46	3/10/2011	2.0	1.00	0.44	0.027	0.106	0.334	1.488	4.220	0.113	1.857	0.038	Checking repeatability
47	3/10/2011	0.8	1.00	0.44	0.008	0.106	0.334	1.488	4.220	0.035	1.857	0.055	-
48	3/10/2011	1.4	1.00	0.44	0.018	0.106	0.334	1.488	4.220	0.074	1.857	0.037	-
49	3/10/2011	2.6	1.00	0.44	0.036	0.106	0.334	1.488	4.220	0.152	1.857	0.042	-
50	3/10/2011	1.1	1.00	0.44	0.013	0.105	0.335	1.488	4.220	0.055	1.857	0.055	-
51	3/10/2011	1.7	1.00	0.44	0.022	0.105	0.335	1.488	4.220	0.094	1.857	0.043	-
52	3/10/2011	1.2	1.00	0.44	0.015	0.105	0.335	1.488	4.220	0.061	1.857	0.045	-
53	3/10/2011	1.3	1.00	0.44	0.016	0.105	0.335	1.488	4.220	0.068	1.857	0.039	-
54	3/10/2011	1.0	1.00	0.44	0.011	0.105	0.335	1.488	4.220	0.048	1.857	0.051	interesting shape to amplitude plot
55	3/10/2011	1.7	1.00	0.44	0.022	0.105	0.335	1.488	4.220	0.094	1.857	0.040	computer crashed
56	3/15/2011	2.0	1.00	0.44	0.027	0.110	0.330	1.488	4.220	0.113	1.857	0.036	Checking repeatability
57	3/15/2011	1.4	0.70	0.44	0.018	0.110	0.330	0.764	8.220	0.145	3.617	0.021	-
58	3/15/2011	2.0	1.00	0.44	0.027	0.116	0.324	1.488	4.220	0.113	1.857	0.032	lutocline blurred,waited few hours
59	3/15/2011	1.4	0.70	0.44	0.018	0.116	0.324	0.764	8.220	0.145	3.617	0.021	blurred again

Data for 256 experiments that were taken during the time 2/4/2011 8/4/2011 2011 in Johns Hopkins Coastal Engineering Laboratory.

Test	Date	S	T (s)	h (m)	a (m)	d_2 (m)	d_1 (m)	L (m)	k_r (m^{-1})	ka	kh	k_i (m^{-1})	Comments
60	3/15/2011	1.6	0.90	0.44	0.021	0.124	0.316	1.236	5.081	0.105	2.236	0.039	-
61	3/15/2011	1.7	1.00	0.44	0.022	0.124	0.316	1.488	4.220	0.094	1.857	0.038	computer crashed after last run
62	3/16/2011	1.7	1.00	0.44	0.022	0.117	0.323	1.488	4.220	0.094	1.857	0.029	-
63	3/16/2011	1.3	0.90	0.44	0.016	0.117	0.323	1.236	5.081	0.082	2.236	0.034	mud blurred at 5.125”
64	3/16/2011	2.0	1.05	0.44	0.027	-	-	1.614	3.891	0.105	1.712	0.026	-
65	3/16/2011	1.0	0.80	0.44	0.011	-	-	0.992	6.331	0.073	2.785	0.144	visible seiche
66	3/16/2011	1.5	0.95	0.44	0.019	-	-	1.362	4.611	0.088	2.029	0.040	-
67	3/16/2011	2.2	1.10	0.44	0.030	-	-	1.739	3.611	0.108	1.589	0.035	slight seiche
68	3/16/2011	1.2	0.85	0.44	0.015	-	-	1.987	3.161	0.046	1.391	-	-
69	3/16/2011	1.1	0.85	0.44	0.013	0.140	0.300	1.212	5.182	0.067	2.280	0.038	-
70	3/16/2011	0.8	0.70	0.44	0.008	0.140	0.300	0.764	8.220	0.069	3.617	-	wave maker stopped working
71	3/16/2011	1.0	0.75	0.44	0.011	0.138	0.302	0.875	7.177	0.077	3.158	0.030	large scatter waves
72	3/16/2011	2.8	1.20	0.44	0.039	0.138	0.302	1.987	3.161	0.124	1.391	0.043	seiche
73	3/16/2011	1.7	1.00	0.44	0.022	0.138	0.302	1.488	4.220	0.094	1.857	0.040	-
74	3/16/2011	1.3	0.90	0.44	0.016	0.138	0.302	1.236	5.081	0.082	2.236	0.044	-
75	3/16/2011	2.2	1.10	0.44	0.030	0.138	0.302	1.739	3.611	0.108	1.589	0.040	-
76	3/16/2011	1.1	0.85	0.44	0.013	0.138	0.302	1.212	5.182	0.067	2.280	0.039	-
77	3/16/2011	1.5	0.95	0.44	0.019	0.138	0.302	1.362	4.611	0.088	2.029	0.042	-
78	3/16/2011	1.0	0.80	0.44	0.011	0.138	0.302	0.992	6.331	0.073	2.785	0.012	-
79	3/17/2011	1.5	0.90	0.44	0.019	0.125	0.315	1.236	5.081	0.097	2.236	0.030	-

Data for 256 experiments that were taken during the time 2/4/2011 8/4/2011 2011 in Johns Hopkins Coastal Engineering Laboratory.

Test	Date	S	T (s)	h (m)	a (m)	d_2 (m)	d_1 (m)	L (m)	k_r (m^{-1})	ka	kh	k_i (m^{-1})	Comments
80	3/17/2011	2.3	0.90	0.44	0.031	0.125	0.315	1.236	5.081	0.160	2.236	0.046	large scatter sonic gauges
81	3/17/2011	0.7	0.90	0.44	0.007	0.124	0.316	1.236	5.081	0.035	2.236	0.034	-
82	3/17/2011	1.9	0.90	0.44	0.025	0.124	0.316	1.236	5.081	0.129	2.236	0.047	-
83	3/17/2011	1.5	0.90	0.44	0.019	0.124	0.316	1.236	5.081	0.097	2.236	0.048	-
84	3/17/2011	2.3	0.90	0.44	0.031	0.124	0.316	1.236	5.081	0.160	2.236	0.049	-
85	3/17/2011	1.9	0.90	0.44	0.025	0.122	0.318	1.236	5.081	0.129	2.236	0.045	-
86	3/17/2011	1.1	0.90	0.44	0.013	0.122	0.318	1.236	5.081	0.066	2.236	0.045	-
87	3/17/2011	1.7	1.00	0.44	0.022	0.122	0.318	1.488	4.220	0.094	1.857	0.035	-
88	3/17/2011	1.4	1.00	0.44	0.018	0.122	0.318	1.488	4.220	0.074	1.857	0.032	-
89	3/17/2011	2.0	1.00	0.44	0.027	0.122	0.318	1.488	4.220	0.113	1.857	0.024	-
90	3/17/2011	1.1	1.00	0.44	0.013	0.122	0.318	1.488	4.220	0.055	1.857	0.043	-
91	3/17/2011	1.0	1.00	0.44	0.011	0.122	0.318	1.488	4.220	0.048	1.857	0.044	-
92	3/17/2011	1.7	1.00	0.44	0.022	0.122	0.318	1.488	4.220	0.094	1.857	0.026	-
93	3/17/2011	1.2	1.00	0.44	0.015	0.122	0.318	1.488	4.220	0.061	1.857	0.041	-
94	3/17/2011	1.8	1.00	0.44	0.024	0.122	0.318	1.488	4.220	0.100	1.857	0.027	-
95	3/17/2011	2.3	1.00	0.44	0.031	0.122	0.318	1.488	4.220	0.133	1.857	0.027	-
96	3/17/2011	0.9	1.00	0.44	0.010	0.122	0.318	1.488	4.220	0.042	1.857	0.046	-
97	3/17/2011	1.3	1.00	0.44	0.016	0.122	0.318	1.488	4.220	0.068	1.857	0.039	-
98	3/17/2011	1.5	1.00	0.44	0.019	0.122	0.318	1.488	4.220	0.081	1.857	0.034	-
99	3/17/2011	1.6	1.00	0.44	0.021	0.122	0.318	1.488	4.220	0.087	1.857	0.028	-

Data for 256 experiments that were taken during the time 2/4/2011 8/4/2011 2011 in Johns Hopkins Coastal Engineering Laboratory.

Test	Date	S	T (s)	h (m)	a (m)	d_2 (m)	d_1 (m)	L (m)	k_r (m^{-1})	ka	kh	k_i (m^{-1})	Comments
100	3/17/2011	1.4	1.00	0.44	0.018	0.122	0.318	1.488	4.220	0.074	1.857	0.033	-
101	7/11/2011	2.0	1.00	0.44	0.027	0.083	0.357	1.488	4.220	0.113	1.857	0.040	Checking repeatability
102	7/11/2011	1.9	0.90	0.44	0.025	0.083	0.357	1.236	5.081	0.129	2.236	0.015	very bad data
103	7/11/2011	2.0	1.00	0.44	0.027	0.083	0.357	1.488	4.220	0.113	1.857	0.028	-
104	7/12/2011	2.0	1.00	0.44	0.027	0.092	0.348	1.488	4.220	0.113	1.857	0.056	-
105	7/12/2011	1.9	0.95	0.44	0.025	0.094	0.346	1.362	4.611	0.117	2.029	0.062	-
106	7/12/2011	1.6	0.85	0.44	0.021	0.094	0.346	1.212	5.182	0.107	2.280	0.050	-
107	7/12/2011	1.4	0.80	0.44	0.018	0.094	0.346	0.992	6.331	0.112	2.785	0.040	-
108	7/12/2011	0.8	0.89	0.44	0.008	0.094	0.346	1.212	5.182	0.043	2.280	0.043	-
109	7/12/2011	1.0	0.89	0.44	0.011	0.095	0.345	1.212	5.182	0.059	2.280	0.040	-
110	7/12/2011	1.2	0.89	0.44	0.015	0.095	0.345	1.212	5.182	0.075	2.280	0.033	-
111	7/12/2011	1.4	0.89	0.44	0.018	0.095	0.345	1.212	5.182	0.091	2.280	0.052	-
112	7/12/2011	1.8	0.89	0.44	0.024	0.095	0.345	1.212	5.182	0.123	2.280	0.062	-
113	7/12/2011	2.2	0.89	0.44	0.030	0.095	0.345	1.212	5.182	0.155	2.280	0.051	-
114	7/12/2011	0.8	1.00	0.44	0.008	0.095	0.345	1.488	4.220	0.035	1.857	0.050	-
115	7/12/2011	1.0	1.00	0.44	0.011	0.095	0.345	1.488	4.220	0.048	1.857	0.033	-
116	7/12/2011	1.2	1.00	0.44	0.015	0.095	0.345	1.488	4.220	0.061	1.857	0.032	-
117	7/12/2011	1.4	1.00	0.44	0.018	0.095	0.345	1.488	4.220	0.074	1.857	0.030	-
118	7/12/2011	1.8	1.00	0.44	0.024	0.095	0.345	1.488	4.220	0.100	1.857	0.035	-
119	7/12/2011	2.2	1.00	0.44	0.030	0.095	0.345	1.488	4.220	0.126	1.857	0.041	-

Data for 256 experiments that were taken during the time 2/4/2011 8/4/2011 2011 in Johns Hopkins Coastal Engineering Laboratory.

Test	Date	S	T (s)	h (m)	a (m)	d_2 (m)	d_1 (m)	L (m)	k_r (m^{-1})	ka	kh	k_i (m^{-1})	Comments
120	7/12/2011	2.5	1.00	0.44	0.035	0.095	0.345	1.488	4.220	0.146	1.857	0.046	-
121	7/12/2011	0.9	1.00	0.44	0.010	0.092	0.348	1.488	4.220	0.042	1.857	0.038	problem with sonic gauge
122	7/12/2011	1.2	0.89	0.44	0.015	-	-	1.212	5.182	0.075	2.280	0.028	-
123	7/12/2011	2.0	1.00	0.44	0.027	-	-	1.488	4.220	0.113	1.857	0.028	Checking repeatability
124	7/13/2011	2.0	1.00	0.38	0.027	0.081	0.294	1.446	4.343	0.117	1.629	0.052	Checking repeatability
125	7/13/2011	0.8	1.00	0.38	0.008	0.081	0.294	1.446	4.343	0.036	1.629	0.056	-
126	7/13/2011	1.0	1.00	0.38	0.011	0.081	0.294	1.446	4.343	0.050	1.629	0.045	-
127	7/13/2011	1.2	1.00	0.38	0.015	0.081	0.294	1.446	4.343	0.063	1.629	0.048	-
128	7/13/2011	1.4	1.00	0.38	0.018	0.081	0.294	1.446	4.343	0.077	1.629	0.049	-
129	7/13/2011	1.8	1.00	0.38	0.024	0.081	0.294	1.446	4.343	0.103	1.629	0.045	-
130	7/13/2011	2.2	1.00	0.38	0.030	0.081	0.294	1.446	4.343	0.130	1.629	0.054	-
131	7/13/2011	0.9	1.00	0.38	0.010	0.081	0.294	1.446	4.343	0.043	1.629	0.056	-
132	7/13/2011	2.0	1.00	0.38	0.027	0.081	0.294	1.446	4.343	0.117	1.629	0.048	Checking repeatability
133	7/13/2011	1.6	1.00	0.38	0.021	0.081	0.294	1.446	4.343	0.090	1.629	0.051	-
134	7/13/2011	0.8	0.89	0.38	0.008	0.095	0.280	1.191	5.273	0.044	1.977	0.039	-
135	7/13/2011	1.0	0.89	0.38	0.011	0.095	0.280	1.191	5.273	0.060	1.977	0.039	-
136	7/13/2011	1.2	0.89	0.38	0.015	0.095	0.280	1.191	5.273	0.077	1.977	0.033	-
137	7/13/2011	1.4	0.89	0.38	0.018	0.095	0.280	1.191	5.273	0.093	1.977	0.046	-
138	7/13/2011	1.8	0.89	0.38	0.024	0.095	0.280	1.191	5.273	0.125	1.977	0.061	-
139	7/13/2011	2.2	0.89	0.38	0.030	0.095	0.280	1.191	5.273	0.158	1.977	0.051	-

Data for 256 experiments that were taken during the time 2/4/2011 8/4/2011 2011 in Johns Hopkins Coastal Engineering Laboratory.

Test	Date	S	T (s)	h (m)	a (m)	d_2 (m)	d_1 (m)	L (m)	k_r (m^{-1})	ka	kh	k_i (m^{-1})	Comments
140	7/13/2011	1.3	0.89	0.38	0.016	0.095	0.280	1.191	5.273	0.085	1.977	0.037	-
141	7/13/2011	1.6	0.89	0.38	0.021	0.095	0.280	1.191	5.273	0.109	1.977	0.067	-
142	7/13/2011	2.0	0.89	0.38	0.027	0.095	0.280	1.191	5.273	0.142	1.977	0.054	-
143	7/13/2011	0.8	0.89	0.38	0.008	0.095	0.280	1.191	5.273	0.044	1.977	0.042	-
144	7/13/2011	1.5	0.89	0.38	0.019	0.095	0.280	1.191	5.273	0.101	1.977	0.057	-
145	7/14/2011	2.0	1.00	0.44	0.027	0.098	0.342	1.488	4.220	0.113	1.857	0.056	Checking repeatability
146	7/14/2011	0.8	1.00	0.44	0.008	0.098	0.342	1.488	4.220	0.035	1.857	0.068	-
147	7/14/2011	1.6	1.00	0.44	0.021	0.098	0.342	1.488	4.220	0.087	1.857	0.054	-
148	7/14/2011	1.2	1.00	0.44	0.015	0.098	0.342	1.488	4.220	0.06	1 1.857	0.050	-
149	7/14/2011	2.	2 1.00	0.44	0.030	0.098	0.342	1.488	4.220	0.126	1.857	0.057	-
150	7/14/2011	1.0	1.00	0.44	0.011	0.098	0.342	1.488	4.220	0.048	1.857	0.059	-
151	7/14/2011	0.7	1.00	0.44	0.007	0.098	0.342	1.488	4.220	0.029	1.857	0.066	-
152	7/14/2011	2.5	1.00	0.44	0.035	0.098	0.342	1.488	4.220	0.146	1.857	0.059	-
153	7/14/2011	0.9	1.00	0.44	0.010	0.098	0.342	1.488	4.220	0.042	1.857	0.060	-
154	7/14/2011	2.0	1.00	0.44	0.027	0.098	0.342	1.488	4.220	0.113	1.857	0.051	Checking repeatability
155	7/15/2011	2.0	1.00	0.44	0.027	0.102	0.338	1.488	4.220	0.113	1.857	0.049	Checking repeatability
156	7/15/2011	1.2	0.85	0.44	0.015	0.100	0.340	1.113	5.642	0.082	2.483	0.047	-
157	7/15/2011	1.8	0.85	0.44	0.024	0.098	0.342	1.113	5.642	0.134	2.483	0.044	-
158	7/15/2011	0.8	0.85	0.44	0.008	0.098	0.342	1.113	5.642	0.047	2.483	0.045	-
159	7/15/2011	1.5	0.85	0.44	0.019	0.098	0.342	1.113	5.642	0.108	2.483	0.043	-

Data for 256 experiments that were taken during the time 2/4/2011 8/4/2011 2011 in Johns Hopkins Coastal Engineering Laboratory.

Test	Date	S	T (s)	h (m)	a (m)	d_2 (m)	d_1 (m)	L (m)	k_r (m^{-1})	ka	kh	k_i (m^{-1})	Comments
160	7/15/2011	2.1	0.85	0.44	0.028	0.098	0.342	1.113	5.642	0.160	2.483	0.041	-
161	7/15/2011	2.0	1.20	0.44	0.027	0.098	0.342	1.987	3.161	0.085	1.391	0.053	large scatter - long Seiche likely
162	7/15/2011	1.0	0.89	0.44	0.011	0.098	0.342	1.212	5.182	0.059	2.280	0.051	-
163	7/15/2011	1.6	0.89	0.44	0.021	0.098	0.342	1.212	5.182	0.107	2.280	0.064	-
164	7/18/2011	2.0	1.00	0.44	0.027	0.102	0.338	1.488	4.220	0.113	1.857	0.058	Checking repeatability
165	7/18/2011	2.0	1.22	0.44	0.027	0.103	0.337	2.036	3.084	0.083	1.357	0.067	interesting long seich shape
166	7/18/2011	1.2	1.22	0.44	0.015	0.105	0.335	2.036	3.084	0.045	1.357	0.065	-
167	7/18/2011	2.0	1.10	0.44	0.027	0.106	0.334	1.739	3.611	0.097	1.589	0.067	another long seiche
168	7/18/2011	2.0	1.24	0.44	0.027	0.106	0.334	2.085	3.012	0.081	1.325	0.065	funky looking seiche
169	7/18/2011	1.2	1.24	0.44	0.015	0.106	0.334	2.085	3.012	0.044	1.325	0.071	still slight seiche
170	7/18/2011	1.6	1.24	0.44	0.021	0.105	0.335	2.085	3.012	0.062	1.325	0.062	-
171	7/18/2011	0.9	1.24	0.44	0.010	0.105	0.335	2.085	3.012	0.030	1.325	0.069	-
172	7/18/2011	2.4	1.24	0.44	0.033	0.105	0.335	2.085	3.012	0.099	1.325	0.060	-
173	7/18/2011	1.4	1.24	0.44	0.018	0.105	0.335	2.085	3.012	0.053	1.325	0.059	-
174	7/18/2011	2.0	1.24	0.44	0.027	0.105	0.335	2.085	3.012	0.081	1.325	0.061	-
175	7/19/2011	2.0	1.00	0.44	0.027	0.102	0.338	1.488	4.220	0.113	1.857	0.053	Checking repeatability
176	7/19/2011	2.0	1.24	0.44	0.027	0.102	0.338	2.085	3.012	0.081	1.325	0.052	-
177	7/19/2011	1.2	1.24	0.44	0.015	0.100	0.340	2.085	3.012	0.044	1.325	0.061	-
178	7/19/2011	1.6	1.24	0.44	0.021	0.100	0.340	2.085	3.012	0.062	1.325	0.060	-
179	7/19/2011	1.4	1.24	0.44	0.018	0.100	0.340	2.085	3.012	0.053	1.325	0.062	-

Data for 256 experiments that were taken during the time 2/4/2011 8/4/2011 2011 in Johns Hopkins Coastal Engineering Laboratory.

Test	Date	S	T (s)	h (m)	a (m)	d_2 (m)	d_1 (m)	L (m)	k_r (m^{-1})	ka	kh	k_i (m^{-1})	Comments
180	7/19/2011	0.9	1.24	0.44	0.010	0.100	0.340	2.085	3.012	0.030	1.325	0.060	-
181	7/19/2011	2.4	1.24	0.44	0.033	0.100	0.340	2.085	3.012	0.099	1.325	0.053	-
182	7/19/2011	2.0	1.24	0.44	0.027	0.100	0.340	2.085	3.012	0.081	1.325	0.049	-
183	7/19/2011	1.8	1.24	0.44	0.024	0.098	0.342	2.085	3.012	0.072	1.325	0.051	-
184	7/19/2011	2.0	1.00	0.44	0.027	0.098	0.342	1.488	4.220	0.113	1.857	0.053	Checking repeatability
185	7/20/2011	2.0	0.95	0.49	0.027	0.111	0.379	1.378	4.557	0.122	2.233	0.035	-
186	7/20/2011	1.2	0.95	0.49	0.015	0.110	0.380	1.378	4.557	0.066	2.233	0.039	-
187	7/20/2011	2.0	1.00	0.49	0.027	0.110	0.380	1.510	4.159	0.112	2.038	0.029	-
188	7/20/2011	1.6	0.95	0.49	0.021	0.114	0.376	1.378	4.557	0.094	2.233	0.037	-
189	7/20/2011	0.8	0.95	0.49	0.008	0.114	0.376	1.378	4.557	0.038	2.233	0.047	-
190	7/20/2011	2.4	0.95	0.49	0.033	0.114	0.376	1.378	4.557	0.150	2.233	0.040	-
191	7/20/2011	1.0	0.95	0.49	0.011	0.116	0.374	1.378	4.557	0.052	2.233	0.048	-
192	7/20/2011	2.0	0.95	0.49	0.027	0.117	0.373	1.378	4.557	0.122	2.233	0.043	-
193	7/20/2011	1.2	0.95	0.49	0.015	0.117	0.373	1.378	4.557	0.066	2.233	0.037	-
194	7/20/2011	1.8	0.95	0.49	0.024	0.117	0.373	1.378	4.557	0.108	2.233	0.039	-
195	7/20/2011	1.1	0.95	0.49	0.013	0.117	0.373	1.378	4.557	0.059	2.233	0.040	-
196	7/20/2011	1.6	0.95	0.49	0.021	0.117	0.373	1.378	4.557	0.094	2.233	0.037	-
197	7/20/2011	1.0	0.95	0.49	0.011	0.116	0.374	1.378	4.557	0.052	2.233	0.039	-
198	7/20/2011	2.0	0.95	0.49	0.027	0.116	0.374	1.378	4.557	0.122	2.233	0.039	-
199	7/20/2011	0.9	0.95	0.49	0.010	0.116	0.374	1.378	4.557	0.045	2.233	0.043	-

Data for 256 experiments that were taken during the time 2/4/2011 8/4/2011 2011 in Johns Hopkins Coastal Engineering Laboratory.

Test	Date	S	T (s)	h (m)	a (m)	d_2 (m)	d_1 (m)	L (m)	k_r (m^{-1})	ka	kh	k_i (m^{-1})	Comments
200	7/21/2011	2.0	0.95	0.49	0.027	0.100	0.390	1.378	4.557	0.122	2.233	0.018	-
201	7/21/2011	2.0	0.95	0.49	0.027	0.100	0.390	1.378	4.557	0.122	2.233	0.028	-
202	7/21/2011	1.2	0.95	0.49	0.015	0.100	0.390	1.378	4.557	0.066	2.233	0.027	-
203	7/21/2011	1.0	0.95	0.49	0.011	0.098	0.392	1.378	4.557	0.052	2.233	0.024	-
204	7/21/2011	2.0	1.20	0.49	0.027	0.098	0.392	2.040	3.078	0.083	1.508	0.217	long seich
205	7/21/2011	2.0	1.25	0.49	0.027	0.098	0.392	2.170	2.894	0.078	1.418	0.027	better looking data
206	7/22/2011	2.0	0.95	0.49	0.027	0.114	0.376	1.378	4.557	0.122	2.233	0.032	-
207	7/22/2011	1.2	0.95	0.49	0.015	0.113	0.377	1.378	4.557	0.066	2.233	0.036	-
208	7/22/2011	1.6	0.95	0.49	0.021	0.113	0.377	1.378	4.557	0.094	2.233	0.034	lutocline slightly cloudy
209	7/22/2011	1.0	0.95	0.49	0.011	0.117	0.373	1.378	4.557	0.052	2.233	0.037	still a little cloudy
210	7/22/2011	0.8	0.95	0.49	0.008	0.121	0.369	1.378	4.557	0.038	2.233	0.046	-
211	7/22/2011	2.0	0.95	0.49	0.027	0.121	0.369	1.378	4.557	0.122	2.233	0.033	-
212	7/22/2011	0.9	0.95	0.49	0.010	0.121	0.369	1.378	4.557	0.045	2.233	0.035	-
213	7/22/2011	2.4	0.95	0.49	0.033	0.121	0.369	1.378	4.557	0.150	2.233	0.037	-
214	7/22/2011	0.9	0.95	0.49	0.009	0.121	0.369	1.378	4.557	0.042	2.233	0.045	-
215	7/22/2011	0.9	0.95	0.49	0.010	0.121	0.369	1.378	4.557	0.045	2.233	0.042	-
216	7/22/2011	1.4	0.95	0.49	0.018	0.121	0.369	1.378	4.557	0.080	2.233	0.035	-
217	8/1/2011	2.0	1.00	0.44	0.027	0.103	0.337	1.488	4.220	0.113	1.857	0.046	-
218	8/1/2011	2.0	1.00	0.44	0.027	0.103	0.337	1.488	4.220	0.113	1.857	0.048	Checking repeatability
219	8/1/2011	2.0	1.00	0.44	0.027	0.103	0.337	1.488	4.220	0.113	1.857	0.049	Checking repeatability

Data for 256 experiments that were taken during the time 2/4/2011 8/4/2011 2011 in Johns Hopkins Coastal Engineering Laboratory.

Test	Date	S	T (s)	h (m)	a (m)	d_2 (m)	d_1 (m)	L (m)	k_r (m^{-1})	ka	kh	k_i (m^{-1})	Comments
220	8/1/2011	2.0	1.00	0.44	0.027	0.103	0.337	1.488	4.220	0.113	1.857	0.049	Checking repeatability
221	8/1/2011	2.0	1.00	0.44	0.027	0.103	0.337	1.488	4.220	0.113	1.857	0.047	Checking repeatability
222	8/1/2011	2.0	1.00	0.44	0.027	0.103	0.337	1.488	4.220	0.113	1.857	0.047	Checking repeatability
223	8/1/2011	2.0	1.00	0.44	0.027	0.100	0.340	1.488	4.220	0.113	1.857	0.050	Checking repeatability
224	8/1/2011	2.0	1.00	0.44	0.027	0.100	0.340	1.488	4.220	0.113	1.857	0.051	Checking repeatability
225	8/1/2011	2.0	1.00	0.44	0.027	0.100	0.340	1.488	4.220	0.113	1.857	0.045	Checking repeatability
226	8/1/2011	2.0	1.00	0.44	0.027	0.100	0.340	1.488	4.220	0.113	1.857	0.043	Checking repeatability
227	8/2/2011	2.0	1.00	0.44	0.027	0.111	0.329	1.488	4.220	0.113	1.857	0.039	Checking repeatability
228	8/2/2011	2.0	1.00	0.44	0.027	0.111	0.329	1.488	4.220	0.113	1.857	0.040	Checking repeatability
229	8/2/2011	2.0	1.00	0.44	0.027	0.111	0.329	1.488	4.220	0.113	1.857	0.038	Checking repeatability
230	8/2/2011	2.0	1.00	0.44	0.027	0.111	0.329	1.488	4.220	0.113	1.857	0.038	Checking repeatability
231	8/2/2011	2.0	1.00	0.44	0.027	0.111	0.329	1.488	4.220	0.113	1.857	0.039	Checking repeatability
232	8/2/2011	2.0	1.00	0.44	0.027	0.110	0.330	1.488	4.220	0.113	1.857	0.042	Checking repeatability
233	8/2/2011	2.0	1.00	0.44	0.027	0.110	0.330	1.488	4.220	0.113	1.857	0.042	Checking repeatability
234	8/2/2011	2.0	1.00	0.44	0.027	0.110	0.330	1.488	4.220	0.113	1.857	0.045	Checking repeatability
235	8/2/2011	2.0	1.00	0.44	0.027	0.110	0.330	1.488	4.220	0.113	1.857	0.045	Checking repeatability
236	8/3/2011	2.0	1.00	0.44	0.027	0.110	0.330	1.488	4.220	0.113	1.857	0.042	Checking repeatability
237	8/3/2011	2.0	1.00	0.44	0.027	0.102	0.338	1.488	4.220	0.113	1.857	0.048	Checking repeatability
238	8/3/2011	2.0	1.00	0.44	0.027	0.102	0.338	1.488	4.220	0.113	1.857	0.050	Checking repeatability
239	8/3/2011	2.0	1.00	0.44	0.027	0.102	0.338	1.488	4.220	0.113	1.857	0.051	Checking repeatability

Data for 256 experiments that were taken during the time 2/4/2011 8/4/2011 2011 in Johns Hopkins Coastal Engineering Laboratory.

Test	Date	S	T (s)	h (m)	a (m)	d_2 (m)	d_1 (m)	L (m)	k_r (m^{-1})	ka	kh	k_i (m^{-1})	Comments
240	8/3/2011	2.0	1.00	0.44	0.027	0.102	0.338	1.488	4.220	0.113	1.857	0.052	Checking repeatability
241	8/3/2011	2.0	1.00	0.44	0.027	0.102	0.338	1.488	4.220	0.113	1.857	0.055	Checking repeatability
242	8/3/2011	2.0	1.00	0.44	0.027	0.102	0.338	1.488	4.220	0.113	1.857	0.050	Checking repeatability
243	8/3/2011	2.0	1.00	0.44	0.027	0.102	0.338	1.488	4.220	0.113	1.857	0.050	Checking repeatability
244	8/3/2011	2.0	1.00	0.44	0.027	0.102	0.338	1.488	4.220	0.113	1.857	0.053	Checking repeatability
245	8/3/2011	2.0	1.00	0.44	0.027	0.102	0.338	1.488	4.220	0.113	1.857	0.050	Checking repeatability
246	8/4/2011	2.0	1.00	0.44	0.027	0.102	0.338	1.488	4.220	0.113	1.857	0.051	Checking repeatability
247	8/4/2011	2.0	1.00	0.44	0.027	0.100	0.340	1.488	4.220	0.113	1.857	0.047	Checking repeatability
248	8/4/2011	2.0	1.00	0.44	0.027	0.100	0.340	1.488	4.220	0.113	1.857	0.412	Checking repeatability
249	8/4/2011	2.0	1.00	0.44	0.027	0.100	0.340	1.488	4.220	0.113	1.857	0.046	Checking repeatability
250	8/4/2011	2.0	1.00	0.44	0.027	0.100	0.340	1.488	4.220	0.113	1.857	0.046	Checking repeatability
251	8/4/2011	2.0	1.00	0.44	0.027	0.100	0.340	1.488	4.220	0.113	1.857	0.040	Checking repeatability
252	8/4/2011	2.0	1.00	0.44	0.027	0.100	0.340	1.488	4.220	0.113	1.857	0.034	Checking repeatability
253	8/4/2011	2.0	1.00	0.44	0.027	0.100	0.340	1.488	4.220	0.113	1.857	0.042	Checking repeatability
254	8/4/2011	2.0	1.00	0.44	0.027	0.100	0.340	1.488	4.220	0.113	1.857	0.042	Checking repeatability
255	8/4/2011	2.0	1.00	0.44	0.027	0.100	0.340	1.488	4.220	0.113	1.857	0.041	Checking repeatability
256	8/4/2011	2.0	1.00	0.44	0.027	0.100	0.340	1.488	4.220	0.113	1.857	0.040	Checking repeatability

Bibliography

Aijaz, S. and Jenkins, S. (1994). On the electrokinetics of shear stress behavior in fluid-mud suspensions. *Journal of Geophysical Research*, **99**(C6), 12697–12706.

Allison, M., Kineke, G., Gordon, E., and Goni, M. (2000). Developing and reworking of seasonal flood deposit on the inner continental shelf off the atchafalaya river. *Cont. Shelf Res.*, **20**, 2267–2294.

Augustin, L., Irish, J., and Lynett, P. (2012). Laboratory and numerical studies of wave damping by emergent and near-emergent wetland vegetation. *Coastal Eng.*, **56**(3), 332–340.

Bai, Y.-C., Ng, C.-O., Shen, H.-T., and Wang, S.-Y. (2002). Rheological properties and incipient motion of cohesive sediment in the haihe estuary of china. *China Ocean Engineering*, **16**(4), 483–498.

Barnes, H., Hutton, J., and Walters, K. (1989). *An introduction to rheology*, volume 3. Elsevier, Amsterdam ;New York.

BIBLIOGRAPHY

Benjamin, T. and Feir, J. (1967). Disintegration of wave trains on deep water. part 1. theory. *J. Fluid Mech.*, **27**, 417–430.

Chan, I.-C. and Liu, P.-F. (2009). Responses of bingham-plastic muddy seabed to a surface solitary wave. *Journal of Fluid Mechanics*, **618**, 155–180.

Chou, H., Foda, M., and Hunt, J. (1993). Rheological response of cohesive sediments to oscillatory forcing in nearshore and estuarine cohesive sediment transport. *Coastal Estuarine Stud.*, **42**, 126–147.

Coussot, P. and Piau, J.-M. (1994). On the behavior of fine mud suspensions. *Rheologica Acta*, **33**(3), 175–184.

Dalrymple, R. and Liu, P.-F. (1978). Waves over soft muds: a two-layer fluid model. *Journal of Physical Oceanography*, **8**(6), 1121–1131.

Dawson, T. (1978). Wave propagation over a deformable sea floor. *Ocean Engineering*, **5**(4), 227–234.

de Boer, G., van Dongeren, A., and Winterwerp, J. (2009). Wave damping by fluid mud; experiments in the scheldt flume. *Deltares report Z4700 / 1200266.007*.

De Wit, P. (1995). Liquefaction of cohesive sediments caused by waves. *Liquefaction of Cohesive Sediments Caused by Waves*.

Dean, R. and Dalrymple, R. (1991). *Water wave mechanics for engineers and scientists*. World Scientific Pub. Co., Teaneck, NJ.

BIBLIOGRAPHY

Elgar, S. and Raubenheimer, B. (2008). Wave dissipation by muddy seafloors. *Geophysical Research Letters*, **35**.

Faas, R. (1985). Time and density-dependent properties of fluid mud suspensions, NE brazilian continental shelf. *Geo-Marine Letters*, **4**(3), 147–152.

Faas, R. (1995). Mudbanks of the southwest coast of india III: role of non-newtonian flow properties in the generation and maintenance of mudbanks. *Journal of Coastal Research*, **11**(3), 911–917.

Feng, J., Mehta, A., Williams, D., and Williams, P. (1992). Laboratory experiments on cohesive soil bed fluidization by water waves. *UFL/COEL (University of Florida. Coastal and Oceanographic Engineering Laboratory)*, (92/015).

Foda, M. (1989). Sideband damping of water waves over a soft bed. *Journal of Fluid Mechanics*, **201**(-1), 189.

Gade, H. (1957). *Effects of a non-rigid impermeable bottom on plane surface waves in shallow water*. Ph.D. thesis, Texas A&M University.

Gade, H. (1958). Effects of a non-rigid impermeable bottom on plane surface waves in shallow water. *Journal of Marine Research*, **16**(2), 61–82.

Geyer, W., Hill, P., and Kineke, G. (2004). The transport, transformation and dispersal of sediment by buoyant coastal flows. *Cont. Shelf Res.*, **24**, 927–949.

BIBLIOGRAPHY

Holland, K., Vinzon, S., and Calliari, L. (2009). A field study of coastal dynamics on a muddy coast offshore of cassino beach, brazil. *Continental Shelf Research*, **29**(3), 503–514.

Hsiao, S. and Shemdin, O. (1979). Interaction of ocean waves with a soft bottom. *Journal of Physical Oceanography*, **10**(4), 605–610.

Hsu, W., Hwung, H., Hsu, T., Torres-Freyermuth, A., and Yang, R. (2013). An experimental and numerical investigation on wave-mud interactions. *Journal of Geophysical Research Oceans*, **118**, 1126–1141.

Hu, S. and Wai, O. (2001). Experimental study on wave energy dissipation and cohesive sediment transport in silt coast. *International Journal of Sediment Research*, **16**(2), 224–233.

Jain, M. (2007). *Wave attenuation and mud entrainment in shallow waters*. Ph.D. thesis.

Jaramillo, S., Sheremet, A., Allison, M., Reed, A., and Holland, K. (2009). Wave-mud interactions over the muddy atchafalaya subaqueous clinoform, louisiana, united states: Wave-supported sediment transport. *Journal of Geophysical Research C: Oceans*, **114**(4).

Jiang, L. and Zhao, Z. (1989). Viscous damping of solitary waves over fluid-mud

seabeds. *Journal of Waterway, Port, Coastal, and Ocean Engineering*, **115**(3), 345–362.

Jiang, L., Kioka, W., and Ishida, A. (1990). Viscous damping of cnoidal waves over fluid-mud seabed. *Journal of Waterway, Port, Coastal, and Ocean Engineering*, **116**(4), 470–491.

Jiang, Q. and Watanabe, A. (1995). Rheological properties of soft mud and a numerical model for its motion under waves. *Coastal Engineering Journal*, **38**(2), 195–214.

Jiang, Q. and Watanabe, A. (1997). Analysis of mud mass transport under waves using an empirical rheological model. volume 4, pages 4174–4187. Penta-Ocean Inst of Technology, Tochigi, Japan.

Kaihatu, J., Sheremet, A., and Holland, K. (2007). A model for the propagation of nonlinear surface waves over viscous muds. *Coastal Engineering*, **54**(10), 752–764.

Kay, S. and Marple, S. (1981). Spectrum analysis-a modern perspective. *Proc. IEEE*, **11**, 1380–1419.

Kessel, T. and Kranenburg, C. (1996). Gravity current of fluid mud on sloping bed. *Journal of Hydraulic Engineering*, **122**(12), 710–717.

Keulegan, G. (1958). Energy dissipation in standing waves in rectangular basins. *Journal of Fluid Mechanics*, **6**, 33–50.

BIBLIOGRAPHY

Kim, T. and Lee, J. (2013). The difference in wave environments between intertidal sand beaches and mud flats. *J. of Coastal Res.*, **65**(517-522).

Kineke, G., Sternberg, R., Trowbridge, J., and Geyer, W. (1996). Fluid-mud processes on the Amazon continental shelf. *Continental Shelf Research*, **16**(5-6), 667–696.

Koftis, T., Prinos, P., and Stratigaki, V. (2013). Wave damping over artificial posidonia oceanica meadow: A large-scale experimental study. *Coastal Eng.*, **73**(71-83).

Kranenburg, W. (2008). *Modelling wave damping by fluid mud, Derivation of a dispersion equation and an energy dissipation term and implementation into SWAN*. Master's thesis, DELFT Hydraulics and DELFT University of Technology.

Kranenburg, W., Winterwerp, J., de Boer, G., Cornelisse, J., and Zijlema, M. (2011). Swan-mud: Engineering model for mud-induced wave damping. *Journal of Hydraulic Engineering*, **137**(9), 959–975.

Krone, R. (1963). A study of rheologic properties of estuarial sediments.

Lian, J.-J., Zhao, Z.-D., and Zhang, Q. (1999). A nonlinear viscoelastic model for bed mud transport due to waves and currents. *Chinese Science Bulletin*, **44**(17), 1597–1600.

Liu, K.-F. and Mei, C. (1990). Approximate equations for the slow spreading of a thin sheet of bingham plastic fluid. *Physics of Fluids A: Fluid Dynamics*, **2**(1), 30–36.

BIBLIOGRAPHY

Liu, K.-F. and Mei, C. (1993a). Long waves in shallow water over a layer of Bingham-plastic fluid-mud-ii. mathematical derivation of long wave equations. *International Journal of Engineering Science*, **31**(1), 145–155.

Liu, K.-F. and Mei, C. (1993b). Long waves in shallow water over a layer of Bingham-plastic fluid mud-i. physical aspects. *Int'l J. Engneering Sci.*, **31**(1), 125–144.

Liu, P.-F. and Chan, I.-C. (2007). On long-wave propagation over a fluid-mud seabed. *Journal of Fluid Mechanics*, **579**, 467–480.

Longuet-Higgins, M. (1953). Mass-transport in water waves. *Phil. Trans. A*, **245**(535-581).

Longuet-Higgins, M. and Stewart, R. (1960). Changes in the form of short gravity waves on long waves and tidal currents. *J. of Fluid Mech.*, **8**(4), 565–583.

Longuet-Higgins, M. and Stewart, R. (1962). Radiation stress and mass transport in gravity waves, with application to 'surf beats'. *J. of Fluid Mech.*, **13**(4), 481–504.

Longuet-Higgins, M. S. (1950). A theory of the origin of microseisms. *Mathematical and Physical Sciences*, **243**(857), 1–35.

Ma, G., Kirby, J., Su, S., Figlus, J., and Shi, F. (2013). Numerical study of turbulence and wave damping induced by vegetation canopies. *Coastal Eng.*, **80**, 68–78.

Ma, Y., Dong, G., Perlin, M., Ma, X., and Wang, G. (2012). Experimental investiga-

tion on the evolution of the modulation instability with dissipation. *J Fluid Mech.*, **711**, 101–121.

Maa, J.-Y. (1986). *Erosion of soft muds by waves*. Ph.D. thesis.

Maa, J.-Y. and Mehta, A. (1987). Mud erosion by waves: a laboratory study. *Continental Shelf Research*, **7**(11-12), 1269–1284.

Maa, J.-Y. and Mehta, A. (1988). Soft mud properties: Voigt model. *Journal of Waterway, Port, Coastal, and Ocean Engineering*, **114**(6), 765–770.

Maa, J.-Y. and Mehta, A. (1990). Soft mud response to water waves. *Journal of Waterway, Port, Coastal and Ocean Engineering*, **116**(5), 634–650.

MacPherson, H. (1980). The attenuation of water waves over a non-rigid bed. *Journal of Fluid Mechanics*, **97**(4), 721–742.

Mallard, W. and Dalrymple, R. (1977). Water waves propagating over a deformable bottom. *Proceedings of the Annual Offshore Technology Conference*, **3**, 141–146.

Mallik, T., Mukherji, K., and Ramachandran, K. (1988). Sedimentology of the kerala mud banks (fluid muds?). *Marine Geology*, **80**(1-2), 99–118.

Mathew, J., Baba, M., and Kurian, N. (1995). Mudbanks of the southwest coast of india. I: wave characteristics. *Journal of Coastal Research*, **11**(1), 168–178.

Mehta, A. (1991). Understanding fluid mud in a dynamic environment. *Geo-Marine Letters*, **11**(3), 113–118.

BIBLIOGRAPHY

Mei, C. and Liu, K.-F. (1987). A Bingham-plastic model for a muddy seabed under long waves. *Journal of Geophysical Research*, **92**(C13), 14581–14594.

Mei, C., Krotov, M., Huang, Z., and Huhe, A. (2010). Short and long waves over a muddy seabed. *Journal of Fluid Mechanics*, **643**, 33–58.

Mimura, N. (1993). Rates of erosion and deposition of cohesive sediments under wave action. In A. Mehta, editor, *Nearshore and Estuarine Cohesive Sediment Transport*, volume 42 of *Coastal Estuarine Studies*, pages 247–264. AGU.

Nagai, T., Yamamoto, T., and Figueroa, J. (1984). A laboratory experimentation on the interaction between water waves and soft clay bed. *Coastal Engineering in Japan*, **27**, 279–291.

Ng, C.-O. (2000). Water waves over a muddy bed: a two-layer Stokes' boundary layer model. *Coastal Engineering*, **40**(3), 221–242.

Nouri, Y. (2013). *Experimental study of water wave interactions with a layer of mud*. Ph.D. thesis, Johns Hopkins University.

Ogus, E., Elginoz, N., Koroglu, A., and Kabdasli, M. (2013). The effect of reed beds on wave attenuation and suspended sediment concentration. *J. of Coastal Res.*, **65**, 356–361.

Otsubo, K. and Muraoka, K. (1988). Critical shear stress of cohesive bottom sediments. *Journal of Hydraulic Engineering*, **114**(10), 1241–1256.

BIBLIOGRAPHY

Oveisy, A. (2009). *A Two-Dimensional Horizontal Wave Propagation and Mud Mass Transport Model on Muddy Coastal Regions*. Ph.D. thesis, Queen's University.

Oveisy, A., Hall, K., Soltanpour, M., and Shibayama, T. (2009). A two-dimensional horizontal wave propagation and mud mass transport model. *Continental Shelf Research*, **29**(3), 652–665.

Phillips, O. (1960). On the dynamics of unsteady gravity waves of finite amplitude. *J. Fluid Mech.*, **9**(2), 193–217.

Piedra-Cueva, I. (1993). Mass transport in mud layer induced by wave action. pages 1189–1193. Inst of Fluid Mechanics and Env Engineering, Montevideo, Uruguay.

Prony, R. (1795). Essai experimental et analytique. *J. de L'Ecole Polytechnique*, **2**, 24–76.

Robillard, D. (2009). *A Laboratory investigation of mud seabed thickness contributing to wave attenuation*. Ph.D. thesis, University of Florida.

Rodriguez, H. (2009). *Mud bottom evolution at open coast*. Ph.D. thesis, University of Florida.

Rodriguez, H. and Mehta, A. (2000). Longshore transport of fine-grained sediment. *Continental Shelf Research*, **20**(12-13), 1419–1432.

Rosenthal, W. (1978). Energy exchange between surface waves and of sediment. *J. Geophys. Res.*, **83**, 1980–1982.

BIBLIOGRAPHY

Ross, M. and Mehta, A. (1990). Fluidization of soft estuarine mud by waves. *The Microstructure of Fine Grained Sediments: From Mud to Shale*, pages 185–191.

Safak, I., Sheremet, A., Allison, M., and Hsu, T. (2010). Bottom turbulence on the muddy atchafalaya shelf, louisiana. *J. Geophys. Res.*, **115**.

Sakakiyama, T. and Bijker, E. (1989). Mass transport velocity in mud layer due to progressive waves. *Journal of Waterway, Port, Coastal and Ocean Engineering*, **115**(5), 614–633.

Shen, D.-X., Carr, C., and Isobe, M. (2003). Wave dissipation and reflection on muddy bottoms. In J. A. Melby, editor, *Proceedings of Coastal Structures 2003*, volume 147, pages 789–801.

Sheremet, A. and Stone, G. W. (2003). Observations of nearshore wave dissipation over muddy sea beds. *Journal of Geophysical Research C: Oceans*, **108**(11), 21–1.

Sheremet, A., Jaramillo, S., Su, S., Allison, M., and Holland, K. (2011). Wave-mud interaction over the muddy atchafalaya subaqueous clinoform, louisiana, united states. *J. Geophys. Res*, **116**.

Shibayama, T. and An, N. N. (1993). A visco-elastic-plastic model for wave-mud interaction. *Coastal Engineering in Japan*, **36**(1), 67–89.

Shibayama, T., Takikawa, H., and Horikawa, K. (1986). Mud mass transport due to waves. *Coastal Engineering Journal*, **29**, 151–161.

BIBLIOGRAPHY

Shibayama, T., Aoki, T., and Sato, S. (1989). Mud mass transport rate due to waves: a viscoelastic model. *IAHR*, pages B567–B574.

Shibayama, T., Okuno, M., and Sato, S. (1990). Mud transport rate in mud layer due to wave action. *Proceedings of the 22nd International Conference on Coastal Engineering*, **1**(22).

Smyth, G. (2000). Employing symmetry constaints for improved frequency estimation by eigenanalysis method. *Technometrics*, **42**(3), 277–289.

Soltanpour, M. and Haghshenas, S. A. (2009). Fluidization and representative wave transformation on muddy beds. *Continental Shelf Research*, **29**(3), 666–675.

Soltanpour, M. and Samsami, F. (2011). A comparative study on the rheology and wave dissipation of kaolinite and natural hendijan coast mud, the persian gulf. *Ocean Dynamics*, **61**, 295–309.

Soltanpour, M., Shibayama, T., and Noma, T. (2003). Cross-shore mud transport and beach deformation model. *Coastal Engineering Journal*, **45**(3), 363–386.

Soltanpour, M., Samsami, F., and Sorourian, S. (2010). A comparative study on the rheology and wave dissipation of kaolinite and natural hendijan coast mud, the persian gulf. *Proceedings of 32nd Conference on Coastal Engineering, Shanghai, China, 2010*, (32), 295–309.

BIBLIOGRAPHY

Stokes, G. (1847). On the theory of oscillatory waves. *Trans Camb. Phil. Soc.*, **8**, 441–455.

Tang, J., Causon, D., Mingham, C., and Qian, L. (2013). Numerical study of vegetation damping effects on solitary wave run-up using the nonlinear shallow water equations. *Coastal Eng.*, **75**(21-28).

Thimakorn, P. (1980). An experiment on clay suspension under water waves. *Proceedings of International Conference on Coastal Engineering*, pages 2894–2906.

Torres-Freyermuth, A. and Hsu, T. (2010). On the dynamics of wave-mud interaction: A numerical study. *Journal of Geophysical Research*, **115**.

Traykovski, P. A., Geyer, W. R., Irish, J. D., and Lynch, J. F. (2000). The role of wave-induced density-driven fluid mud flows for cross-shelf transport on the eel river continental shelf. *Continental Shelf Research*, **20**(16), 2113–2140.

Tsuruya, H. and Nakano, S. (1987). Interactive effects between surface waves and a muddy bottom. volume 1, pages 50–62. Ministry of Transport, Yokosuka, Japan.

Tsuruya, H., Nakano, S., and Takahama, J. (1986). Proceedings of japanese conference on coastal engineering. **33**, 317–321.

Tubman, M. W. and Suhayda, J. N. (1976). Wave action and bottom movements in fine sediments. *Proceedings of* 15^{th} *International Conference on Coastal Engineering*, pages 1168–1183.

BIBLIOGRAPHY

Vinzon, S., Winterwerp, H., Nogueira, R., and De Boer, G. (2009). Mud deposit formation on the open coast of the larger patos lagoon-cassino beach system. *Cont. Shelf Res.*, **29**(3), 572–588.

Vinzon, S. B. and Mehta, A. J. (1998). Mechanism for formation of lutoclines by waves. *Journal of Waterway, Port, Coastal, and Ocean Engineering*, **124**(3), 147–149.

Wells, J. (1983). Dynamics of coastal fluid muds in low-, moderate-, and high-tide-range environments. *Canadian Journal of Fisheries and Aquatic Sciences*, **40**, 130–142.

Wells, J. and Coleman, J. (1981). Physical processes and fine grained sediment dynamics, coast of surinam, south america. *Journal of Sedimentary Petrology*, **51**(4), 1053–1068.

Whitford, D., Waers, J., and Vieira, M. (2001). Teaching time-series analysis ii. wave height and water surface elevation probability distributions. *American Journal of Physics*, **69**(4), 497–504.

Winterwerp, J., De Boer, G., Greeuw, G., and Van MAREN, D. (2012). Mud-induced wave damping and wave-induced liquefaction. *Coastal Eng.*, **64**, 102–112.

Winterwerp, J. C., de Graaff, R. F., Groeneweg, J., and Luijendijk, A. P. (2007).

BIBLIOGRAPHY

Modelling of wave damping at guyana mud coast. *Coastal Engineering*, **54**(3), 249–261.

Yamamoto, T. (1982a). Experiments of wave-driven soil transport in clay beds. *Geo-Marine Letters*, **2**(3), 205–208.

Yamamoto, T. (1982b). Non-linear mechanics of ocean wave interactions with sediment beds. *Applied Ocean Research*, **4**(2), 99–106.

Yamamoto, T. (1983). Numerical integration method for seabed response to water waves. *International Journal of Soil Dynamics and Earthquake Engineering*, **2**(2), 92–100.

Yamamoto, T. and Schuckman, B. (1984). Experiments and theory of wave-soil interactions. *Journal of Engineering Mechanics*, **110**(1), 95–112.

Yamamoto, T. and Takahashi, S. (1985). Wave damping by soil motion. *Journal of Waterway, Port, Coastal, and Ocean Engineering*, **111**(1), 62–77.

Yamamoto, T., Koning, H., Sellmeijer, H., and Hijum, E. (1978). On the response of a poro-elastic bed to water waves. *Journal of Fluid Mechanics*, **87**(01), 193.

Yamamoto, T., Takahashi, S., and Schuckman, B. (1983). Physical modeling of seabed interactions. *Journal of Engineering Mechanics*, **109**(1), 54–72.

Yamamoto, T., Nagai, T., and Figueroa, J. (1986). Experiments on wave-soil interac-

tion and wave-driven soil transport in clay beds. *Continental Shelf Research*, **5**(4), 521–540.

Zhang, Q.-H. and Zhao, Z.-D. (1999). Wave-mud interaction: Wave attenuation and mud mass transport. *Coastal Sediments '99*, pages 1867–1880.

Zhang, Q.-H., Wai, O., and Lee, J. (2003). Wave attenuation over mud bed: A pseudo-plastic model. *Journal of Hydrodynamics*, **15**(6), 32–38.

Zhang, X. and Ng, C. (2006b). Mud-wave interaction: A viscoelastic model. *China Ocean Eng.*, **20**(1), 15–26.

Zhao, Z.-D., Lian, J.-J., and Shi, J. (2006). Interactions among waves, current, and mud: Numerical and laboratory studies. *Advances in Water Resources*, **29**(11), 1731–1744.

Zhou, X. and Wang, J. (1992). The wave attenuation on the mud bed. *Acta Mechanica Sinica*, **8**(3), 215–223.

Vita

Nourah Mohammed Almashaan received the B.S. degree in Civil Engineering (Structural Engineering) From Kuwait University (KU), Kuwait on 2003. Then she worked as a teaching assistance in Kuwait University and worked in many Laboratories in Kuwait University such as (Structural, Geotechnical and Transportation) from (2003-2010). During this period, Nourah received M.Sc. in Civil Engineering (Environmental Engineering) from Kuwait University on 2007. She enrolled in the Civil Engineering (Coastal Engineering) Ph.D. program at Johns Hopkins University on 2010. She also received the M.Sc. degree in Civil Engineering (Coastal Engineering) from Johns Hopkins University on 2012. Her research focuses on the water wave mechanisms that cause wave energy dissipation when passing over a muddy bottom in shallow, intermediate and deep water depths by conducting experimental tests in Coastal Engineering Laboratory in Johns Hopkins University. Starting in September 2014, Nourah will

work as assistance professor in Kuwait University and she will create her own Coastal Engineering Laboratory to continue her career and contribute in solving many of the coastal processes problems in Kuwait and the Gulf area.